CHRISTOF SCHNEIDER

Friction Stir Welding of Magnesium and Steel

Supervised by

Univ.–Prof. Dr. Christof SOMMITSCH

Institute for Material Science and Welding

Graz University of Technology, Austria

Ass.–Prof. Dr. Norbert ENZINGER

Dr. Thomas WEINBERGER

Institute for Material Science and Welding

Graz University of Technology, Austria

Professor Toshihiko KOSEKI

Associate Professor Junya INOUE

Department of Materials Engineering, School of Engineering

University of Tokyo, Japan

A diploma thesis submitted to the

FACULTY OF MECHANICAL ENGINEERING

GRAZ, UNIVERSITY OF TECHNOLOGY

Graz, June 2010

STATUTORY DECLARATION

I declare that I have authored this thesis independently, that I have not used other than the declared sources/resources, and that I have explicitly marked all material which has been quoted either literally or by content from the used sources.

Date _____   Signature: _____

EIDESSTATTLICHE ERKLÄRUNG

Ich erkläre an Eides statt, dass ich die vorliegende Arbeit selbstständig verfasst, andere als die angegebenen Quellen/Hilfsmittel nicht benutzt, und die den benutzten Quellen wörtlich und inhaltlich entnommenen Stellen als solche kenntlich gemacht habe.

Graz, am _____   Unterschrift: _____

Acknowledgements

Abstract

Friction stir welding (FSW) is well known as a solid state welding process with the possibility to join dissimilar materials which are almost impossible with other welding techniques. During this diploma thesis the magnesium alloy AZ31B-O was joined in lap configuration with zinc coated ultra low carbon steel DX54D.

After the parameter study, judged by the fracture strength, the interface and fracture path of key samples were investigated by SEM. The fracture strength increases with increasing welding speed and the majority of the samples fractured not at the interface, which means that the interface is stronger as the measured fracture strength.

For higher welding speeds, an eutectic magnesium zinc layer, which is a sign for melting during the joining process, was detected at the interface. This eutectic layer flows out of the joining interface for lower welding speeds. To get more information about the influence of zinc on the fracture strength and the interface, the zinc coating was removed from the steel sheet before friction stir welding. The fracture strength was lower than with zinc coating and no evidence for melting during the FSW was found.

Contents

1 Introduction

The automobile industry is a tough market. The legislator expects cars with a lower or non carbon dioxide CO_2 emission, the demanding customer only buys cars with good driving properties and the customers with highest sales are expecting low cost cars with low fuel consumption. In the continuous struggle to improve car body properties and at the same time reduce the weight of the structure, new materials and new technologies are being required.

Magnesium is no new material in this field. In 1938 the German auto maker Volkswagen produced the Volkswagen Type 1 called Beetle with approximately 20kg of magnesium [**?**]. Volkswagen used the casted magnesium for gearboxes and cylinder blocks to upgrade the driving properties. Nowadays, magnesium sheet metals are used for e.g. A-pillars, floor pans in the luggage trunk in the car industry and for a lot of other applications in other industries [**?**]. Figure **??** shows the Porsche Panamera body structure where the different materials are highlighted with different colours.

Figure 1.1: Porsche Panamera body structure, boron alloyed - red, polyphase - orange, micro alloyed - yellow, steel - green, aluminum - blue, magnesium torqouise [**?**]

Use the right material at the right place. The conclusion from this technical axiom is dissimilar ma-

terials at the joint. In 2006, the Japanese auto maker Mazda started joining aluminum and steel with the Friction Stir Welding process in serial production. Two big advantages of Friction Stir Welding are 40% lower energy cost compared with Resistance Spot Welding and the possibility to join totally different materials [?]. Friction Stir Welding (FSW) is a relatively new welding process and only some material combinations are reviewed so far. During this diploma thesis the focus was on joining an IF-steel (DX54D) and a magnesium alloy (AZ31) with FSW in a lap joint configuration.

The basic optimization of the strength of the joint is done by improvement of the welding parameters to produce sound and well performing welds. The joints are analyzed on base of cross section metallography, hardness measurement as well as cross tensile tests. Based on these results the plunge depth and welding speed were varied to investigate the basic properties of the magnesium steel interface with respect to pressure and heat input by enhanced methods and knowledge provided at University of Tokyo.

This diploma thesis was a result of the international cooperation between the University of Tokyo particularly the Department of Materials Engineering School of Engineering[a] and Graz University of Technology particularly Institute of Material Science and Welding (IWS)[b].
In Graz, basic optimization of the welding parameters of the joint by means of basic metallography, measurement of hardness as well as cross tension test were conducted. The detailed microscopy investigations of joint was done at the University of Tokyo.

1.1 The Flow in Graz

The project started in Graz with a literature study (see Figure ??) to become acquainted with the friction stir welding process and the basic characteristics of the magnesium alloy and the steel. Based on the welding parameters from the literature studies the pretest period started. Through the pretest period focus was on getting a feeling for the process and the material. During this period the common friction stir welding parameters were tested and the influence of the rolling direction of the magnesium sheet and the clamping distance was investigated. The next step was the optimization of the welding joint. This took place in the experiment period where the strength of the joint the bottom line was. During this period the heat input was varied through the welding parameters. The influence of the heat input on the welding joint was investigated by cross tensile tests, basic light microscopy and

---

[a]The University of Tokyo, Department of Materials Engineering School of Engineering: http://www.material.t.u-tokyo.ac.jp/

[b]Graz University of Technology,Institute of Material Science and Welding: http://www.iws.tugraz.at/

scanning electron microscopy (SEM) of the cross section. Sometimes it was necessary to do a step backwards because new possible influences on the joint were founded. Further, the measurement of the temperature during the welding process was done in Graz.
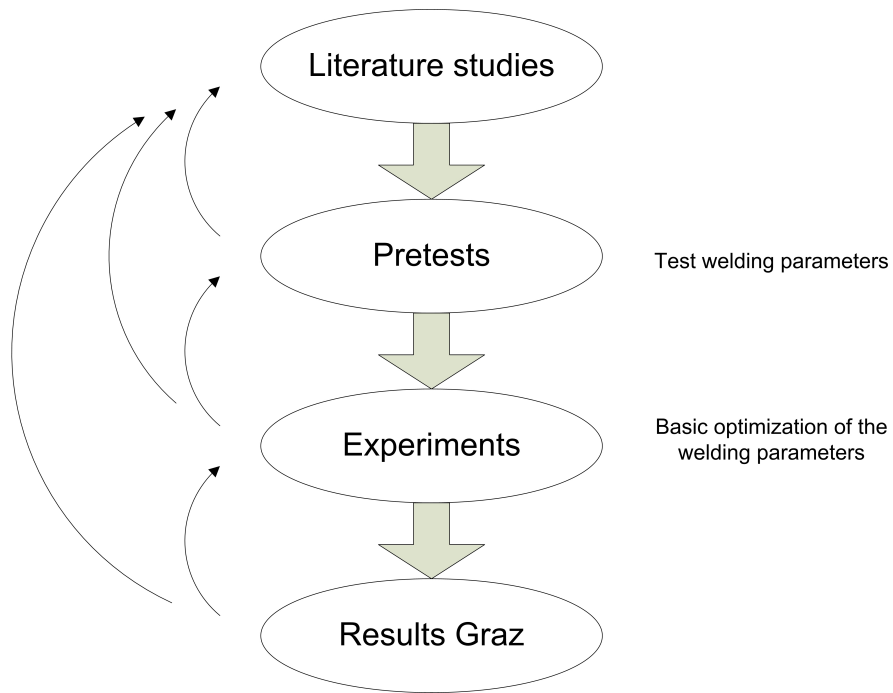

Figure 1.2: Flow of the diploma thesis in Graz

1.2 The Flow in Tokyo

During a stay of three month at Koseki/Inoue Laboratory at the University of Tokyo the interface and fracture path were investigated in detail. The samples were polished with different techniques and investigated by SEM, EDS and EDSB. The steel sheets for welding parameter study in Graz were zinc coated. The influence of the zinc on the microstructure was not investigated before. Due to that, some samples welded with the same welding parameters and base material but without the zinc coating were investigated as well. Because of the conducted temperature measurement and the known welding force from the experiments in Graz, all parameters for diffusion welding could be estimated. To get more information about the interface steel - magnesium, some samples were welded with diffusion welding with the estimated parameters from FSW.

1.3 Thesis Overview

Chapter 1 presents an introduction of this work.

Chapter 2 provides an introduction of the FSW process considering different parameters.

Chapter 3 provides an overview of the used materials.

Chapter 4 presents the parameter study and the temperature measurement during the friction stir welding process.

Chapter 5 presents the investigation of the interfaces, the fracture pathes and fracture morphologies.

Chapter 6 presents additional experiments and investigation, concatenating on the influence of the zinc coating.

Chapter 7 the work presented in this thesis is summarised and future directions of research are shared.

Appendix presents the sample preparation and additional figures.

2 Friction Stir Welding

Friction stir welding is a relatively new solid-state welding technique. In FSW, a rotating tool traverses along the joint seam of the material to be joined and accomplishes welding via mechanical stirring. It was invented at The Welding Institute (TWI) of UK in 1991 as a joining technique whereas aluminum alloys were the first applications [**?**].

The fundamental operation can be explained clearly with reference to Figure **??**. The FSW tool rotates about the Z axis and the pin (or probe) plunges into the material. The shoulder of the tool applies force to the top of the material. The friction between the rotating shoulder of the tool and the material generates the major heat input which softens the material. The tool traverses along the weld line, and the rotating tool probe drags the plasticized material to the back of the probe. In figure **??** the left side is the retreating side and the right side the advancing side. On the retreating side the velocity between tool and material is higher than on the advancing side. Therefore different heat generation and different material flow can be observed leading to different microstructures.

FSW has been verified to be appropriate to a number of joint types, including butt (demonstrated in Figure **??**), lap-, T-joints etc.. Lap welds, the subject of this research, occur when two horizontal members are placed on top of one another. The tool is plunged completely through the top member and partly into the bottom member and traversed along the blind joint seam.

2.1 Process Parameters

Processing parameters for friction stir welding includs welding velocity, tool rotation, tool attitude (tilt angle), plunge depth and welding forces will be explained here. Alternatively to welding velocity are welding speed, traversing rate or traversing speed. The direction of rotation, clockwise or counter-clockwise, is described when observing the tool from above. The force parallel to the rotational axis (or Z axis) is the down force or axial force. The force parallel to the travel axis (X direction) is the traversing force. In the same plane and orthogonal to the traversing force is the side or lateral force. The welding energy per unit length is the ratio between tool rotation, the syntonized torque and
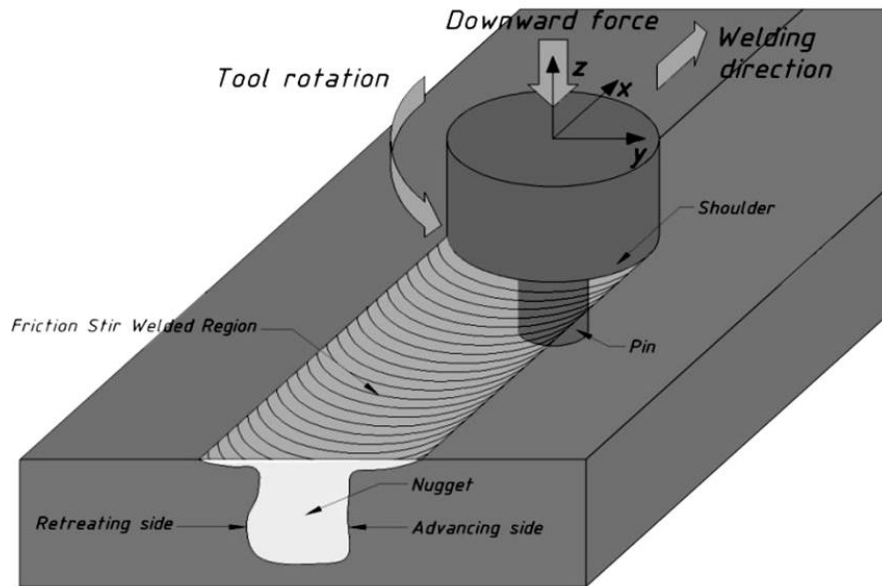
Figure 2.1: Friction stir welding process, source: IWS

welding velocity.

$$E = T * \frac{2 * \pi * n}{v} \tag{2.1}$$

The number T denotes the torque at the spindle axis, n the tool rotation and v the welding speed. Another, very important welding parameter is the plunge depth. The tool plunges through the top sheet into the bottom sheet. The plunge depth is the distance which the tool dips into the material.

2.2 Tool

The shape, material, and structure of the FSW tool is defined by the work piece material as well as rotation and traversing speed. The geometry of the pin could be cylindrical, square or conical and different threads may be machined into the pin to improve the material flow, to influence the process forces and prevent different weld defects. Different tool materials are used (mild steel, stainless steel, armour steel, high carbon steel, high speed steel, tungsten carbide and so on) [**?**]. The main parameter for the heat input are the shoulder diameter as well as the tool rotation.

The tool has two different functions: localized heating, and (b) material flow. At the beginning, heat is generated by friction between the pin and the work piece. The material deformation produces an additional heating. If the shoulder touches the work piece, the shoulder is the major heat generator. The second function of the tool is to stir and to move the material. The design of the tool has an big

influence on the process loads and the material flow.

2.3 Lap Configuration [?]

Figure **??** shows T- joint which is a special type of lap configuration. For a lap configuration sheets overlap and the FSW - tool plunge through the top sheet into the bottom sheet where the interface pulls up adjacent to the nugget. This pull ups are called tears, upturns or clamps and are of fundamental importance. One effect of this pull ups is, that the effective sheet thickness of the weld is reduced. This pull ups are the reason for a notch effect at the interface.

If the hardness of the materials is about the same, some pull downs will be at the interface (see figure **??**) which reduces the effective sheet thickness. For harder material as bottom sheet, the effect of the pull downs is not so critical.
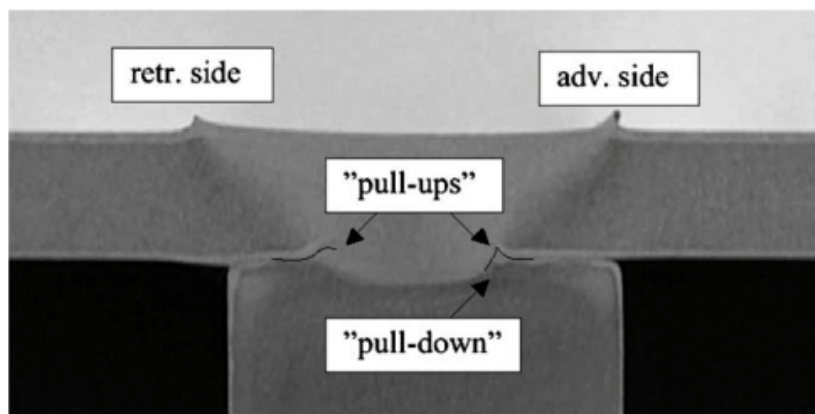

Figure 2.2: Cross-section of a T - joint with similar materials

2.4 Weld Zones

Friction stir welding is a process which involves complex interactions between a multiplicity of simultaneous thermomechanical processes. Figure **??** shows a cross section of a friction stir welding joint. The joint consists of four different zones, the base metal, the heat-affected zone (HAZ), the thermomechanically affected zone (TMAZ) and the stirred (nugget) zone. The central nugget region is the one which experiences the most deformation because a (threaded) tool deposits material from the front to the back of the pin. Sometimes in the cross section of the nugget region "onion rings" are observed [**?**]. The nugget size is significantly larger than the pin size.

The heat-affected zone (HAZ) is similar to that in conventional fusion welds but varies not in temperature so significantly. The main difference between the friction stir HAZ and the conventional welds HAZ is the temperature. In the friction stir HAZ the maximum temperature is significantly lower than the solidus temperature. This can be the reason for different microstructures when compared with fusion welding processes. The thermomechanically affected zone (TMAZ) lies between the HAZ [**?**] and nugget and experiences both temperature and deformation during FSW. The grains around the nugget were deformed in flowing pattern.

Figure 2.3: Cross-section of a AZ31 welded by FSW: (a) stirred (nugget) zone, (b) thermomechanically affected zone, (c) heat-affected zone and (d) base material [**?**]

2.5 Friction Stir Welding Process

Figure **??** shows a chronological sequence of a friction stir weld run. The red line displays the position of the tool, the green line the down force and the blue line the spindle rotation. First of all the tool moves to the surface of the top sheet and touches it (1). If the down force reaches 1 kN the spindle starts to rotate (2) and the tool plunge into the top sheet. At the beginning the pin plunges into the material and later the shoulder plunges into the material. The shoulder diameter is larger than the the pin diameter and this is the reason why the forge force is lower (3) at the beginning and increase when

the tool is plunging in the bottom layer (4). At the moment it is only a spot weld. The tool starts to move through the material and produce a weld seam. At the end position of the weld seam, the tool is pulled out of the material and shortly after the spindle stops.
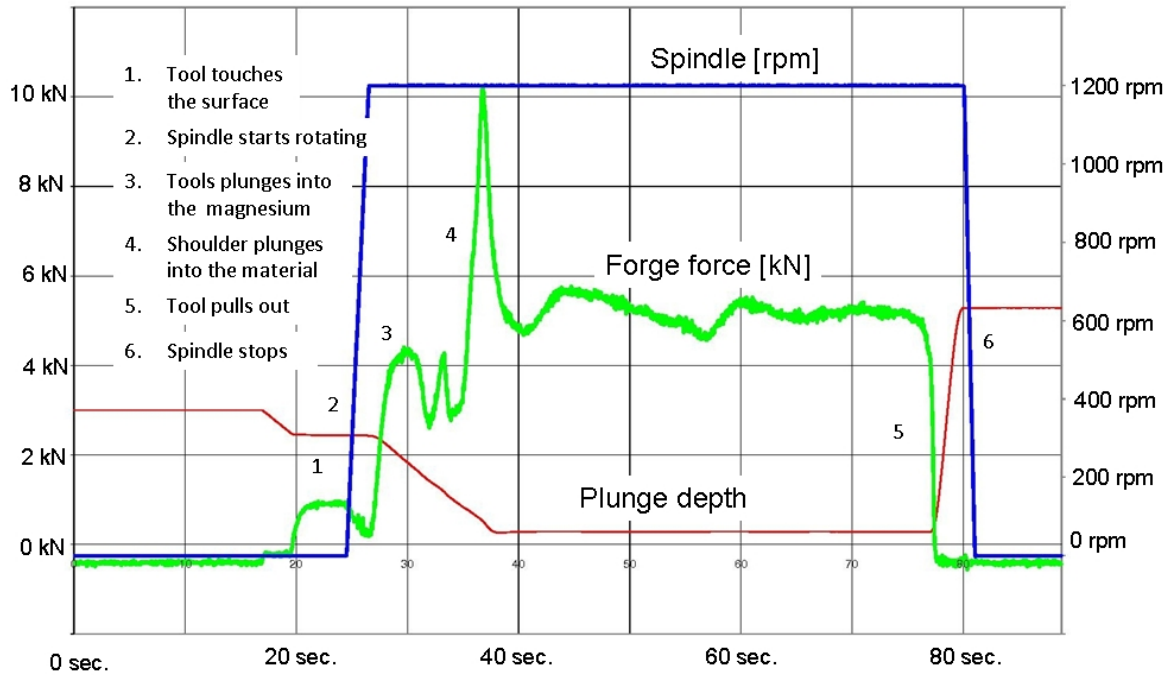

Figure 2.4: Friction stir welding prozess

2.6 Used Machine, Tool and Fixture

The friction stir welding machine used for this experiment is MTS ISTIR BR4 manufactured by MTS Systems Corporation located at the welding lab in Graz. The machine is fully automated, provids 4 degrees of control in the X, Y, and Z directions in addition to rotational speed control. The tool is rotating about the Z axis and the machine head traverse in X and Z directions. The machine table moves in X direction. The FSW machine is controlled by a computer, allowing for accurate data collection and varying of parameters. In table **??** specifications of the welding machine are listed.

The tool used in the present study was a tool with an exchangeable pin. The shaft material was a tool steel H13 and the pin consists of 75% tungsten and 25% rhenium. The shoulder had a diameter of 12.7 mm and the underside was scrolled. The pin length was 2.1 mm and the pin had a square shape (3.3 mm x 3.3 mm).

The fixture during the friction stir welding process it is very important. Especially in the lap joint

Table 2.1: Specifications of FSW machine

Max. Welding velocity	6.4 m/min
Max. Tool Rotation	3200 rpm
Max. Torque of Spindle	180 Nm
Max. Down force	35.6 kN

configuration of thin sheets it is necessary to apply a very low distance between clamping. If the distance of clamping is too large the upper plate deforms and the material flow between the plates. The result is a bad quality join or even no join. This effect is stronger the thinner the plates are. The pneumatic fixture used in the present study is show in figure **??**. The fixture consists of four pneumatic cylinders which can be actuated with a maximal air pressure of 10 bar, actuated with 6 bar which leads to a clamping force per terminal strip of 3.7 kN.
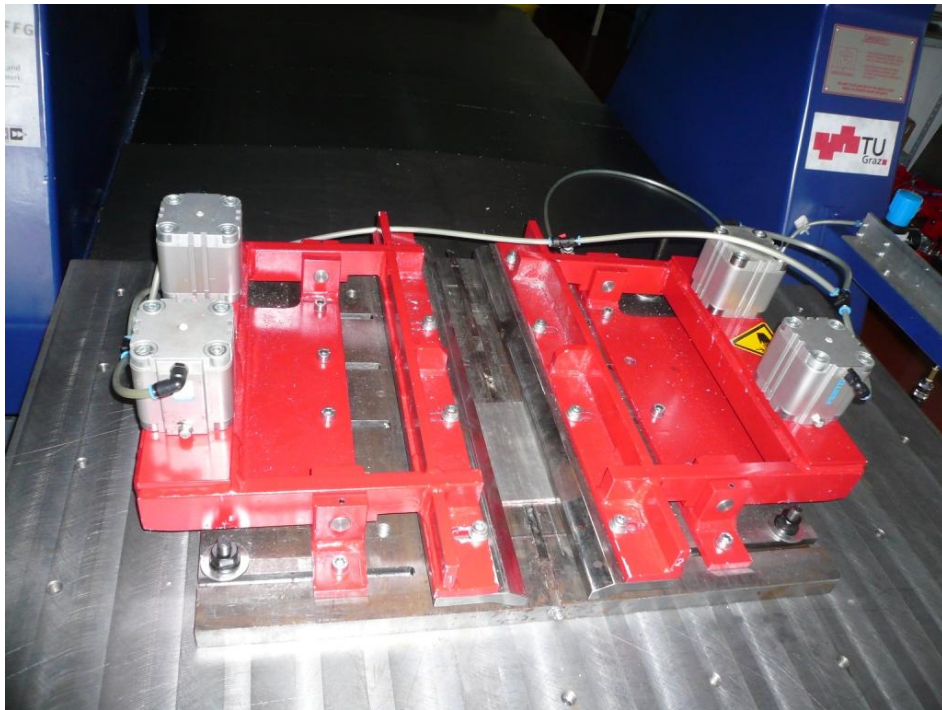

Figure 2.5: Pneumatic Fixture at IWS

3 Materials

During this diploma thesis the focus was on joining an IF-steel and a magnesium alloy.

3.1 Magnesium

3.1.1 Element Magnesium

Magnesium is the eighth most abundant element in the earth's surface by mass and ninth in the Universe as a whole. It belongs to Group 2 of the periodic table along with other elements like Calcium (Ca), Beryllium (Be), Strontium (Sr), Barium (Ba) and Radium (Ra). These elements are called alkaline Earth metals. Magnesium has the symbol Mg and the atomic number 12. It's found in sea water, brines and magnesiumbearing minerals which offer almost unlimited reserves.

The most widely used method for the extraction of magnesium is based on the electrolysis of magnesium chloride obtained from the seawater. Magnesium (1.74 g/cm^3) metal has two thirds the density of aluminum (2.7g/cm^3), a very low melting point (650 °C), it is castable and its alloys can be joined and welded [**?**]. The industry usage of magnesium alloys increased extreamly the past years.

Magnesium has a hexagonal close-packed (hcp) (see figure **??** crystal structure. The hexagon at the top and the bottom of the unit cell consist of seven atoms. Six atoms form regular hexagons and surround a single atom in the center. Another plane is situated between the top and bottom plane with three additional atoms.

Deformation of magnesium at low temperatures occurs by slip and twinning. Slipping takes place on definite slip planes and along slip directions. A slip plane is characterized by the greatest atomic density while the slip direction is the closest packed direction within the slip plane. The combination of the slip plane and the slip direction is termed the slip system. At low temperature the main deformation takes place at the slip plane 0001 with three slip directions. To achieve a deformation without cracking, five independent slip or twinning systems are required [**?**]. Hcp crystal structure has two other slip planes but these planes are twinning. Twinning is of importance for materials where deformation by slip is difficult whereas a hcp crystal structure material has a low tendency to twinning. Due
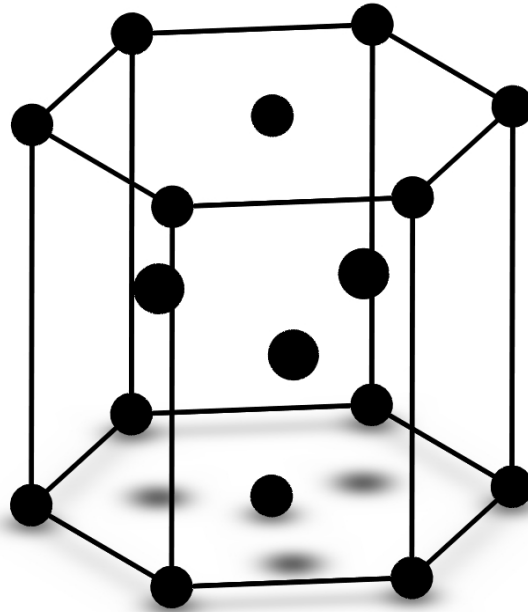
Figure 3.1: Hexagonal close-packed (hcp) unit cell

to its hcp structure, magnesium shows a very limited forming ability at room temperature [**?**]. Alloying elements or increasing the temperature can produce more than one additional slip plane. Table **??** shows different physical properties of magnesium.

The oxide layer of magnesium metals is not closed which is the reason why magnesium does not have a high resistant to corrosion as aluminum. Magnesium in finely divided form is readily ignitable and can ignite spontaneously in the presence of water or cutting fluids containing fatty acids. Smoking and the use of open flame or electrical welding must be forbidden in areas where magnesium is being machined or sawed. In case of a fire, water must not be used because the water will dissociate into oxygen and hydrogen, accelerating the fire and creating an explosion hazard.

Table 3.1: Physical properties of magnesium [**?**]

Standard atomic weight	24.31 g/mol
Atomic radius	160 pm
Density (near r.t.)	1.74 g/cm^3
Melting point	650 °C
Boiling point	1090 °C
Crystal structure	hcp
Thermal conductivity	156 W/(mK)
Thermal expansion	24.8 μm/(mK)
Young's modulus	44.8 GPa
Shear modulus	16.6 GPa

3.1.2 Friction Stir Welding of Magnesium

Welding of magnesium is considered as being difficult because of the porosity formation during in the weld. The large coefficient of expansion of magnesium alloys effects large deformation and distortions of the weld. Friction stir welding is a solid state welding process with low temperature and therfore lower distortions. This is the reason why friction stir welding the best choice for magnesium alloys is [**?**]. Table **??** shows the welding parameters for different similar and dissimilar FSW welds. The tool rotation varied from 475 rpm to 2500 rpm and the welding speed is between 45 mm/min to 2000 mm/min for butt weld configuration. For lap weld configuration the tool rotation is 1500 rpm and the welding speed between 20 mm/min and 300 mm/min.

Table 3.2: FSW parameters for different magnesium alloys

Material 1	Material 2	Thickness [mm]	Configuration	Tool rotation [rpm]	Welding speed [mm/min]	Reference
AZ31-O	AZ31-O	2	butt	2000	600	[?]
AZ31	AZ31	2	butt	700 - 1400	600 - 2000	[?]
AZ31	AZ31	5	butt	1000	40 - 600	[?]
AZ31	AZ31	6.3	butt	800	100	[?]
AZ31	Al1050	5	butt	2450	90	[?]
AZ31	AA6040Al	1.5	butt	1400	105	[?]
AZ31B	Ti	2	butt	850	50	[?]
AZ31B-O	A5052P-O	2	butt	800 - 1600	300	[?]
AZ31	low carbon steel	1.6 /0.8	lap	1500	100 - 300	[?]
AZ31	AC4C	3 /2.5	lap	1500	20 - 80	[?]
AZ31B-H24	AZ31B-H24	2	butt	2000	300 - 1800	[?]
AZ31B-H24	AZ31B-H24	4.88	butt	1000	120	[?]
AZ31B-H24	AZ91B	2	butt	800	90	[?]
AZ31B-H24	AM60B	2	butt	800	90	[?]
AZ31B-H24	Al2040-T3	4.88	butt	2500	45	[?]
AZ31B-H24	Al6061-T6	2	butt	800	90	[?]
AZ61	AZ61	2.5	butt	475	75	[?]
AZ61A	Ti	2	butt	850	50	[?]
AM60B	Al6061-T6	2	butt	800	90	[?]
AZ91B	AM60B	2	butt	800	90	[?]
AZ91B	Al6061-T6	2	butt	800	90	[?]
AZ91D	Ti	2	butt	850	50	[?]

3.1.3 AZ31B-O

Magnesium AZ31B-O is a wrought alloy which is used in the automobile industry. AZ31B-O is a standard designation according to ASTM - standard. The letters A and Z represents the alloying elements aluminum and zinc in accordance with ASTM A 275 [**?**] and the numbers 3 and 1 represents the content of aluminum and zinc. AZ31 is made up 3% aluminum and 1%zinc. The letter B stands for the impurity level of alloying elements. Table **??** shows the alloy contents which are allowed in the impurity level B and the actual alloy content of the used magnesium sheets investigated by Salzgitter Magnesium, Germany[a]. The last character is a symbol for temper designation in accordance with ASTM B 296 [**?**]. O is a character for annealed. The standard designation of AZ31 in DIN 1729 [**?**] is $MgAl_3Zn_1$ with the material number of 3.5312. The used, hot rolled AZ31B-0 magnesium sheets was produced by Salzgitter Magnesium.

Table 3.3: Impurity level B for AZ31B [**?**] and actual alloy content (Salzgitter)

Elements	Al	Zn	Mn	Si	Cu	Ni	Fe	Ca	Other
Min.%	2.5	0.6	0.2						
Max.%	3.5	1.4	1	0.1	0.05	0.005	0.005	0.04	0.3
Actual%	3.11	0.94	0.43	0.004	<0.01	0.001	0.028		

3.1.4 The ternary alloy

Figure **??** shows a ternary alloy phase diagram of Mg - Al - Zn- at 1 wt.% Zn with four different phases.

The ϕ phase is a tertiary phase because it consists of magnesium, aluminum and zinc.

The γ phase is a binary phase which is $Mg_{17}Al_{12}$. The other phases are the liquid phase and (Mg)-phase.

Melting temperature of AZ31B - O (3wt.% of aluminum) is at about 630 °C. The diagram shows between 630 °C and about 550 °C a two phase region which consists of the liquid and (Mg) phase. Below 550 °C and above 220 °C it is a one phase field which consists of the (Mg) - phase. In the diagram between 220 °C and 100 °C a two phase region appears which consists of (MG) - phase and the γ phase. Below 110 °C is a three phase region with the γ, (Mg) and the ϕ - phase. At room temperature the AZ31B-O consists of (Mg), γ and ϕ phase in equilibrium state after slow cooling.

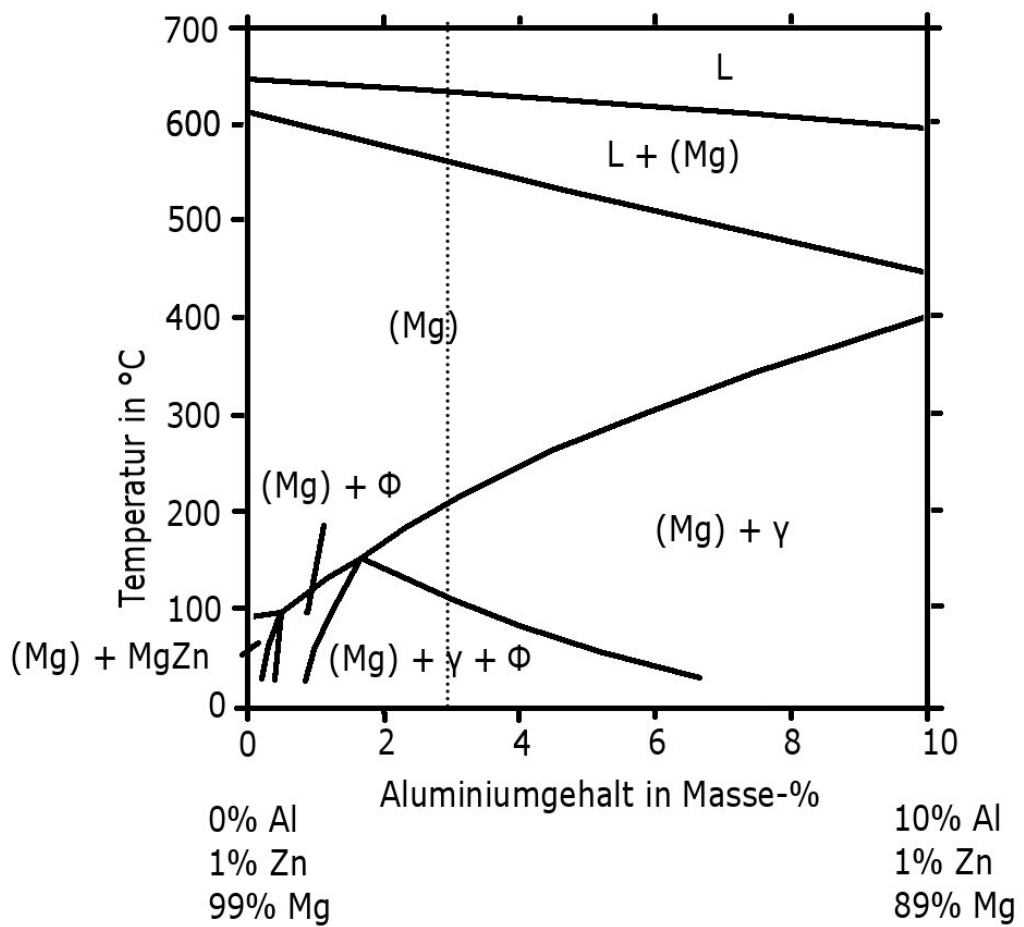[a]Salzgitter Magnesium-Technologie GmbH,Eisenhüttenstr. 99, 38239 Salzgitter, Germany

Figure 3.2: Phase diagram [**?**]

3.2 Steel

Deep drawing steel was chosen because of the application for automobiles. This steel is an interstitial free (IF) steel.

> *"The interstitial is an atom occupying an interstitial site not normally occupied by an atom in the perfect crystal structure or an extra atom inserted into the perfect crystal structure such that two atoms occupy positions close to a singly occupied atomic site in the perfect structure." [?]*

This interstitial atoms are hydrogen, nitrogen, oxygen or carbon atoms which are small enough to fit into the interstitial positions [?]. It is particularly important to control the precipitate characteristics because they have a strong influence on the properties. Precipitations hinder the locations in moving which reduce the formability. Deep drawing steels should have a high formability and deep drawability and that is the reason why they should be an IF steel. IF steels are ultra low carbon (<6 mass ppm) steels manufactured by adding carbide, nitride and sulphide forming elements such as titanium and/or niobium [?].

The used steel is DX54D+Z 150 produced by voestalpine[b] for cold forming according to DIN EN 10327 [?]. The sheets were hot dip zinc coated with a zinc layer thickness of 7 to 15 μm. Table **??** show the chemical composition and table **??** the mechanical properties of the sheets used in this study. Rp_{02} is the lowest stress at elongation of 0.2% with the unit Megapascal (MPa). Rm displays the tensile strength which is the maximum stress in a stress - strain curve. Ag is the elongation before necking starts in percent. A80 is the elongation at fracture in percent. The value 80 indicates is the gauge length of 80 mm.

Table 3.4: Chemical composition of DX54D (Voest Alpine)

Elements	C	Si	Mn	P	Cu	Al	S	Cr	Mo	Cu
wt.%	0.0017	0.006	0.12	0.0075	0.0098	0.045	0.0098	0.021	0.001	0.02
max. wt.%	0.12	0.5	0.6	0.1	-	-	0.045	-	-	-
Elements	Ni	Nb	Ti	V	B	N				
wt.%	0.01	0.002	0.065	0.002	0.0002	0.003				
max.%	-	-	0.3	-	-	-				

---

[b]Voest Alpine Stahl GmbH, voestalpine-Straße 3, 4020 Linz, Austria

Table 3.5: Mechanical properties of DX54D (Voest Alpine)

	Rp$_{02}$	Rm	Ag	A80
Unit	MPa	MPa	%	%
	168	286	23.8	46.5

3.3 Binary Systems

To weld two different metals without any filler metal together, solid solubility is desirable. The result of solid solubility is mixed crystals. Three different conditions are essential for formation mixed crystals [?]:

- same crystal lattice

- ratio of atomic radius < 14%

- chemically similar

Table ?? shows the physical properties of magnesium and iron. The melting temperatures (iron - 1536 °C, magenesium - 650 °C) and crystal structures (iron - bcc, magnesium - hcp) are totally different.

Table 3.6: Physical properties of magnesium [?] and iron [?]

Elements	Magnesium	Iron
Atomic radius	160 pm	140 pm
Melting point	650 °C	1536 °C
Crystal structure	hcp	bcc
Thermal expansion	24.8 μm/(mK)	12.2 μm/(mK)
Thermal conductivity	156 W/(mK)	80.2 W/(mk)

3.3.1 Magnesium - Iron

The crystal structure of magnesium is hexagonal close-packed (hcp) and the iron has a body center cubic structure (bcc). Magnesium and iron have totally different melting points. Magnesium melts at about 923K (650 °C) and iron at 1536 °C. The magnesium - iron binary alloy phase diagram (Figure ??) shows an eutectic phase diagram with an eutectic temperature of 650 °C. The maximum

solid solubility of iron in magnesium is 0.00043 at.%. Cooling of a Mg - Fe alloy containing more than 0.008 at.% magnesium, of the melt, the phase diagram illustrates that the liquid Mg alloy undergoes eutectic solidification at 650 °C to form (Mg) containing 0.00043 at.% iron in solid solution plus the BCC -phase.
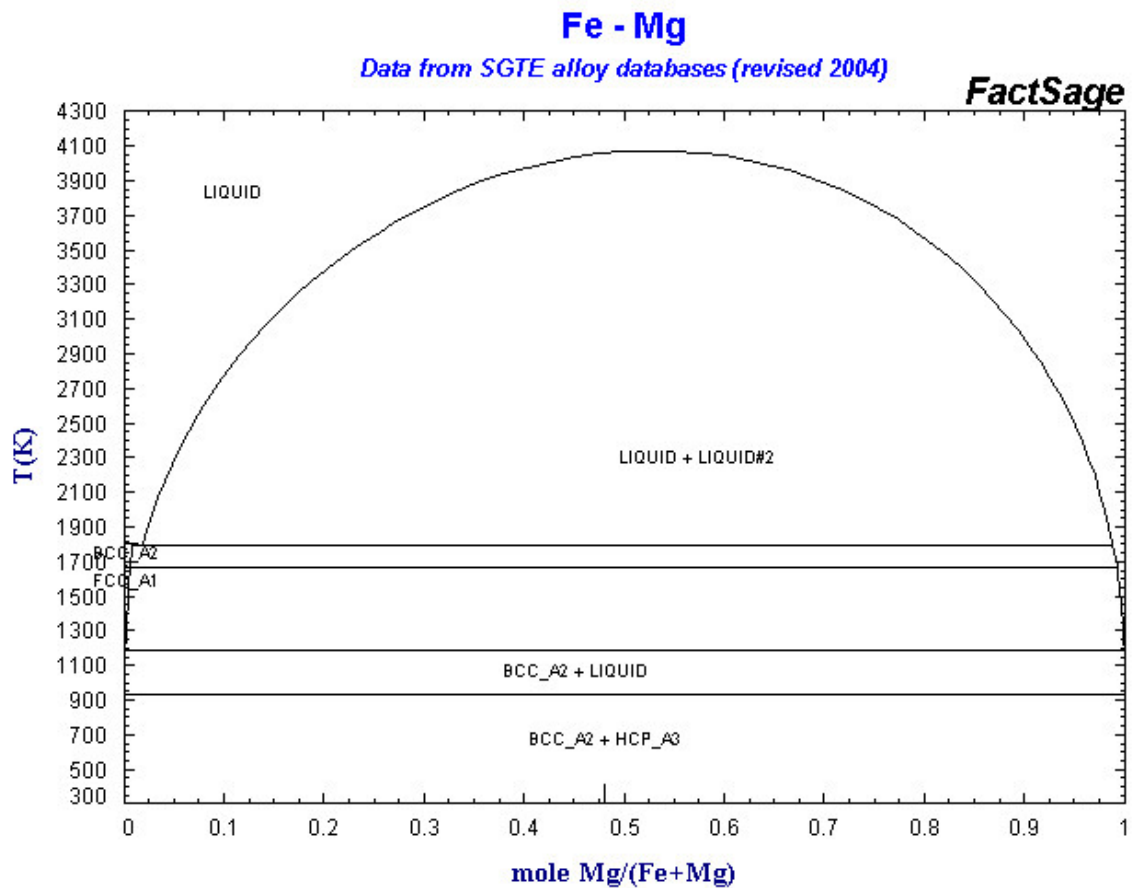
Figure 3.3: Phase diagram Fe - Mg [?]

3.3.2 Magnesium - Zinc

The crystal structure of zinc and magnesium is hexagonal close-packed. The melting point of zinc is 420 °C and for Magnesium 650 °C. The binary alloy phase diagram of magnesium and zinc (Figure ??) shows eutectic and peritectic points. The melting temperature of the eutectic on the magnesium rich side is 340 °C and on the zinc rich side 419 °C. Figure ?? shows, that the solubility of magnesium in zinc is low (0.4 at.%). On the other hand the solubility of zinc in magnesium is 2.4 at.%. Between the magnesium rich side and zinc rich side is the phase $MgZn_2$ (C14) which is a Laves phase. Laves

phases are intermetallic phases which has a close packed structure from A and B atoms with the ideal ratio of radii.
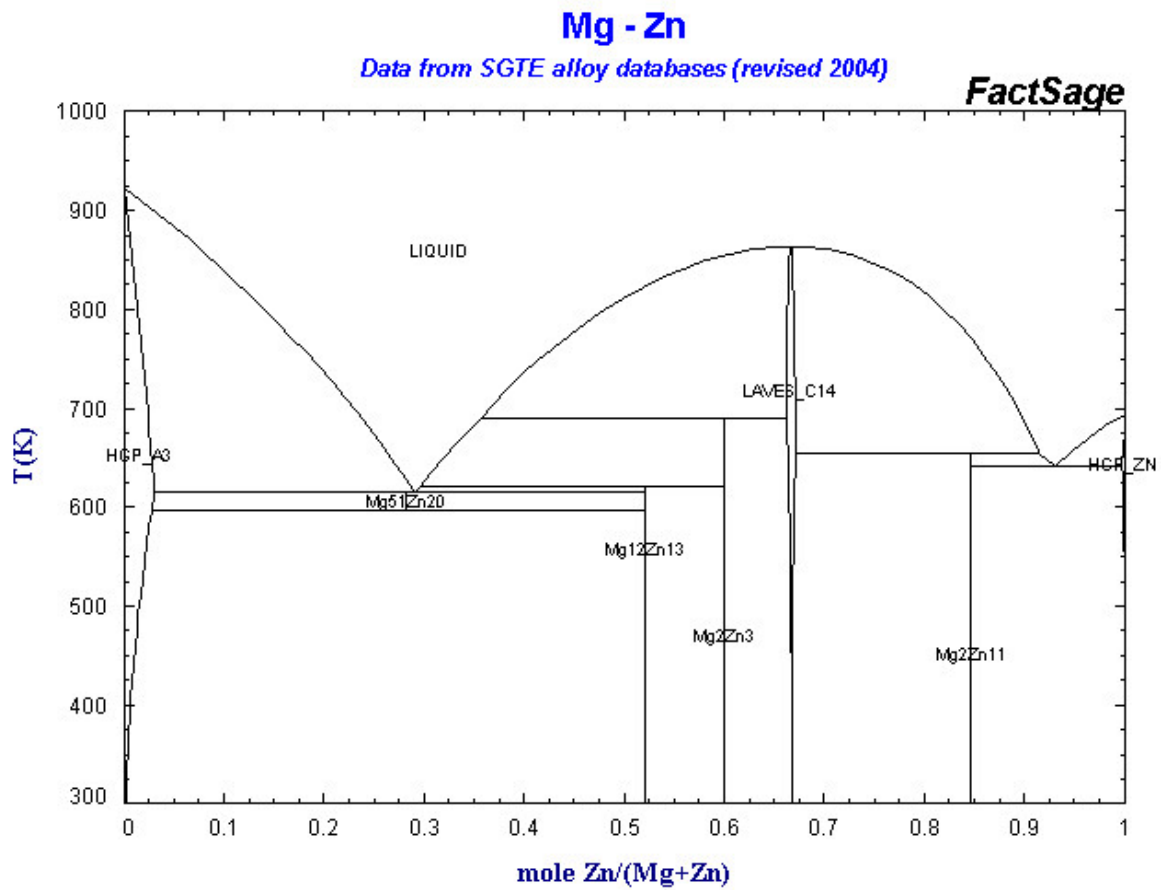
Figure 3.4: Phase diagram Mg - Zn [**?**]

4 Experimental procedure

The sheets used in this study were quadratic with a length of 150mm and 2 mm thick (Figure **??**) and were welded in lap joint configuration using FSW. The top sheet was magnesium and the bottom sheet of the weld joint was made of steel. The sheets overlapped 65 mm and the total weld length was 125 mm. Before the welding all sheets were sprayed with ethanol and cleaned with a cleaning cloth.
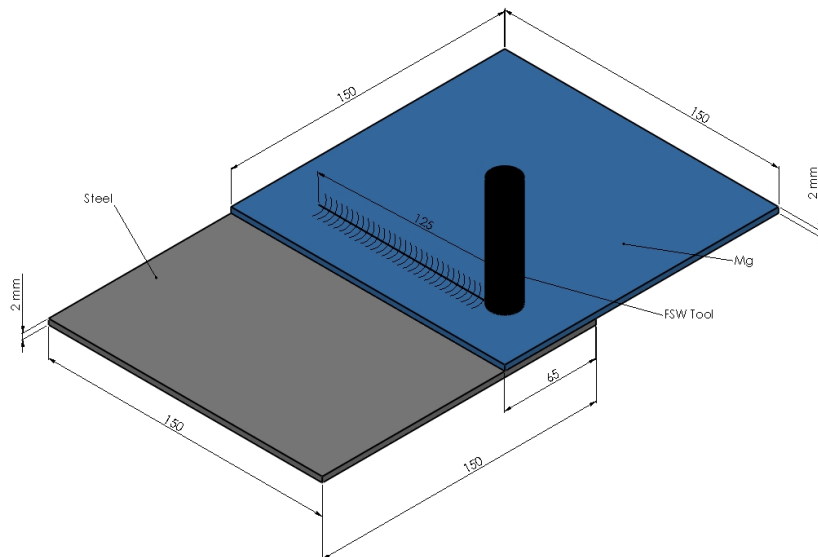
Figure 4.1: Joint configuration

4.1 Parameter Study

There are many different parameters from the friction stir welding process, the material and the clamping situation which have influence on the quality of the joint. To weld sound seams it is necessary to find a good parameter mix. Figure **??** and table **??** shows the different welding parameters and the range were the parameter study was done.

In this investigation the tilt angle was set to zero degree. This angle was defined through the tool which was used.

Table 4.1: Welding Parameters Range

Welding parameters	
Tool rotation r	900 to 1200 rpm
Plunge depth t	-0.05 to -0.2 mm
Welding speed v	150 to 1000 mm/min
Tilt angle α	0 °
Control system	Forge Force Controlled - Plunge Depth Controlled
Material	
Direction of rolling AZ31B-0	Welding normal or in direction of rolling
Clamping Situation	
Clamping distance δ	40 to 120 mm
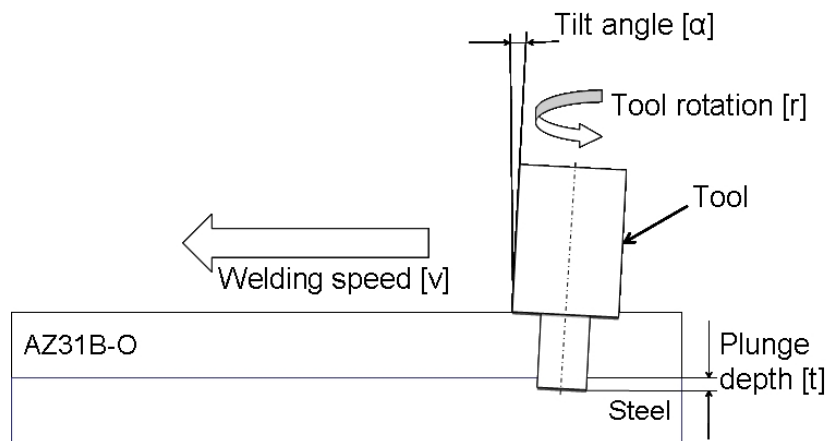
Figure 4.2: Welding parameters

Every parameter study needs a starting point. Chen et al. [**?**] studied the effect of tool geometry on microstructure and mechanical properties of friction stir lap welded magnesium alloy and steel. They used a AZ31 magnesium alloy for their investigation with a thickness of 1.6 mm and a zinc coated low carbon steel with a thickness of 0.8 mm. They suggested a tool rotation speed of 25 rad per second (about 238 rpm) and a welding speed of 1.67 mm/s to 5 mm/s (about 100 mm/min to 300 mm/min) and their upsetting force was 3.92 kN. It was impossible to weld with these parameters. The friction stir welding engine at IWS stopped because the upsetting force reached the maximum of 35 kN (see figure **??**).

Tool rotation for welding AZ31 magnesium alloy between 500 rpm [**?**] and 2000 rpm [**?**] were reported in other literature. With a tool rotation of 1200 rpm and a welding speed of 150 mm/min the
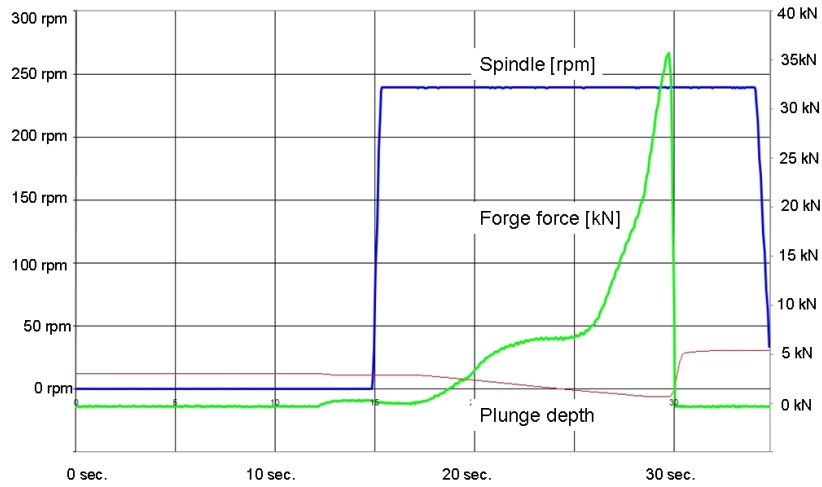
Figure 4.3: FSW - prozessdiagram with tool rotation 235 rpm

magnesium was weldable. The judgment was based on result of tensile tests. During the tensile test two different fracture pathes have been detected (figure **??**). Fracture location 1 displays the fracture in the stir zone and fracture location 2 shows the fracture in the joining interface (see figure **??** and **??**). Because of different fracture locations of the joint sheets and for a better comparison of the results following assumptions were made:

- The tensile stresses were calculated with the thickness of the base material and not with the effective sheet thickness (see **??**).

- Tensile stress = max. failure force per cross section area of the base material.
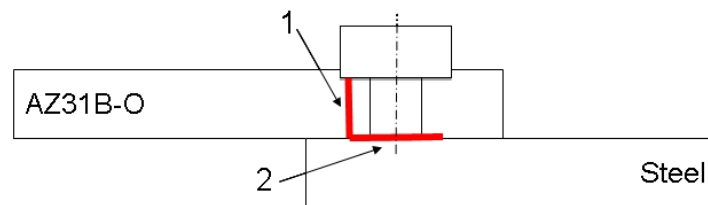
Figure 4.4: Fracture path: 1 at the stir zone, 2 at the joining interface
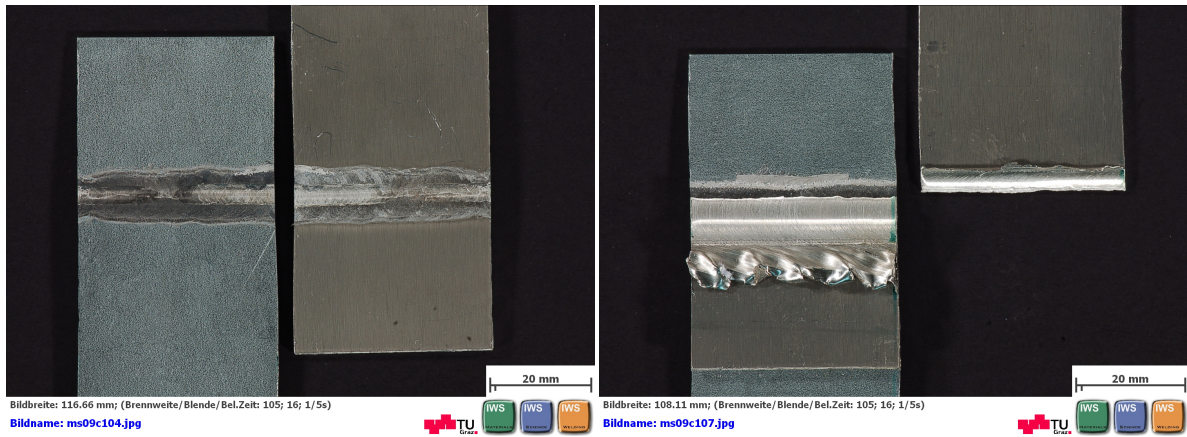
Figure 4.5: Fractured at the interface   Figure 4.6: Fractured at the stir zone

4.1.1 Variation of the Plunge Depth

Figure **??** shows the definition of the algebraic sign of the plunge depth. If the pin is in the steel sheet the algebraic sign is minus.
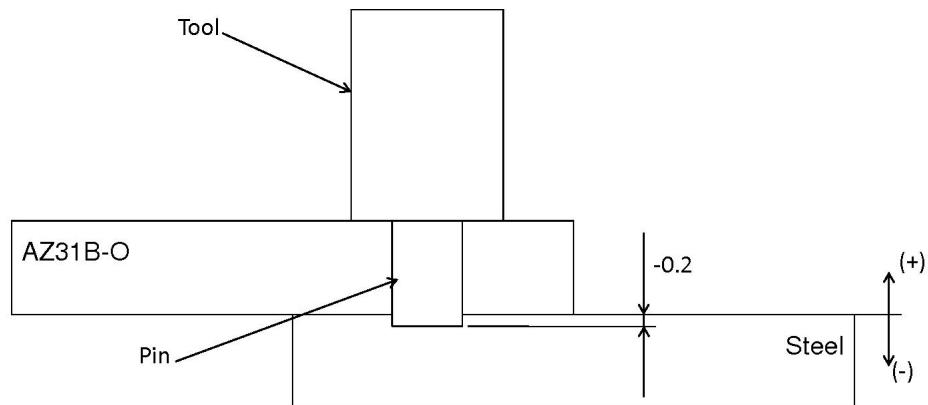
Figure 4.7: Definition of the algebraic sign for the plunge depth

Experiment:

The influence of the plunge depth on the tensile stress was investigated with the following welding parameters:

- **Plunge depth: -0.05 to -0.2 mm**

- Welding speed: 150 mm/min

- Tool rotation: 1200 rpm

- Distance of clamping: 40 mm

- Welding orthogonal to the direction of rolling

- Load on advancing side

- Displacement controlled

Result:

With a minor plunge depth into the steel (-0.05 to -0.1 mm) the specimen fractured at the joining interface (see Figure **??**) and with increasing plunge depth the specimen fractured at the stir zone. The tensile stress increases with increasing plunge depth (-0.05 to -0.15 mm) and reached a maximum at (−0.15mm). If the plunge depth increases more, the tensile stress decreases a little bit which is assumed to be caused by the decreasing effective sheet thickness. (The effective sheet thickness of the top sheet is the thickness of the base material minus the plunge depth of the shoulder.)

Discussion:

There are different influences on the plunge depth for example the tolerance of thickness of the metal sheet. For this reason the friction stir welding program has a touch loop (Figure **??**). During this touch loop the tool is not rotating. The tool moves very slowly to the surface of the top sheet and the pin touch the surface. If the machine measures a down force of 0.5 kN, the machine stops moving and set a reference point. This reference point is very important to guarantee always the same plunge depth of the tool shoulder in displacement controlled mode but through this touch loop the same plunge depth of the pin into the bottom sheet can not be guarantee.

For example, the pin length is 2.1 mm and the top sheet has a thickness of 2 mm and the desired plunge depth from the pin into the bottom sheet is 0.15 mm. The thickness tolerance of the top sheet (magnesium with 2 mm thickness) is ±0.1 mm[a]. The real plunge depth into the bottom layer as result of the tolerance of thickness is between 0.05 mm and 0.25 mm. To reduce the influence of the

---

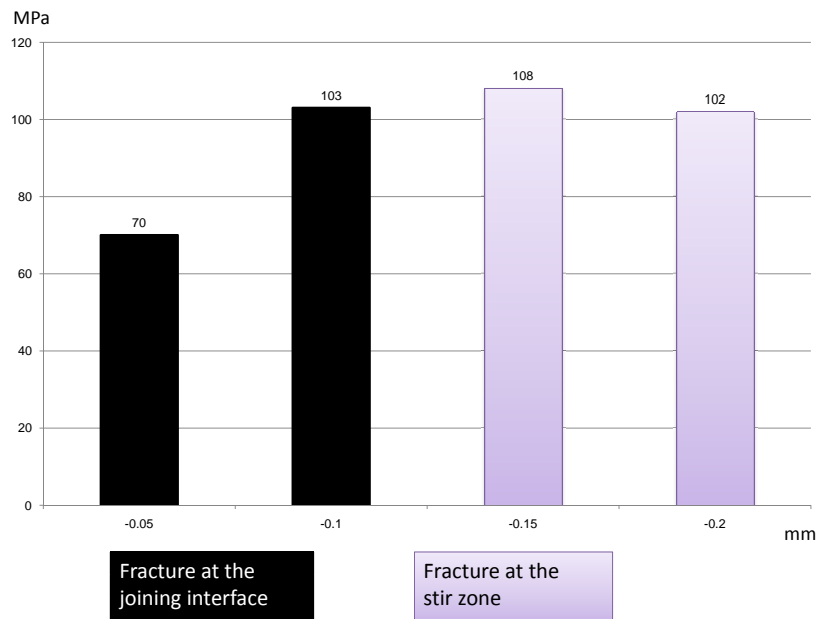[a]Salzgitter Magnesium-Technologie GmbH,Eisenhüttenstr. 99, 38239 Salzgitter, Germany

Figure 4.8: Plunge depth variation

tolerance of thickness all the sheets used during the investigation were cut out of one big sheet. The thickness of the sheets which were used was 2.00 mm.

Another influence on the plunge depth has the control systems of the friction stir welding machine. As well known, the forge force is combined with the plunge depth. That means, if the forge force increases, the plunge depth increases as well and if the forge force decreases, the plunge depth decreases too, but this happens always with some delay. Figure **??** shows a forge force - forge depth diagram over time. The red line displays the forge depth, the green line the forge force and the blue line displays the top and the bottom of the magnesium sheet. Is the pin of the tool in the magnesium (from 38 to 48 sec.) the forces are not as high as the pin is in the steel sheet (from 48 to 59 sec.).

For fast welding (1000mm/min), the tool makes an oscillating motion and the plunge depth varies from 0.108 mm to 0.178 mm. This effect decreases with decreasing welding speed. The plunge depth varied only 0.02 mm for a welding speed of 500 mm/min and for a welding speed of 150 mm/min the plunge depth varied 0.004 mm. A reason for this could be the slow control system of the friction stir welding machine or it is inertia.

Wear of the pin length has a big influence on the plunge depth of the shoulder in the top sheet but no influence on the plunge depth of the pin in the bottom sheet. The result of this is that the effective
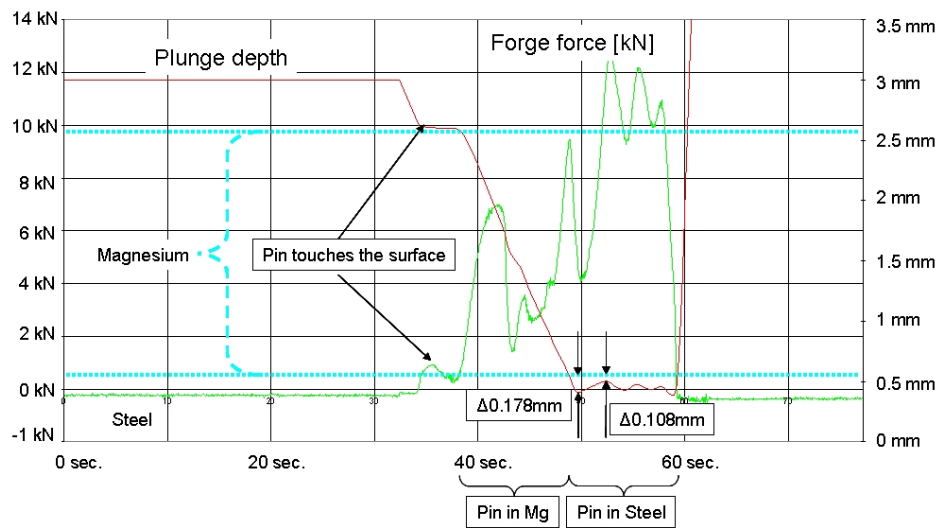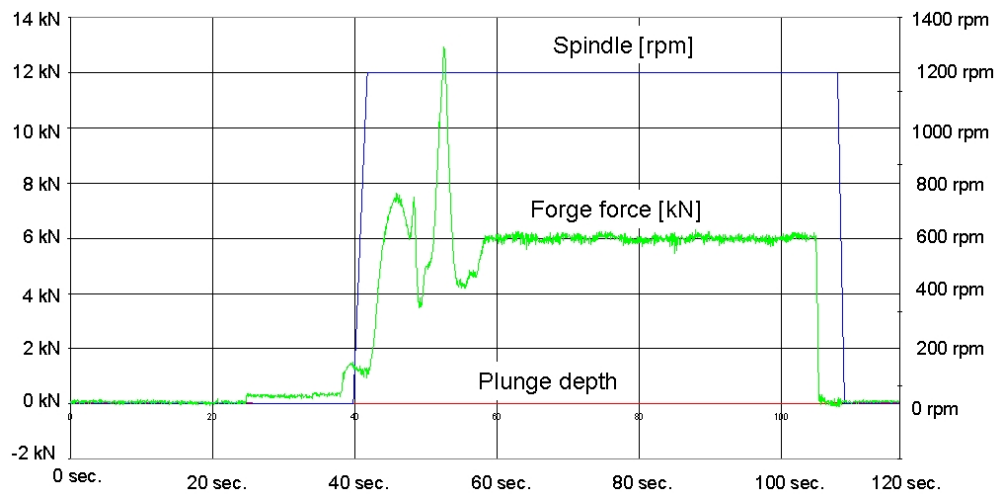
Figure 4.9: Forge force and forge depth - time diagram. Welding parameter: tool rotation: 1200 rpm, welding speed: 1000 mm/min, plunge depth: –0.15 mm, tilt angle 0 °, displacement controlled

sheet thickness of the top sheet decreases with increasing wear. The effective sheet thickness of the top sheet is the thickness of the base material minus the plunge depth of the shoulder.

4.1.2 Control System of the FSW

For welding with FSW, two different control systems are available:

- The plunge depth is defined and the forge force is an outcome (plunge depth controlled).

- The forge force is defined and the plunge depth is due to the forge force (forge force controlled).

For the investigation of the plunge depth, the plunge depth controlled control system was used. Chen et al. [?] studied the effect of tool geometry on microstructure and mechanical properties of friction stir lap welded magnesium alloy and steel. They reported a welding forge force of 3.92 kN. Figure ?? and figure ?? show that the forge force is not constant during the welding process. Figure ?? shows a forge force and forge depth - time diagram.

Except for the beginning of the welding, the forge force is fairly constant. Plunge depth controlled welding has an oscillating forge force and forge force controlled welding has an oscillating plunge depth. The influence of the plunge depth on the tensile strength is very big (see figure ??). As a result of this investigation, only the plunge depth controlled systems was used.

Figure 4.10: Forge force and forge depth - time diagram. Welding parameter: tool rotation: 1200 rpm, welding speed: 150 mm/min, forge force: 4 kN, tilt angle 0 °

4.1.3 Clamping Distance

The clamping distance is the distance between the right and left side of the fixture which press the sheets down (see figure **??**).

Experiment:

The influence of the clamping distance on the tensile stress was investigated with the following welding parameters:

- **Clamping distance: 40 to 125 mm**

- Plunge depth: -0.15 mm

- Welding speed: 150 mm/min

- Tool rotation: 1200 rpm

- Welding orthogonal to the rolling direction

- Load on advancing side

Result:

For the first experiment the clamping distance was 125 mm, the overlap was 150 mm and the tensile stress was could not be measured, because the probe split in the preparation for the tensile test.

In the second experiment the clamping distance was 40 mm and the tensile strength was 100 MPa and the fracture was at the joining interface.

Discussion:

As result of these experiments, all following welds had a clamping distance from 40 mm. If the clamping distance is too large, the material flows between the sheets and push the top sheet up. As Result of this, the pin plunges not the expected value into the bottom sheet.

4.1.4 Strength on Advancing or Retreating Side

For lap weld configuration, two different configurations are possible. These configuration are sometimes called right-handed and left handed lap [**?**]. At the right handed lap the load is on the retreating side and at the left handed lap the load is on the advancing side (see figure **??**. Reynolds et al. [**?**] reported a different tensile strength measured on advancing or retreating side for aluminum alloy 2024 and 7075.
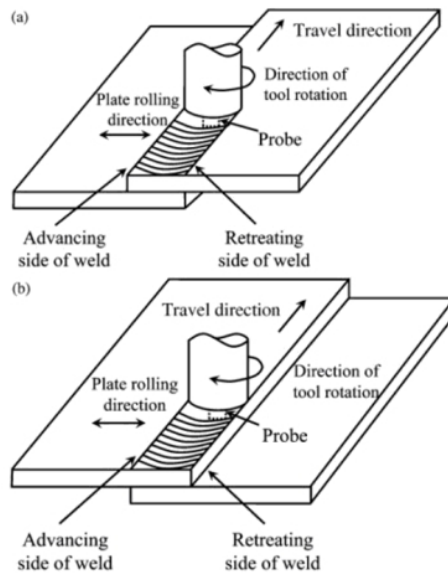
Figure 4.11: Lap weld configuration: a) left handed lap, b) right handed lap

Experiment:

The influence of strength on advancing or retreating side was investigated with the following welding parameters:

- **Strength on advancing or retreating**

- Plunge depth: -0.15 mm

- Welding speed: 150 mm/min

- Tool rotation: 1200 rpm

- Distance of clamping: 40 mm

- Welding orthogonal to the direction of rolling

Result:

The measured strength on the advancing side was 95 MPa and the strength on the retreating side was 87 MPa.

Discussion:

The difference is about 10%. This investigation was done only with one sample.

4.1.5 Welding Speed

The welding speed has a big influence on the energy input per unit length(see equation **??**). With increasing welding speed the energy input per unit length is decreasing and the process temperature decreases with increasing welding speed. Cao et al. [**?**] investigated the effect of welding speed on the quality of friction stir welded joints of a magnesium alloy. They report that the yield strength increases with increasing welding speed. The tensile strength increases first with increasing welding speed but remains constant from 15mm/s to 30mm/s (900mm/min to 1800mm/min).

Experiment:

The influence of the welding speed on the tensile strength was investigated with the following welding parameters:

- Welding speed: 150 to 1000 mm/min

- Plunge depth: -0.15 mm

- Tool rotation: 1200 rpm

- clamping distance: 40 mm

- Welding orthogonal to the direction of rolling

- Load on advancing side

- displacement controlled

Result:

Figure **??** shows the effect of welding speed on the tensile strength. The tensile stress increased with

increasing welding speed from 150 to 500 mm/min and the specimen fractured at the stir zone. With a higher welding speed the fracture path was at the interface and the tensile strength decreases and increases with a welding speed of 1000 mm/min. The highest tensile strength was reached with a welding speed of 500 mm/min. ***Discusion:***
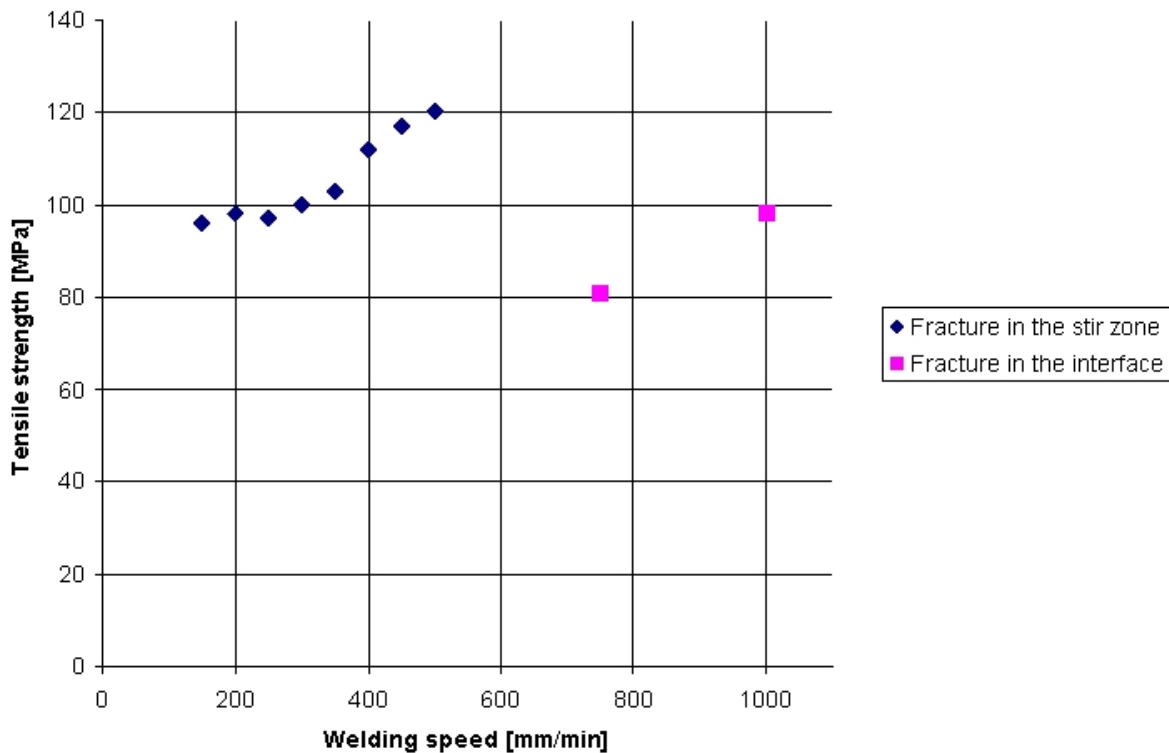
Figure 4.12: Effect of welding speed on tensile stress

With a welding speed higher than 500 mm/min the process got unstable and the plunge depth was not constant (see **??** Variation of the Plunge Depth). The reason for this instability is the control system of the friction stir welding machine because it is to slow to regulate the plunge depth. Figure **??** shows that with a higher welding speed the strength of the magnesium sheet increases. Midling et al. [**?**] investigated the effect of tool shoulder material on heat input during friction stir welding. Equation **??** shows energy input for friction stir welding.

$$Q = 4/3 * \Pi * \mu * F * n * R \qquad (4.1)$$

The number μ donates the friction coefficient (0.1[ ]), F the forge force [N], n the tool rotation (1200rpm) and R the shoulder diameter (12.7mm). The friction coefficient changes with changing temperature but for a simplification the coefficient is for all welding speeds the same. The tool diameter was for all joints the same. To compare the heat input per unit length, the forge force was

divided through the welding speed and multiplied with the tool rotation. Table **??** shows the welding speeds and the forge forces for the welding speed 1200 rpm. The last column displays the result of the simplified heat input per unit length. Figure **??** shows the energy input per unit length over the welding speed. The energy input per unit length decreases with increasing welding speed.

Table 4.2: Energy input per unit length for the tool rotation 1200rpm

Welding speed [mm/min]	Forge Force [kN]	Heat Input [J/mm]
150	5	106
200	5.3	85
250	5.6	71
300	6	64
350	6.5	59
400	7.2	57
450	7.6	54
500	8.2	52
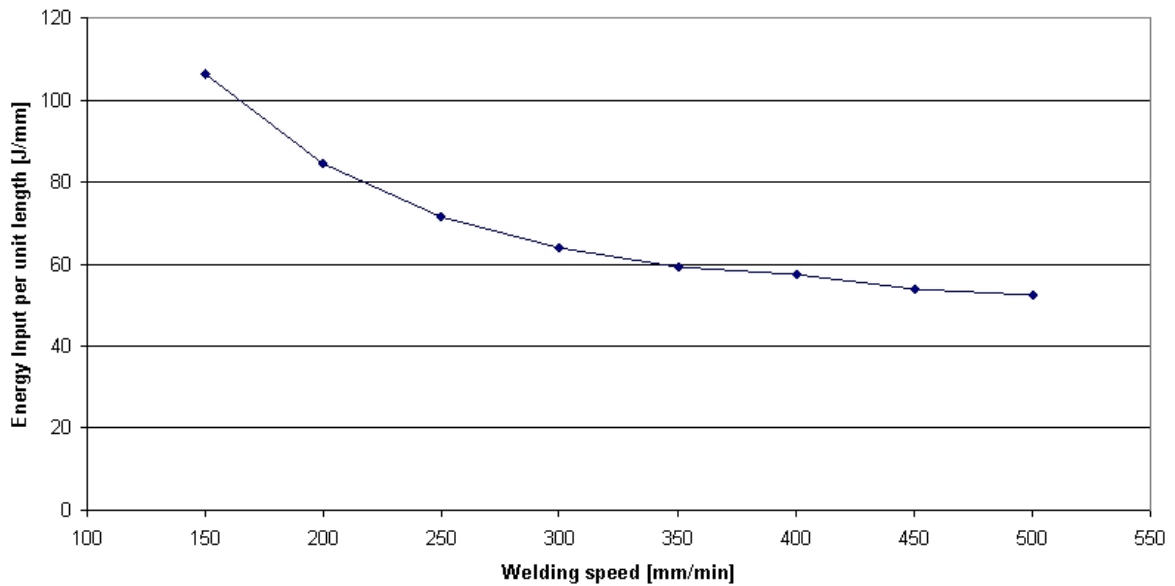
Figure 4.13: Heat input per unit lenght over the welding speed

4.1.6 Tool Rotation

Equation **??** shows that the heat input increases with increasing tool rotation. The strength increases with decreasing heat input and due to this some experiments with the tool rotation 900 rpm were done.

Experiment:

The influence of the tool rotation on the tensile strength was investigated with the following welding parameters:

- Welding speed: 200 to 500 mm/min

- Plunge depth: -0.15 mm

- Distance of clamping: 40 mm

- Welding orthogonal to the direction of rolling

- Load on advancing side

- displacement controlled

Result:

Table **??** shows the tensile strength for different welding speeds with a tool rotation of 900 rpm. For the welding speeds 200 mm/min and 300 mm/min the strength was 110 MPa. With a welding speed of 500 mm/min the strength was much lower.

Table 4.3: Tensile strength for welding with 900 rpm

Welding speed [mm/min]	Tensile strength [MPa]
500	52
300	110
200	110

Discusion:

For a welding speed of 500 mm/min the process got unstable this means that the plunge depth was not constant. Because of the higher welding efficiency with the tool rotation of 12000 rpm, a further investigations with tool rotation 900rpm was stopped at this point.

4.1.7 Conclusion of the Parameter Study

The optimal welding parameters for the used tool and material are:

- Welding speed: 500 mm/min

- Tool rotation: 1200 rpm

- Plunge depth: -0.15

- Distance of clamping: 40 mm

- Load on advancing side

This parameter combination and the welding parameter combination with a welding speed of 150 mm/min, and the other parameters were the same as for the optimal combination, were welded more then 3 times and the difference in strength was lower than 4 MPa. All other parameter combinations were welded only once.

The fracture paths were at the stir zone in the magnesium sheet, exempted from the unstable parameter combinations (high welding speeds, plunge depth controlled) and the low plunge depth.

Overlap Shear Testing

The primarily load for lap joints is in shear or by peel. In an ideal lap shear test, the bending moment does not influence the test and the tensile strength decreases from a maximum at the loaded end to zero at the unloaded end [**?**]. Figure **??** shows the theoretical tensile stress distribution in a lap joint. Bending at the sheet interface is neglected. In a real tensile test, the bending moment has a big
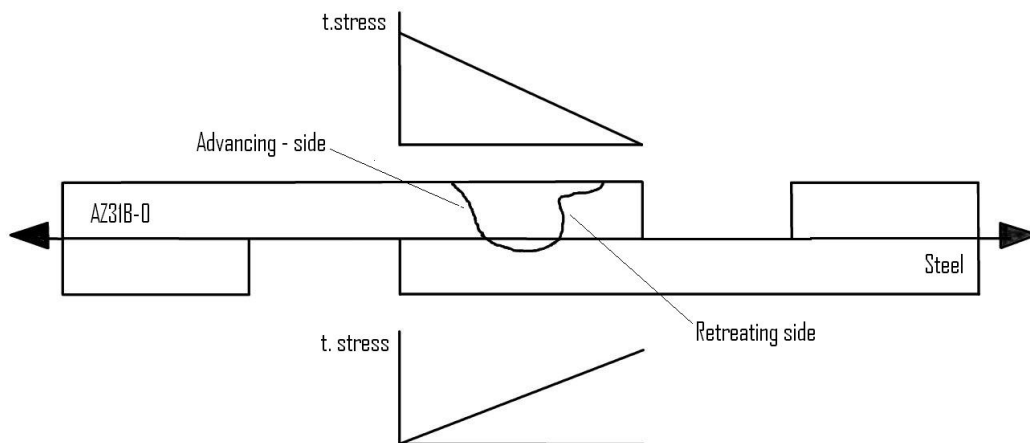
Figure 4.14: Tensile stress distribution in an ideal shear test [**?**]

influence on the overlap shear testing result. If no guides are used the bending moment generates an additional tensile stress at the bottom of the loaded side of the top sheet and at the top of the loaded

side of the bottom sheet. According to this compression stresses will be generated in the top of the loaded side of the top sheet and at the bottom of the loaded side of the bottom sheet. These stresses, as result of the bending moment, increase the test severity and may be destructive when the lap joint interface has components in sheet thickness direction [**?**]. Because of the asymmetric nature of FSW, lap joints can be loaded with the advancing side or the retreating side.

4.2 Temperature Measurement

Friction stir welding has a lower energy input as other welding processes. The process temperature during the friction stir welding process is below the melting temperature which is for AZ31B-O is about $650\,°C$ [**?**]. With increasing welding speed, the thermal gradient increases. A thermocouple is a sensor for measuring temperature. Two different wires are joined together at one end. If a change of temperature takes place at the junction a voltage is produced that can be correlated back to the temperature [**?**]. For the investigation thermocouples produced by Omega Engineering with the following characteristics were used (see table **??**)

Table 4.4: Characteristics of the thermocouples [**?**]

Type	K
Diameter	0.01 Inch
Length	12 Inch
max. Temperature	$760\,°C$
Limits of Error	$2\,°C$

The welding parameters for the temperature measurements were:

- Tool rotation: 1200 rpm

- Welding speed: 500 mm/min and 150 mm/min

- Plunge depth: –0.15 mm

- Clamping distance: 40 mm

- Welding orthogonal to the rooling direction

The measurement of temperature took place at 3 different areas (see Figure **??**):

- On the top sheet, 2 and 3 mm away from the retreating side of the joint

- Between the sheets (Interface), 3 mm to 4.5 mm away from the clamp

- Under the bottom sheet, assembly of the 5 thermocouples shown in Figure **??**
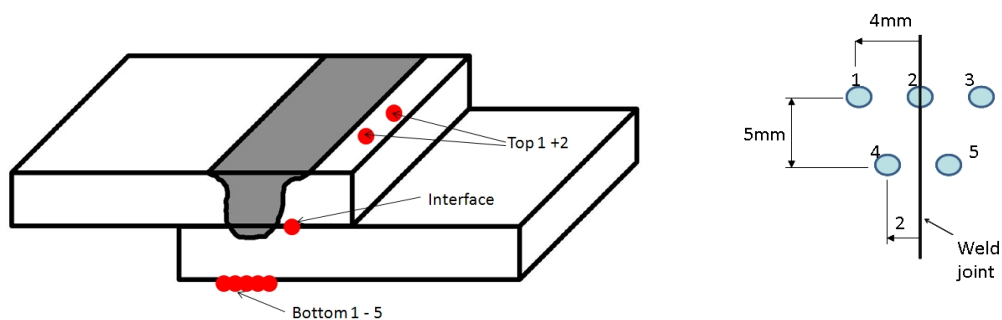
Figure 4.15: Position of the thermocouples

Figure 4.16: Position of the thermocouples at the bottom

The length of the welded joint was 125 mm and the measurement of temperature was in the middle of the joint (between 60 mm and 70 mm from the start point). The thermocouples on the top were fixed with a mixture of water glass (sodium silicate) and quartz sand (silica sand). The distance between the thermocouples on the top was 15 mm in direction of welding. Measuring point Top 1 is closer to the joining start point than measuring point Top 2. At the interface the thermocouple was welded on the steel sheet and the thermocouples on the bottom were fixed in the support and touched the bottom sheet. The sampling rate was 3Hz.

4.2.1 Temperature Measurement with a Welding Speed of 500 mm/min

Figure **??** shows the measured temperatures for all 8 measuring points. The maximum measured temperature on the top is about 100 °C and the temperature is about 9 sec. between 100 °C and 90 °C. At the measuring point in the interface the highest measured temperature was 317 °C. The temperature rate was very high, this means that the temperature increases and decreases very fast. One second before the highest temperature was measured, the temperature was 263 °C and one second after the highest temperature, the temperature was 288 °C. The temperature at the bottom of the steel sheet was nearly the same as at the interface measuring point. The maximum measured temperature was 308 °C.
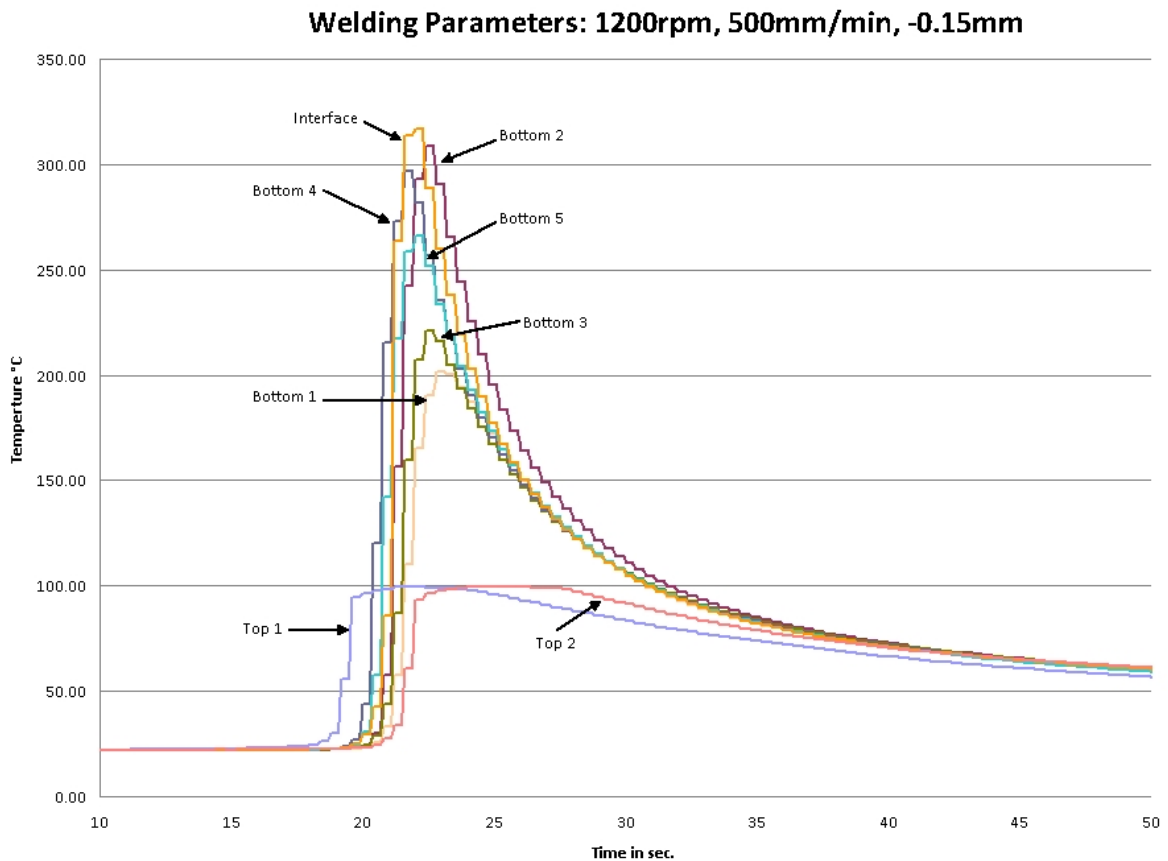
Figure 4.17: Temperature measurement at welding speed 500 mm/min

4.2.2 Temperature Measurement with a Welding Speed of 150 mm/min

The thermocouple at measuring point Top 2 measured non realistic temperatures during the whole measuring time because of contact problems. Figure **??** shows the temperature gradation of 7 measuring points. The temperature at measuring point Top 1 reached a maximum temperature of 200 °C. The graph for the measuring point at the interface shows at the temperature of 160 °C a short period of time where the temperature is constant. The reason is the burr created during the friction stir welding process. The burr pushed the thermocouples a little (less than one millimeter) bit away from the joint. The temperature at the top was 31 sec. higher than 90 °C. At the interface the highest temperature was measured which was 328 °C. The temperatures under the steel sheet were just a little bit lower than in the joining interface.
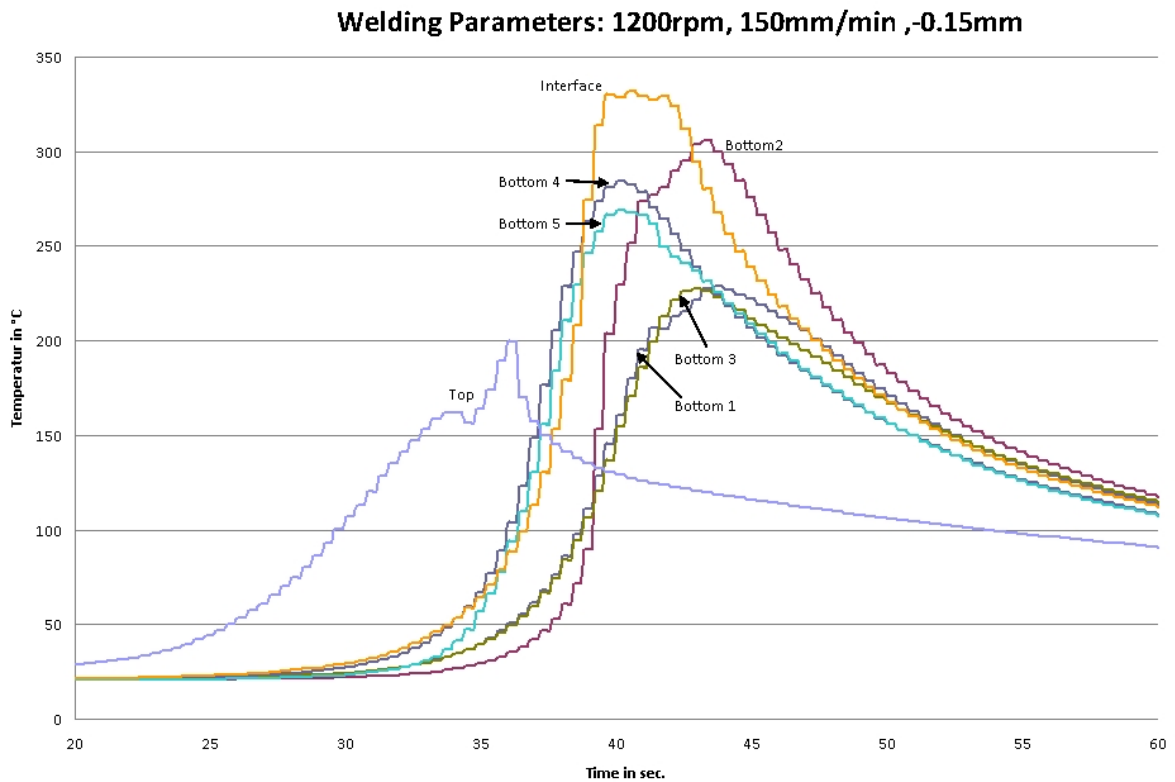
Figure 4.18: Temperature measurement at welding speed 150 mm/min

4.2.3 Conclusion of the Measurement of Temperature

The differences between the temperature measurement with a welding speed of 500 mm/min or 150 mm(min were very small. The maximum temperature at the measuring point interface and bottom were about the same. The biggest difference was at the measuring point Top 1. The temperature at a welding speed of 150 mm/min was 100 °C higher as at welding speed 500 mm/min.

The tool shoulder is generating the heat. If the welding speed is low and the tool rotation is the same, the energy input is higher with lower welding speed and this is the reason for the higher temperature at the top of the magnesium sheet.

Another logical difference was the time of the high temperature because of the welding speed. With a lower welding speed the temperature is a longer time at a certain level.

Nandan et al. [?] investigated the recent advances in friction stir welding - process, weldment structure and properties. They reported that the temperature for steel welding at the advancing side is 100°C higher than on the retreating side. During this investigation the temperature was measured at the retreating side.

5 Investigations

Only the key samples and the base material were investigated with different methods. Table **??** show the welding parameters for the investigated samples and the denotation for the samples which will be used in this chapter. Different investigations were done with the samples. Table **??** shows an overview of the investigations.

Table 5.1: Investigated samples

	Tool rotation [rpm]	Welding speed [mm/min]	Plunge depth [mm]	Tensile strength [MPa]
Optimal Parameters	1200	500	–0.15	120
Low welding speed	1200	150	–0.15	96
Fracture at the interface	900	300	–0.2	107

Table 5.2: Investigations of the samples

	Base material	Optimal Parameters	Low welding speed	Fracture at the interface
Hardness	X	X	X	X
Metallography interface		X	X	X
Fracture surface		X		X
Fracture path		X	X	X
Possible fracture path	X	X	X	X

5.1 Measurement of Hardness

The Vickers hardness test was used for the measurement of hardness with a hardness number of HV1 and HV0.1, where HV gives the hardness scale (Vickers) and 1 or 0.1 indicates the load used in kg. The measurement of hardness took place on a polished cross section in the magnesium sheet. The measuring points were in the middle of the two millimeter thick magnesium sheet and the duration of load was 10 sec.

Afrin et al. [**?**] investigated microstructure and tensile properties of friction stir welded AZ31B magnesium alloy. They used AZ31B-H24 and reported a hardness of the base material of about 70 HV1 and about 50 HV1 in the center of the stir zone. Woo et al. [**?**] investigated the microstructure, texture and residual stresses in a friction stir processed AZ31B-O magnesium alloy. They detected no changes of hardness due to friction stir welding.

5.1.1 HV1

The distance between the measuring points was 1.5 mm. The hardness of the based metal was between 50.2 HV1 and 56.3 HV1 (see **??**).
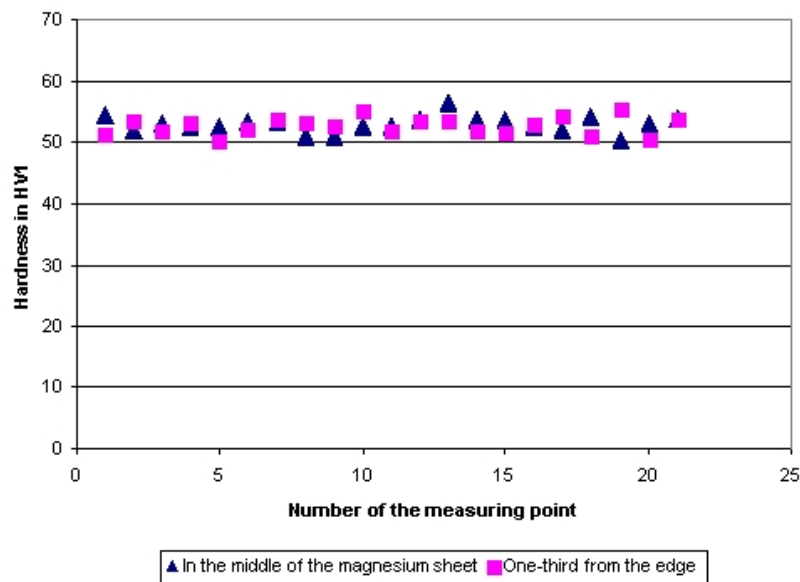
Figure 5.1: Hardness of the base material magnesium

The hardness was measured at a sample welded with following parameters:

- Tool rotation: 1200 rpm

- Welding speed: 500 mm/min and 150 mm/min

- Plunge depth: –0.15 mm

- Distance of clamping: 40 mm

- Welding orthogonal to the direction of rolling

Figure **??** shows the hardness for the sample with optimal welding speed of 500 mm/min. The hardness varied between 48.6 HV1 and 57.8 HV1 and no significant change of the hardness could be detected in the stir zone.

Figure **??** shows the measurement of hardness for the welding speed of 150 mm/min. The hardness was between 40.2 HV1 and 60.1 HV1. The hardness of only one measuring point was 40.2 HV1 and the measuring points before and after these points was about 45 HV1. No significant change of the hardness in the stir zone could be detected.
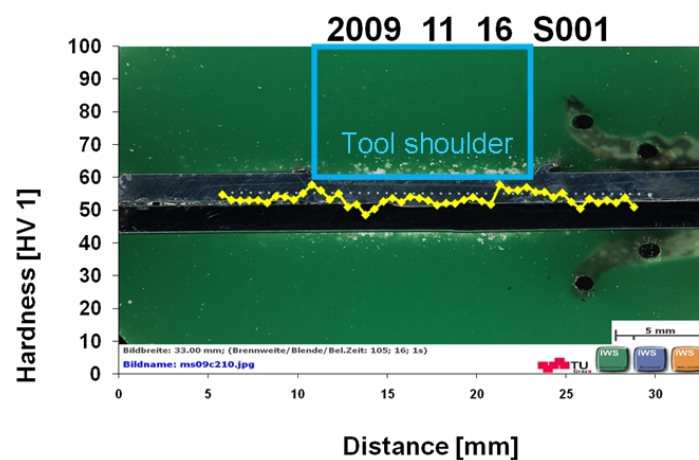
Figure 5.2: Measurment of hardness [HV1], welding speed 150 mm/min

5.1.2 HV0.1

For measuring the hardness with HV1 the distance between the measuring points was 1.5 mm. For a better detection of changes in hardness, the step size between the points of measuring has to be reduced. Because of the deformation during the hardness measurement and following changes of material properties, the load for the measurement was reduced to HV0.1. The welding parameters of the
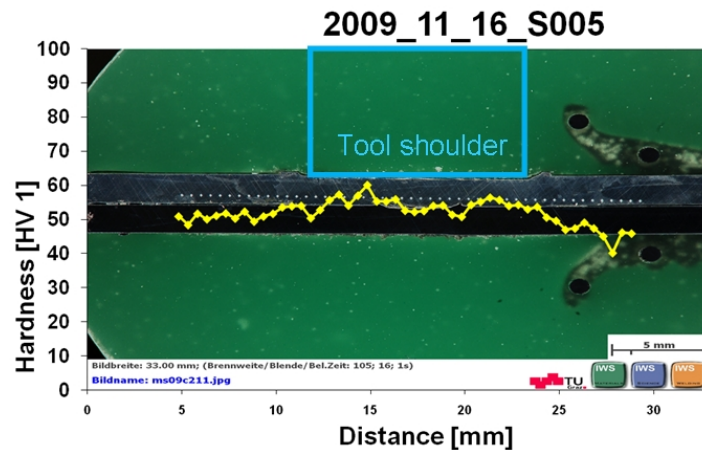
Figure 5.3: Measurment of hardness [HV1], welding speed 500 mm/min

used samples were the same as for the HV1 measurement.

Figure **??** shows the measurement of the hardness for the welding speed of 150 mm/min. The hardness was between 50.7 HV0.1 and 76.8 HV0.1. There only was one measuring point with hardness higher than 70 HV0.1. This measurement point was on a steel particle. The average of hardness is 61.6 HV0.1. Figure **??** shows the measurement of hardness for the welding speed of 500 mm/min. The maximal hardness was 72.8 HV0.1 and the lowest hardness 56.2 HV0.1. The average of the hardness was 66.1 HV0.1.
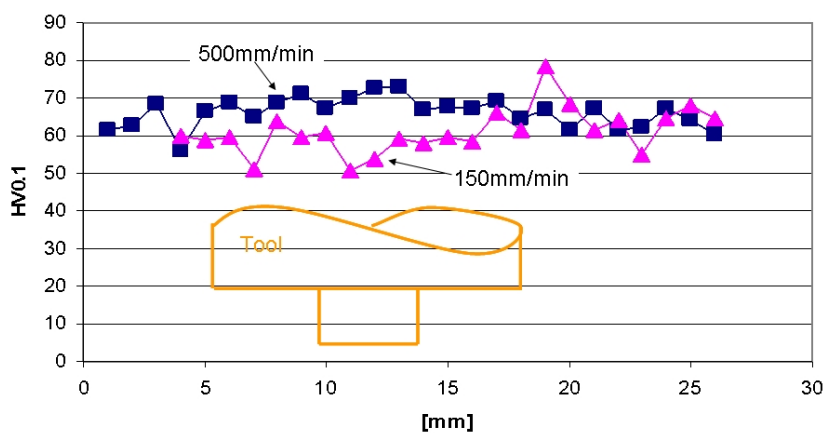
Figure 5.4: Measurment of hardness [HV0.1], welding speed 150 mm/min and 500 mm/min

5.1.3 Discussion of the Hardness Measurement:

The hardness of the AZ31B-O is in the stir zone, HAZ, TMAZ, and base material is about the same. The measured hardness was for the welding speed 500mm/min higher than for the welding speed 150mm/min. The measured hardness was higher for HV0.1 than for HV1. The reason for this difference could the time between welding and measuring be, but no literature about this was found.

5.2 Metallography of the Base Material AZ31B-O

For the investigation of the base material the sample was grinded and afterwards polished with particles with a size of 1 micron. After polishing the sample was etched with 6g picric acid, 10 ml acetic acid, 100ml ethanol and 10ml water. Figure **??** shows a grain size of about 20 microns and a propensity of large deformation twins (T).
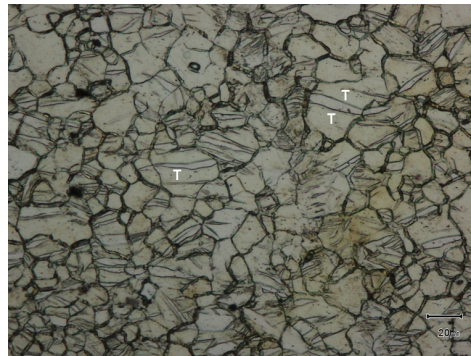
Figure 5.5: Base material AZ31B-O (T... large deformation twins)

Figure **??** shows the grain structure and pole figure for the base material. The direction of rolling was easy to detect and this view is orthogonal to the direction of rolling, this means that the rolling direction was the transverse direction (TD) in the pole figure. The grains have a preferential orientation to the reference direction (RD) because of rolling.
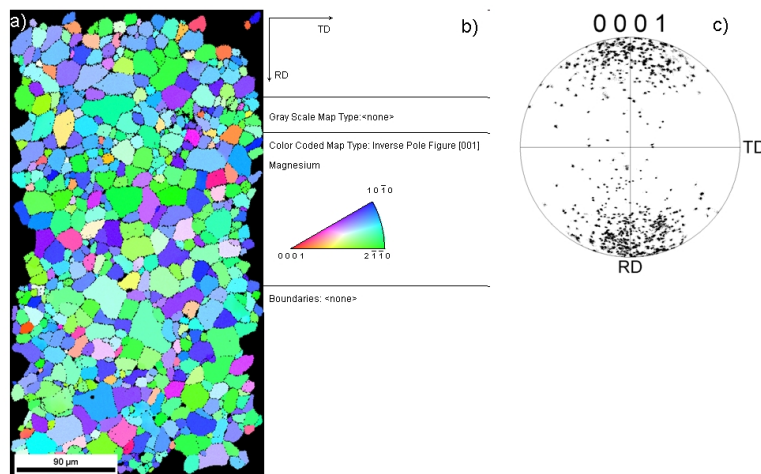
Figure 5.6: Grainstructure and pole figures of the crack area. a) grain size, b) color code triangle c) pole figure

5.3 Metallography of the Interface

During the metallography the grain size, grain structure and particles were investigated with SEM, EDS and EBSD. The sample with the lowest heat input per unit length was the sample with the optimal welding parameters (see figure **??**).

To investigate the influence of the heat input the sample with the highest heat input per unit length was investigated as well. These two samples fractured at the stir zone but there was one sample which had higher fracture strength than the sample with the high heat input but fractured at the interface. This was investigated too. The welding parameters for this optimal welding parameters, low welding speed and sample which fractured at the interface shows table **??**.

The samples could not be polished with micro particles because of the oxide layer at the interface. For this investigation ion beam polishing (IP) system was used. The size of the sample was 4 x 4 x 2 mm which was mechanically polished with one micron particles and afterwards polished with the ion beam.

EDS is a good tool to define the chemical elements. For the investigation with EDS an accelerating voltage of 15keV was used. With this voltage an interaction diameter of about two microns was produced which explains why an investigation with a very high magnification makes no sense. If the acceleration voltage is reduced to 5keV the interaction volume is about one micron but it is impossible to detect the heavy elements like iron or zinc.

5.3.1 Optimal Welding Parameters

The welding parameters for this sample were donated in table **??**.

Basic Light Microscopy and EDS of the Interface Cross Section

The cross section of the sample with the optimal welding parameters shows (figure **??**) a view in the direction of welding without etching. At the top of figure **??** is the magnesium sheet and at the bottom is the steel sheet. On the left and right-hand side of the stir zone are steel clamps which are in the magnesium sheet. The advancing side (AS) is on the left-hand side and the retreating side (RS) is on the right-side. The clamp on the advancing side always points out of the stir zone and the clamp on the retreating side points in the stir zone. During the welding process particles move to the advancing side. An EDS mapping of the cross section is shown in figure **??**. Red represents the magnesium, green the iron and blue the zinc. The particles in the magnesium sheet are iron particles and the layer

between the magnesium and steel sheet consists of zinc. The steel sheet was hot dip zinc coated with a layer thickness of 15 microns(see figure **??**).
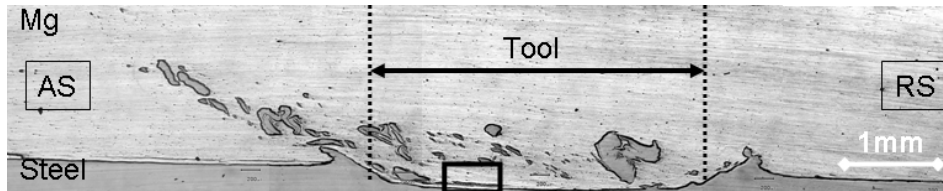
Figure 5.7: Cross section welding speed 500 mm/min
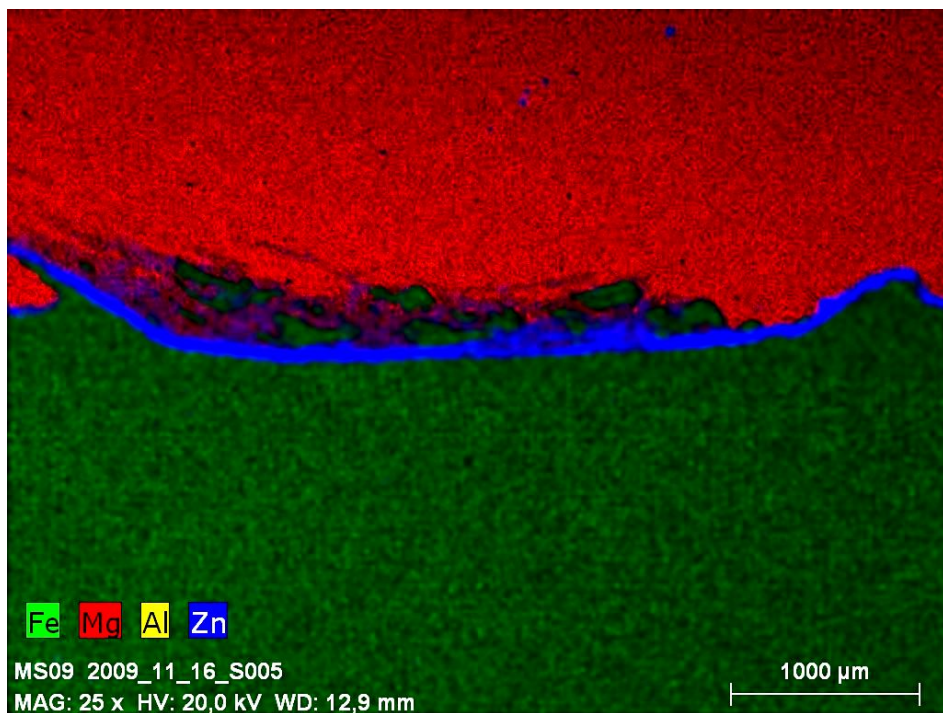
Figure 5.8: EDS of the stir zone from figure **??**

Investigation of the Interface with SEM and EDS

Figure **??** shows the area between the clamps. The ion beam polished area is easy to detect. The white particles are from the aluminium foil which was used to get a better conductivity between the sample holder and a sample. The steel sheet is on top. In the magnesium sheet near the steel sheet is a layer with a thickness of 50 microns. In the stir zone are many steel particles with lengths up to 800 microns and a thickness of less then 150 microns.

Figure **??** (detail A in figure **??**) shows the interface where magnesium - zinc layer or the magnesium at
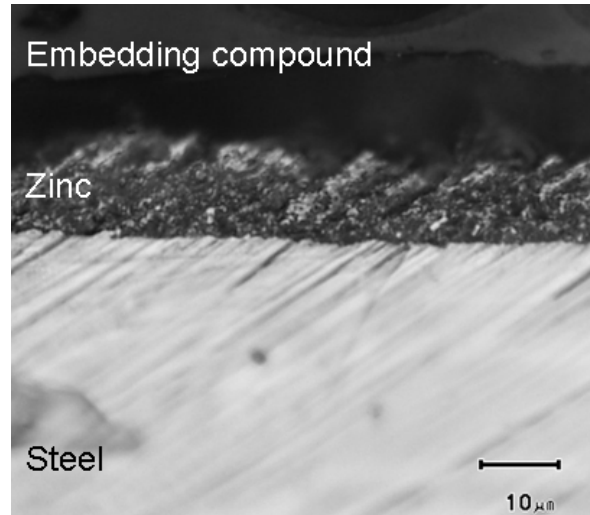
Figure 5.9: Zinc layer of the steel sheet
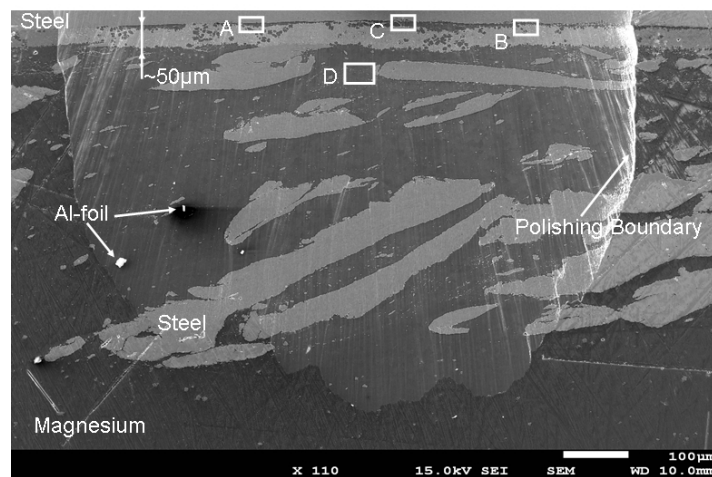
Figure 5.10: Ione beam polished area in the center of the stir zone from figure **??**

the interface is. The microstructure of the zinc looks lamellar and in the layer are particles. Figure **??** shows the EDS map of Figure **??** where red gives the magnesium, violet displays the zinc, yellow stands for the iron and green for aluminium. The particles in the layer are magnesium particles and the layer consists of 45 wt.% of magnesium and 53wt.% of zinc. The chemical composition of the layer was defined by EDS spot and is given in table **??**.

Table 5.3: chemical composition of the zinc layer

Element	wt.%	at.%
Mg	44.56	67.65
Al	1.17	1.59
Fe	1.2	0.79
Zn	53.7	29.97
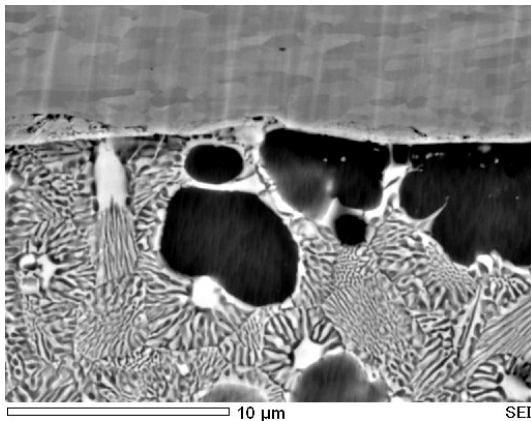
Figure 5.11: Interface steel - zinc- mangnesium, detail A in figure **??**
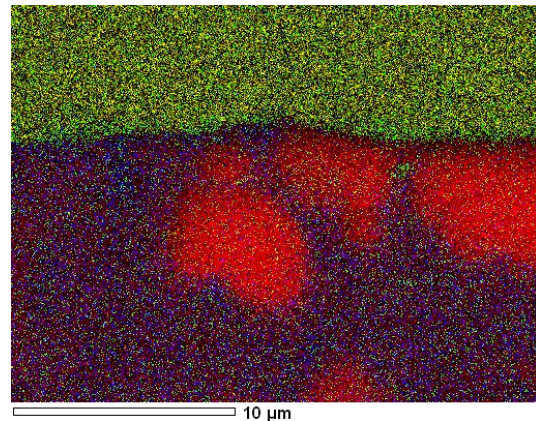
Figure 5.12: EDS of detail A, Mg - red, Zn - violet, Fe - yellow, Al - green

Figure **??** (detail B in figure **??**) shows the only void which was detected. The size of this void is about one micron.

Some EDS line scans are necessary. The EDS lines scan over the interface of magnesium - steel (figure **??**, detail C in figure **??**, line 1 diagram **??**, line 2 diagram **??**) show sometimes a high zinc content at the interface. The zinc content in the steel and magnesium is higher as in the base material. The EDS line 3 scan across the steel particle (diagram **??**) shows also high zinc content at the interface. Different particles were detect in the magnesium in the stir zone. Figure **??** (detail D in figure **??**) shows particles in the stir zone. The shape of the particle top right looks different compared with the

other particles. The EDS map (figure **??**) shows steel particles and the particle top right consists of aluminium and manganese with a size of about 7 microns.
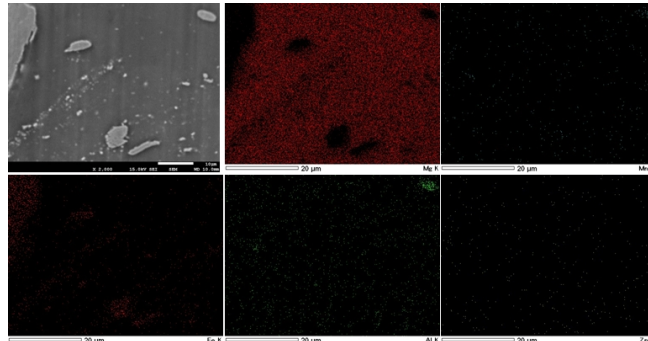
Figure 5.13: Particles and EDS of detail D in figure **??**
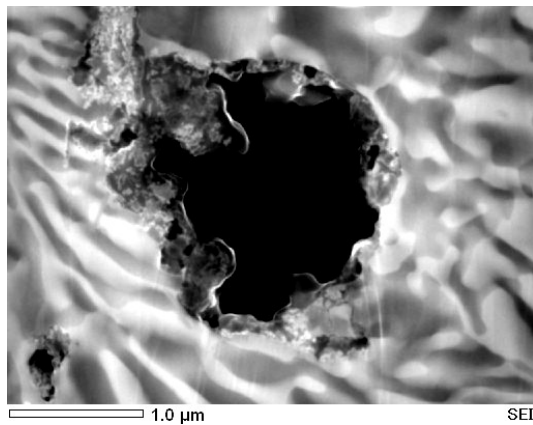
Figure 5.14: Void, detail B in figure **??**
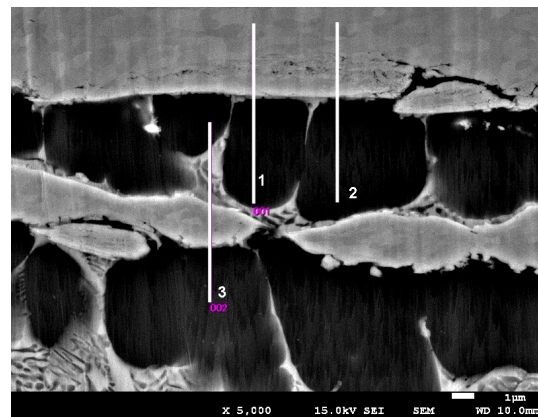
Figure 5.15: EDS lines, detail C in figure **??**
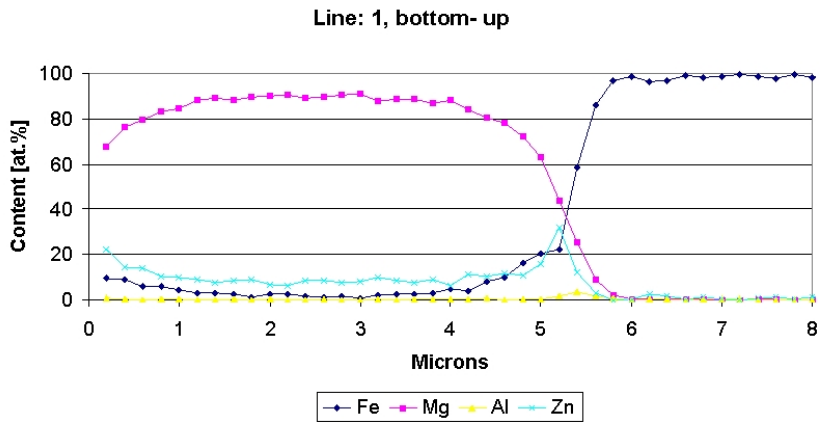
Figure 5.16: EDS line scan diagram for line 1 of figure **??**
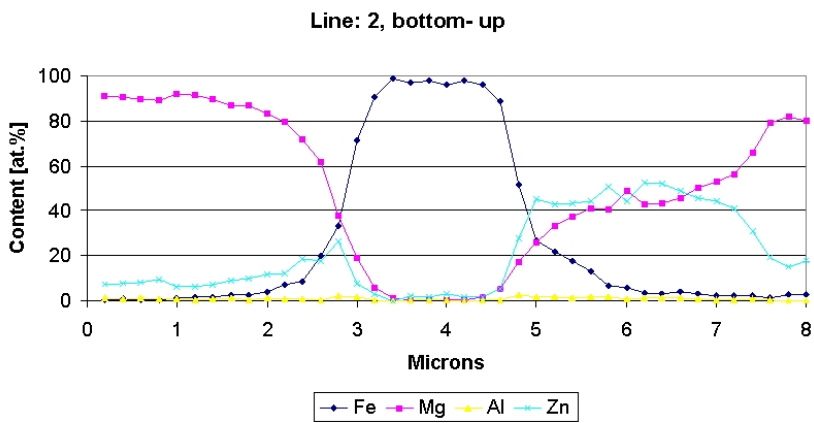
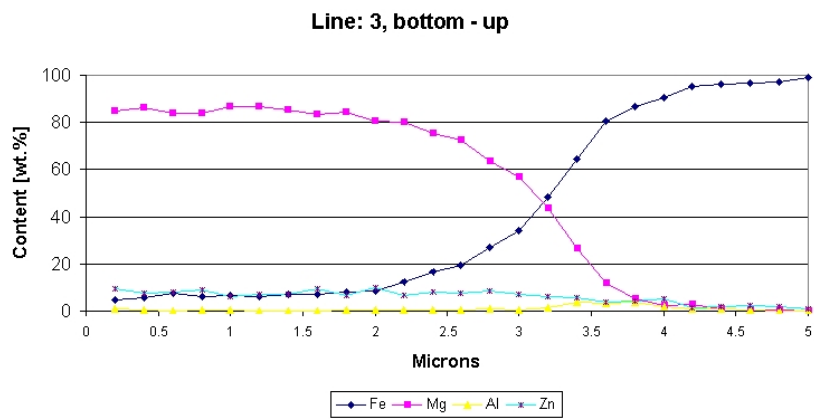Figure 5.17: EDS line scan diagram for line 2 of figure **??**

Figure 5.18: EDS line scan diagram for line 3 of figure **??**

Grain Size and Orientation

Figure **??** shows the characteristic microstructure only of the magnesium in the stir zone. The other elements were removed. The step size of this investigation was 0.2 microns and the detected grain size is about 7 microns. Figure **??** and **??** shows the magnesium grains and pole figures. In figure **??** are white lines which are the borders of different areas. From the top to the first line is the interface area. From the second to the third line is the detail middle and between the fourth line and the bottom is the detail top. The pole figure from the interface shows that the grains near the interface are random but the other two pole figures show that the grains has a preferential orientation.
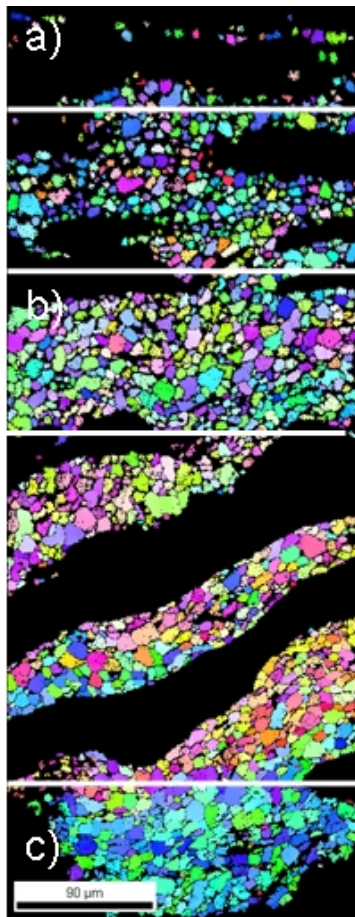
Figure 5.19: EBSD map of the stir zone for the welding speed 500 mm/min
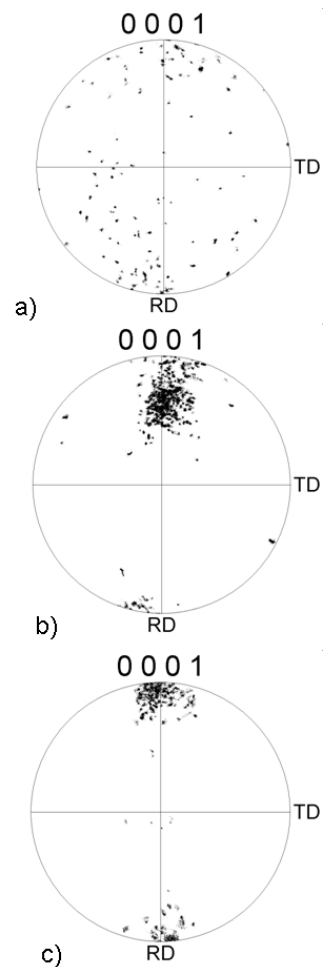
Figure 5.20: Pole figure for the stir zone of the welding speed 500 mm/min, a) at the interface, b)at the middle, c) at the top

Investigation of the Stir Zone

Figure **??** shows the clamp on the advancing side and the stir zone. The steel sheet is on the top and the magnesium sheet on the bottom. The layer between the steel and magnesium is a magnesium - zinc layer. The white particles on the picture are aluminium particles because aluminium foil was used to get a better electrical conductivity from the sample to the sample holder. The with lines on the right and left handed side is the border of the ion beam polished area after 12 hours of polishing. On the right handed side of the clamp is the gap between the magnesium and steel sheet easy to detect. This means that outside of the clamp the sheets are not joined.

Figure **??** shows detail A from figure **??**, which shows a part of the horizontal line of defects in the stir zone. No line like this was located during the investigation of the interface. Figure **??** shows the EBSD map of the crack area and the pole figures from the top of the crack and the bottom side of the crack. The grain size is about the same but the orientation of the grains is different. Pole figure from the top b) shows no preferential orientation of the grains.The pole figure from the bottom c) shows a preferential orientation. This could be a sign for that the stirring process was to less because of the different layers which are not joined.
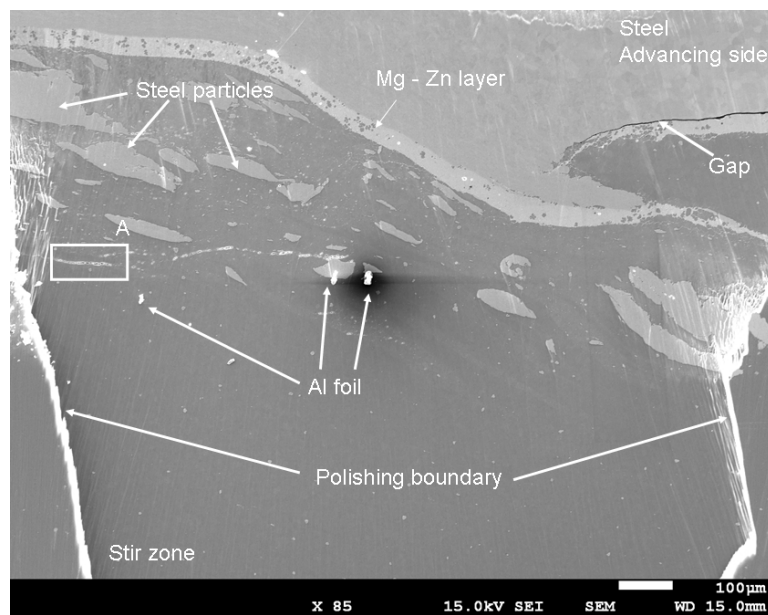
Figure 5.21: Clamp on the advancing side
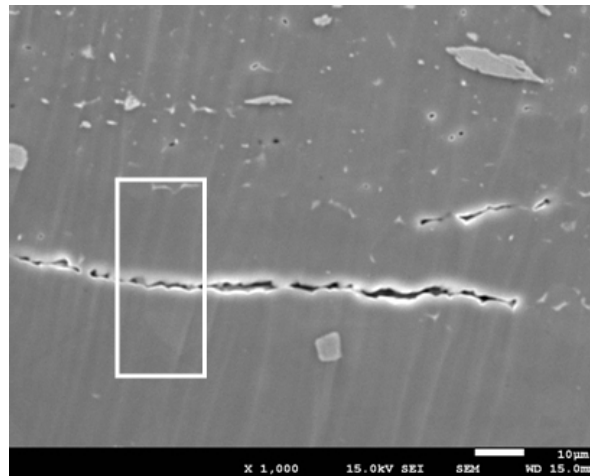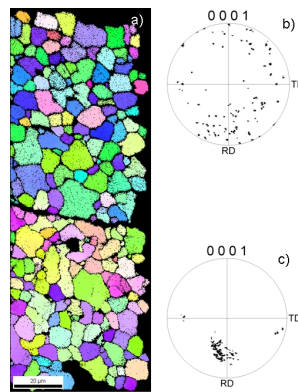
Figure 5.22: Crack in the stir zone, detail A in figure **??**

Figure 5.23: Grainstructure and pole figures of the crack area. a) grain size, b) pole figure of the top, c) pole figure of the bottom

Conclusion and Discussion

There are no defects at the interface but small voids in this zinc - magnesium layer. Big particles made of steel are in the stir zone. This layer in the interface has a chemical composition of about 67at.% of magnesium and 39at.% of zinc and a lamellar micro structure. The thickness of the layer is about 50 microns and the zinc coating from the steel was 15 microns which is about one - third and the same ratio of atomic percent zinc to atomic percent magnesium.

The phase diagram **??** shows that the melting temperature of the magnesium is about 650°C. During the welding process the zinc diffused into the magnesium and due to that the melting temperature decreased. A eutectic point is at 32 at.% zinc and 68at.% magnesium and has a melting temperature of 340°C. The measured temperature was 320°C which was 4 mm away from the interface. The magne-

sium particles between the layer and the steel are segregations from the melt during the solidification. The temperature during the FSW process was definitely higher than 340°C and it is assumed that the layer melted during the joining process. At the interface sometimes a higher content of zinc was detected but there are areas without non interlayer between the steel sheet and the magnesium grains. The reason for this could be the segregation of magnesium which has a higher melting temperature than the zinc due to that the magnesium segregations are in the melt and the zinc is around these segregations.

A line of defects was detected at the stir zone which is parallel to the interface. The grain orientation on the two sides of the crack is different which could be the reason for a wrong material flow during the welding process.

5.3.2 Low Welding Speed

The welding parameters for this sample were donated in table **??**.

Basic Light Microscopy and EDS of the Interface Cross Section

Figure **??** shows the cross section of the sample with the low welding speed. The top sheet is the magnesium and the bottom sheet is the steel sheet. The advancing side is on the left-hand side and particles were moving to the advancing side. On the left-hand side of the stir zone is the advancing side where the clamp points out of the stir zone and on the right-hand side is the retreating side where the clamp points into the stir zone. An EDS mapping of the cross section shows figure **??**. Red gives the magnesium, green the iron and blue the zinc. The particles in the magnesium sheet are steel particles. For this investigation the steel was zinc coated but there is no zinc concentration in the stir zone or at the joined interface. The zinc flows out of the joining area and is on the left and right-hand side of the stir zone.
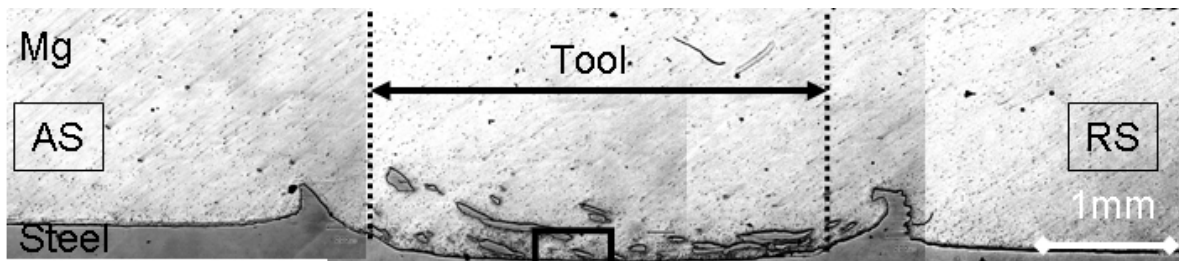
Figure 5.24: Cross section welding: speed 150 mm/min
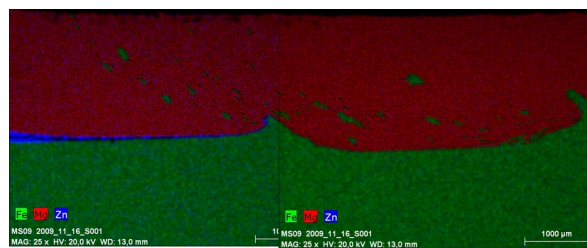
Figure 5.25: EDS of the stir zone from figure **??**

EDS Investigation of Zinc which flows out of the Joining Area

For this investigation the steel sheet was removed from the magnesium sheet. On the magnesium sheet a thin layer which flows out of the joining area was detected. Figure **??** shows the advancing side of

the magnesium sheet after removing the steel sheet. On the right-hand side of figure **??** was the joined area where the area of the pin is marked. The welding direction was from the bottom - up. Figure **??** shows the chemical contents of the EDS spots in Figure **??** in a diagram. The chemical composition of EDS spot 1 shows that there is the magnesium sheet but the EDS spots 2 up to 8 are at the eutectic magnesium - zinc alloy but not EDS spot 4 which has a higher zinc content. EDS spot 9 up to 12 are on the magnesium sheet.
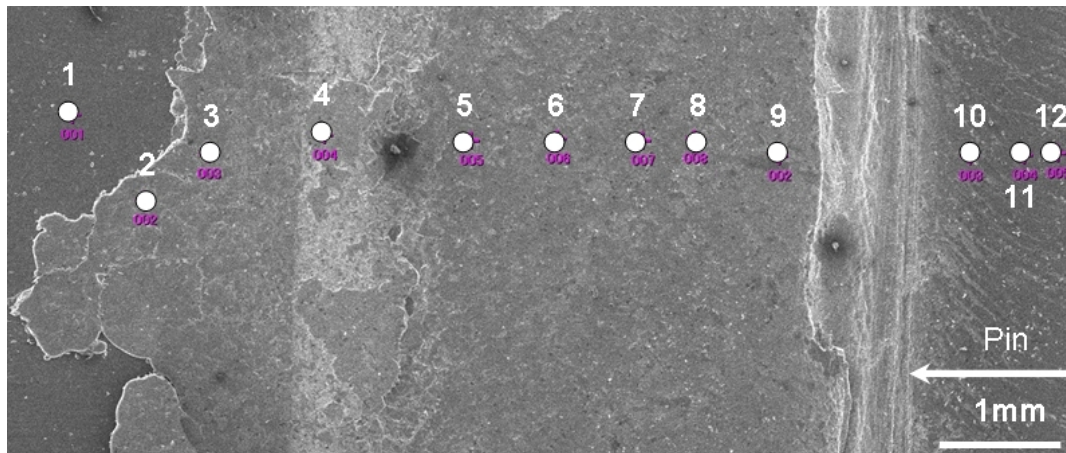
Figure 5.26: Advancing side and joined area on the magnesium sheet
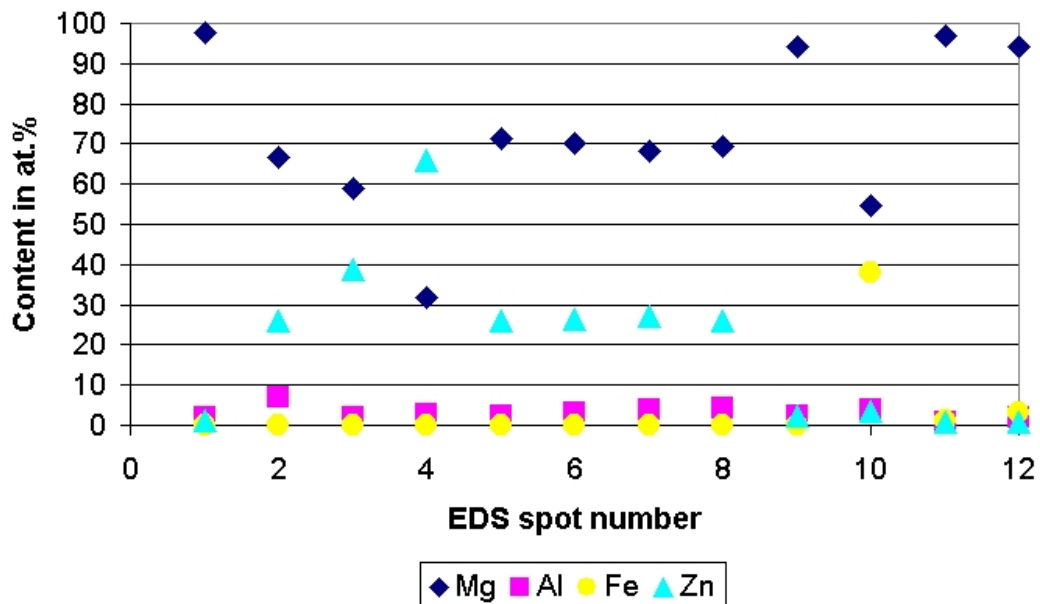
Figure 5.27: EDS spots from firgure **??**

Investigation of the Interface with SEM and EDX

Figure **??** shows the detail in figure **??**. The iron beam polished area is easy to detect. The steel sheet is at top and the magnesium sheet at the bottom. The ion beam polished area shows no magnesium-zinc layer in the stir zone.

Figure **??** (detail A in Figure **??**) shows the interface and steel particle. The EDS line scan (Diagram **??**) over the interface of steel and magnesium shows a little zinc peak at the interface. The second line scan diagram (Diagram **??**) over the interface steel - magnesium and the interface of the particle shows a little zinc peak at the interface between the sheets but no zinc peak at the particle. The line scan shows that the particle is made of iron. The details in figure **??** are voids.
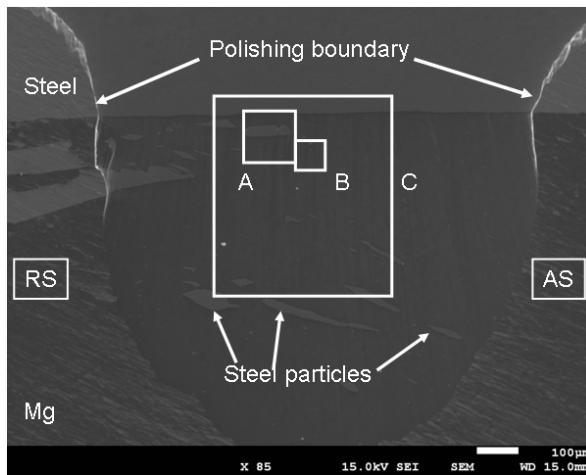
Figure 5.28: Ione beam polished area in the center of the stir zone from figure **??**
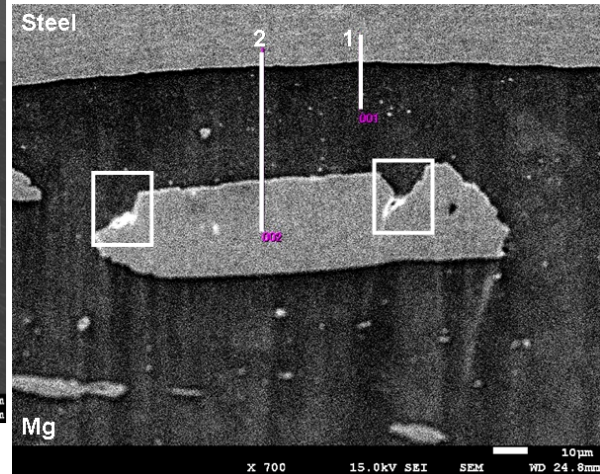
Figure 5.29: EDS lines, detail A in figure **??**

During the investigation of the interface different particles were detect in the magnesium in the stir zone. Figure **??**(detail B in figure**??**) shows particles with the EDX map in the stir zone. The particles consists of aluminium and manganese. The size of the particles is up to 10 microns.
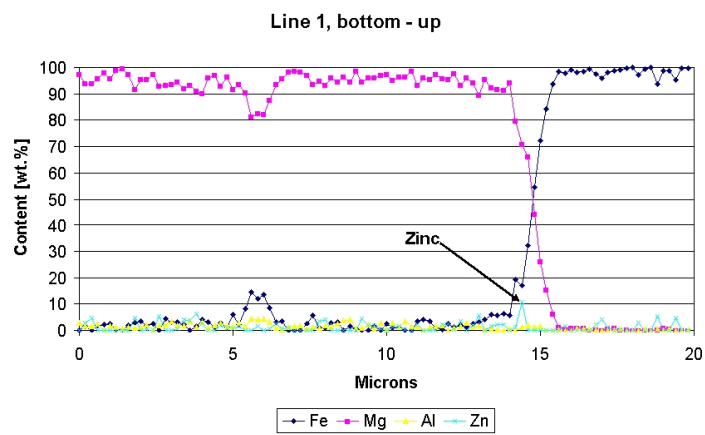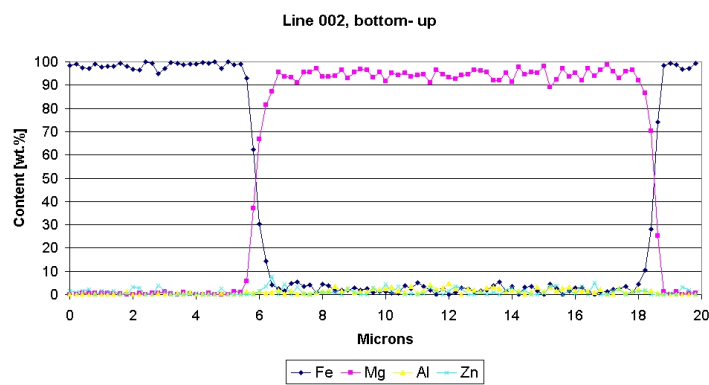
Figure 5.30: EDS line scan diagram for line 1 of figure **??**

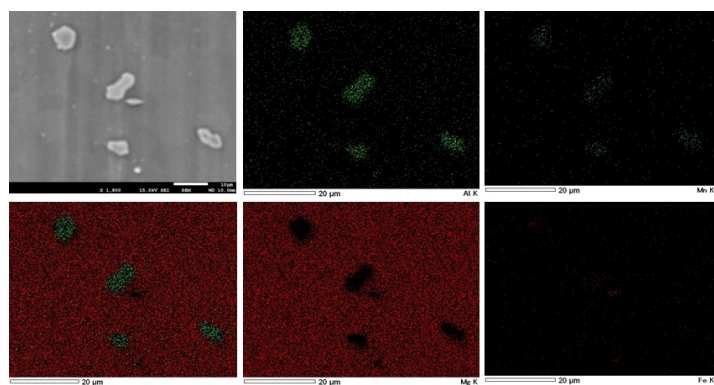Figure 5.31: EDS line scan diagram for line 2 of figure **??**

Figure 5.32: Particles and EDS of detail D in figure **??**

Grain Size and Orientation

Most of the ion beam polished area was investigated with an EBSD to define the grain size at the interface(see figure **??**). The step size for this investigation was 0.75 microns. Figure **??** shows the characteristic microstructure of the magnesium in the stir zone. The steel sheet is on the bottom and displayed by the large black area. The black particles in the magnesium are steel particles. The grain size is increasing with a rising distance to the interface. The average grain size at the interface is about 7 microns and about 100 microns away from the interface the grain size is about 9 microns (see: figure **??**). Figure **??** shows the preferential orientation of the magnesium grains. The white lines divide the figure in the parts interface, middle and top. The pole figure in figure **??** shows the orientation of the magnesium grains at the interface, at the middle of the figure **??** and at the top.
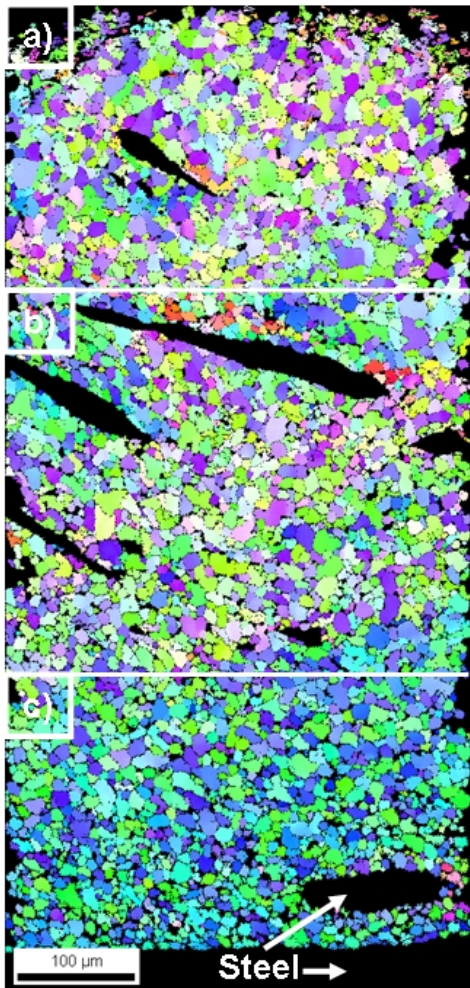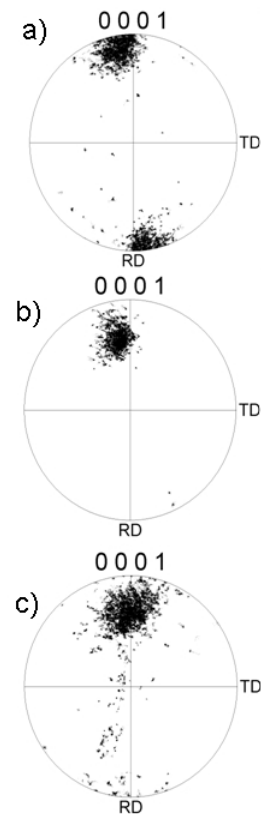

Figure 5.33: EBSD map of the stir zone

Figure 5.34: Pole figure for the stir zone of the welding speed 150 mm/min, a) at the interface, b) at the middle, c) at the top

Conclusion and Discussion

No significant defects were detected at the interface and in the stir zone. The steel particles in the stir zone have a length of up to 700 microns and a width of up to 100 microns. There is no layer at the interface like at a the welding speed 500 mm/min. During the joining process zinc diffused into the magnesium and a thin layer melted (see chapter **??**). This melted layer flows out of the joining interface because of a higher heat input and/or different material flow in the stir zone.

5.3.3 Fracture at the Interface

The welding parameters for this sample were donated in table **??**.

Basic Light Microscopy and EDS of the Interface Cross Section

The cross section of the sample which fractured at the interface is shown in figure **??**. The sample is not etched and the direction of viewing is the welding direction. On top is the magnesium plate and bottom the steel sheet. On the left and right-hand side of the stir zone are steel clamps which are in the magnesium sheet. In the centre of the stir zone, in the top sheet are steel particles. An EDX mapping of the cross section is shown in figure **??**. Red gives the magnesium, green the iron and blue the zinc. The particles in the magnesium sheet are iron particles and the zinc layer was stirred into the magnesium sheet.
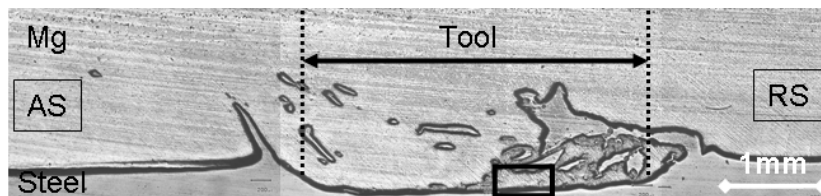

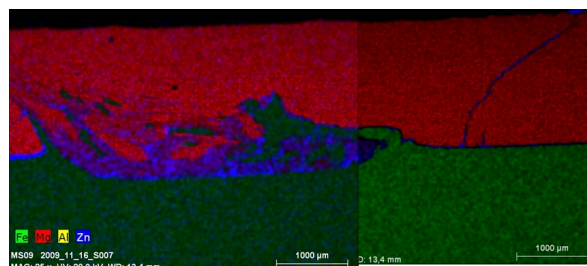Figure 5.35: Cross section, welding speed 300 mm/min and tool rotation 900 rpm

Figure 5.36: EDS of the stir zone from figure **??**

Investigation of the Interface with SEM and EDS

Figure **??** shows the area between the clamps and the polished area is easy to detect. There are big particles in the stir zone and different layers with different shapes are in the stir zone. Figure **??** (detail A in figure **??**) shows the interface between the steel and the magnesium sheet and the EDS maps. The layer consists of magnesium and zinc and there are aluminium - manganese particles in the zinc layer and in the magnesium which was detected in all other samples.

On the right hand side the zinc - magnesium layer is between the steel and the magnesium but on the left hand side the magnesium is between the steel and the zinc - magnesium layer. In the layer are magnesium particles and in the magnesium sheet are iron particles. Figure **??** (detail B in Figure **??**) shows the interface steel - magnesium at another position. There are some voids in the layer and the microstructure looks lamellar. The big round particle with a diameter of about 15 microns is an aluminium - manganese particle with iron at the boundary (see appendix **??**). The micro structure of the steel particle looks a little bit deformed
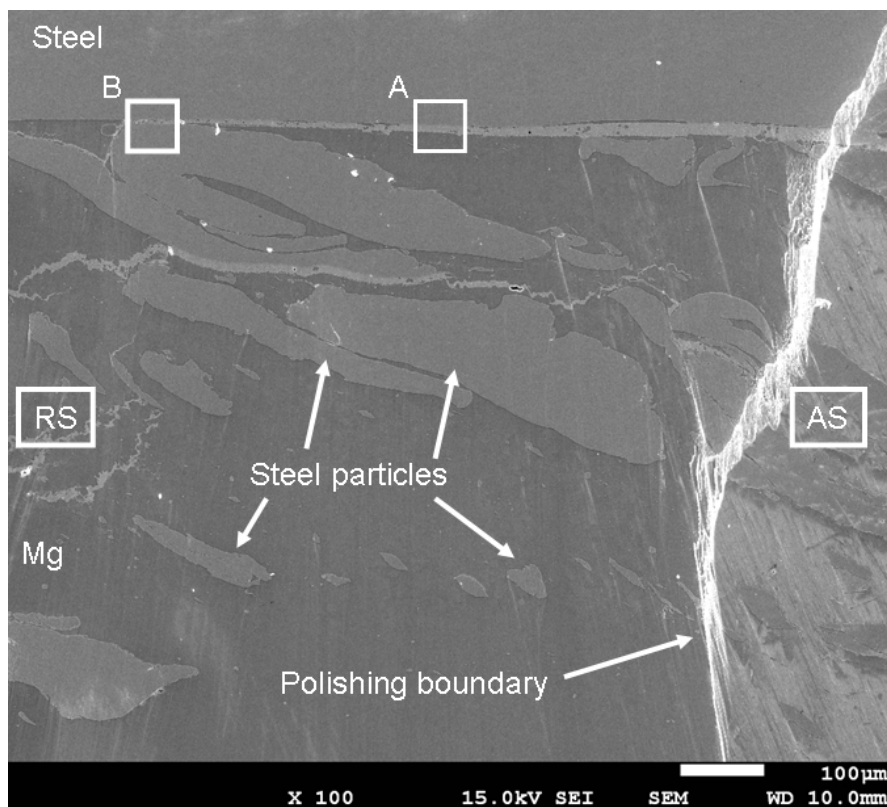

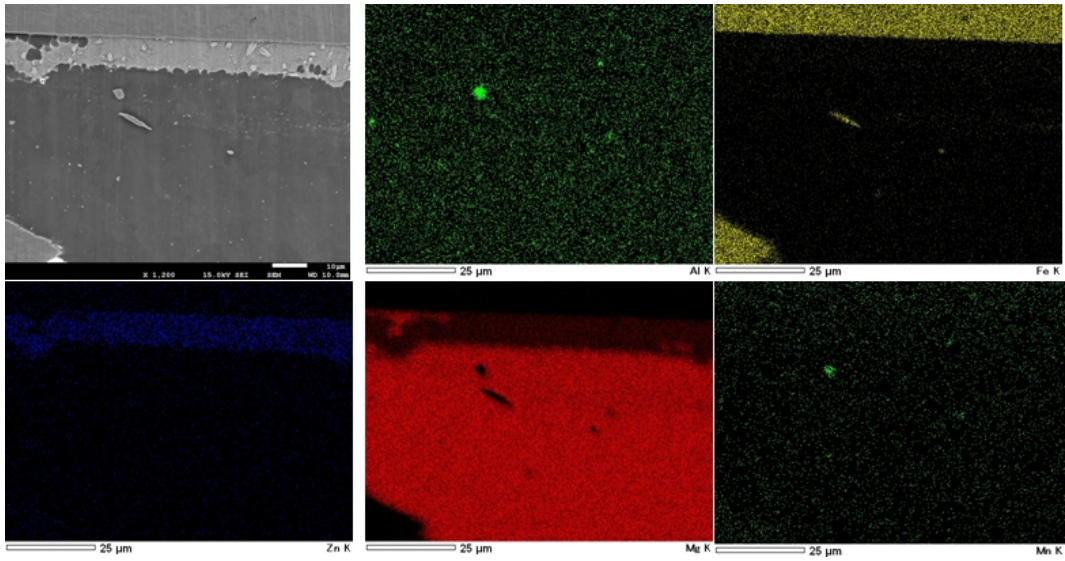Figure 5.37: Ione beam polished area in the center of the stir zone from figure **??**
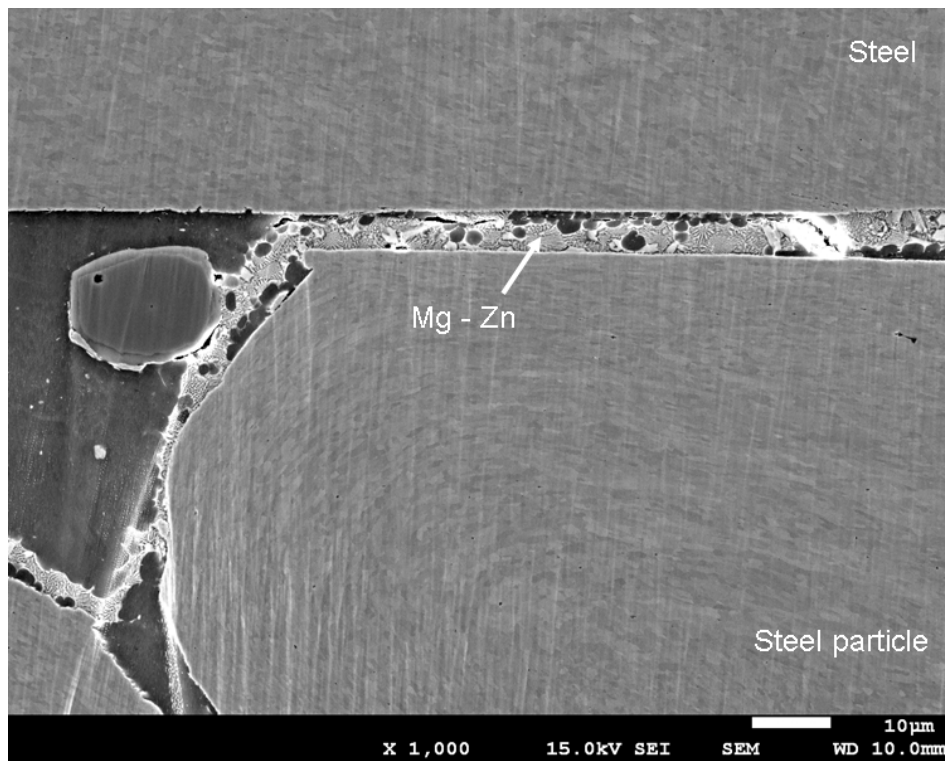
Figure 5.38: Ione beam polished interface, detail A in **??**

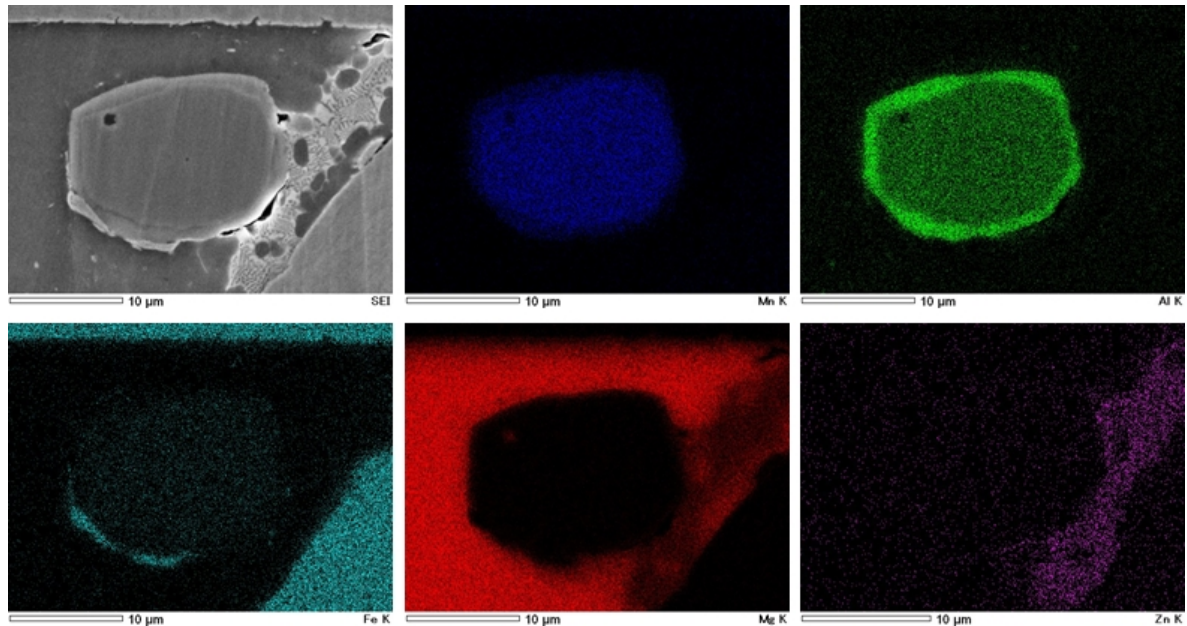Figure 5.39: Interface with voids, detail B in **??**

Figure 5.40: Particle from figure **??**

Conclusion and Discussion

This sample fractured at the interface because of the defects at the interface. Big steel particles are in the stir zone and the zinc layer was stirred into the magnesium. The steel particles move during the stirring process to the advancing side but the zinc layer in the magnesium sheet is at the retreating side.

Nandan et al. [**?**] investigated the recent advances in friction-stir welding - process, weldment structure and properties. They reported that the temperature at the interface could be $100°$C higher than at the retreating side. Because of that the zinc could melt at the advancing side and flow away or diffuse into the magnesium. During the tensile test the sample was loaded on the advancing side, this means that no statement about strength of the zinc layer is possible.

5.3.4 Conclusion and Discussion of the Metallography of the Interface Cross Sections

The grain size and orientation was assayed with EBSD. During EBSD the sample is tilt for $70°$ and the electron beam of the SEM is working in the spot mode scan with a defined step size. Three spots are necessary to define one grain. If the step size was 0.75 microns a grain should be larger than 2.25 microns to be detected as grain. If the grain size is too small the EBSD software can not define the

right element and just chose one of the selected elements which have a similar grain structure as the detected one. For a small grain size or a deformed shape the step size should be very small.

Sometimes the IPF map shows precipitations at the grain boundaries. If there is something at the grain boundaries it should be detected with the EDS, but with the EDS no grain boundary precipitation neither something else was detected. One reason for these small grains at the grain boundary is the step size. The step size is too large and this is the reason why EBSD can not detect the grain boundary. Another reason could be the confidential index. The confidential index range is from 0 (bad) to 1 (good). Low confidential index can be found in areas with very poor pattern quality such as scratches, oxide layers or the camera setting is bad.

Optimal Welding Parameters The AZ31B-O alloy has a melting temperature of about 620 °C (see phase diagram AZ31 **??**) and the melting temperature of magnesium is 650 °C (see phase diagram Mg - Zn figure **??**). The steel was zinc coated with a coating thickness of about 15 microns. The layer in the stir zone consists of 67.65 at.% of magnesium and the zinc content is 29.97 at.%. The layer in the stir zone has a thickness of about 50 microns and a lamellar micro structure which is an indication for an eutectic alloy. The melting temperature of the magnesium is more than 200 °C higher than the melting temperature of the zinc. The measured temperature near the interface was about 350 °C. To get an eutectic alloy the zinc diffuse into the magnesium due to that the melting point of this alloy decreases and melts. Between the steel and the layer are magnesium grains which are segregations of the melted magnesium - zinc alloy (see phase diagram Mg - Zn figure **??**). The melting temperature for the eutectic alloy is about 340 °C but the temperature at the interface is definitely higher.In the zinc layer are some void defects with a diameter of one micron, magnesium and steel particles. The void defect could act as a crack initiation site during the tensile test. The investigation of the stir zone shows a line of defects (see figure **??**. This line could be a sign for that the material flow during the welding process was wrong. This line of defects is parallel to the stress direction during the tensile test due to that these defects were not detected before.

Low welding speed In this sample was no zinc - magnesium layer in the stir zone observed. The size and amount of the steel particles in the magnesium was less compared with the welding speed 500 mm/min. Some voids were detected around the particles but there are no voids at the interface. Magnesium - zinc alloy melts during the joining process and flows out of the joining area. Probably the higher heat input per unit length and different stirring conditions compared with the welding speed 500 mm/min are the reason why the magnesium - zinc alloy flows out of the joining area. The forge force (see figure **??**) for the welding speed 150 mm/min was lower than for the welding speed of 500

mm/min and due to this the forge force is not the reason why the magnesium zinc flows out of the joining area.

Fractrure at the interface There are many voids which are the reason why the fracture path is at the interface. The zinc magnesium layer is widely spread in the stir zone but at different positions. Due to the deeper plunge depth of the tool into the steel compared to the other samples, the clamps and particles are bigger. The heat input per unit length is compared to the welding speed 500 mm/min higher but there are many defects at the interface and the zinc layer is in the stir zone. During the stirring process the steel particles moves to the advancing side but there is a zinc layer at the retreating side.

Commin et. al. [**?**] investigated friction stir welding of AZ31-O magnesium alloy rolled sheets. They report that the grain size in base material is about the same as in the stir zone. Suhuddin et al. [**?**] investigated the grain structure evolution during friction stir welding of AZ31-O and they report that the grain size was decreasing during the friction stir welding process. In this investigation the grain size in the stir zone is smaller than in the base material.

In this investigation the grain size on top is bigger than on the bottom of the magnesium sheet. The reason for this is the higher heat input through the tool shoulder.

In all investigated samples aluminium - manganese particles were found. Commin et al. [**?**] investigated friction stir welding of AZ31 magnesium alloy rolled sheets. They used AZ31 produced by Salzgitter and found Al_8Mn_5 particles in the base material and in the stir zone. The size of the particles was a few nanometers. The remaining particles ar an indicater that in the stir zone the friction stir welding process does not achieve the melting temperature which is 610 °C for the Al_8Mn_5. Laser et al. [**?**] investigated the influence of manganese of the microstructure and mechanical properties of AZ31 gravity die cast alloys. They investigated AZ31 alloys with Mn content form 0.28 to 0.80 wt.% and found Al_8Mn_5 particles in all different alloys. Their calculated phase diagram shows that below 400 °C Al_8Mn_5 should transform to $Al_{11}Mn_4$ but they did not detect it.

The chemical composition of the aluminum - manganese particles was not investigated during this work.

5.4 Investigation of the Fracture Surface

5.4.1 Fracture at the stir zone

The welding parameters for this sample were donated in table **??** which was the sample with the optimal welding parameters.

The fracture path is through the stir zone and therefore one part of the tensile specimen consists of the joined steel and magnesium sheets and the other part is only the magnesium sheet. The fracture surfaces look homogeneous macroscopic and with the naked eye no inclusion are visible.

Figure **??** shows the fracture surfaces of the joined steel and magnesium sheets. The welding direction was from the left-hand side to the right-hand side.

Figure **??** shows the fracture surface of the magnesium sheet with a welding direction from the right-hand side to the left-hand side.

Figure **??** displays the fracture surface at position A. The secondary electron detector was on the top left-hand side and this is the reason for the darker area on the right - hand side. The scanning electron fractograph shows a surface with three different areas. On the top of the magnesium sheet, that means near the area where the tool shoulder was is a small area which is brittle. From the top down there is a small ductile area and a largest area is a shear zone. Figure **??** looks not so homogeneous but this was a small part of the fracture surface.

Figure **??** displays the element analysis of the detail A in figure **??** where blue gives the zinc, red the magnesium and green the iron. The fracture surface has no iron or zinc inclusions. On the steel sheet the large percentage is zinc. With this EDS mapping no statement about zinc in the joining interface is possible. The fracture surface of detail B of figure **??** which is the opposite fracture surface of detail A is shown in Figure **??**.

The fracture surface has logically the same structure as the opposite part. Figure **??** shows the element analysis of the fracture surface of the magnesium sheet. The EDS-mapping displays iron and zinc particles at the fracture surface. These particles are all on the bottom, which means that these iron particles were near the steel sheet before the tensile test.
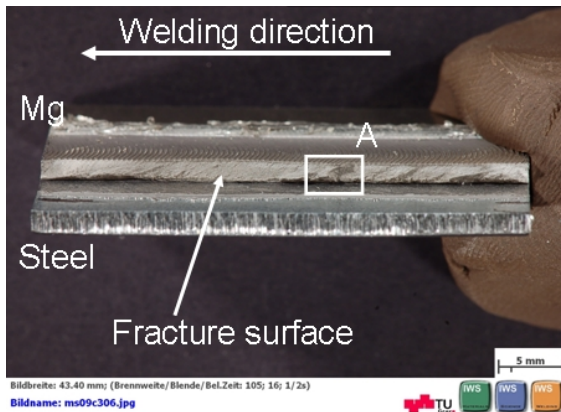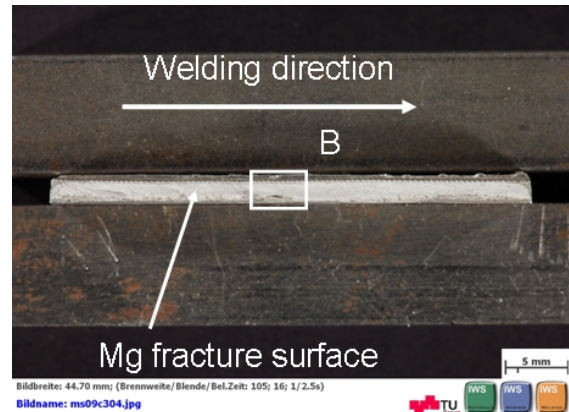
Figure 5.41: Fracture surface 1
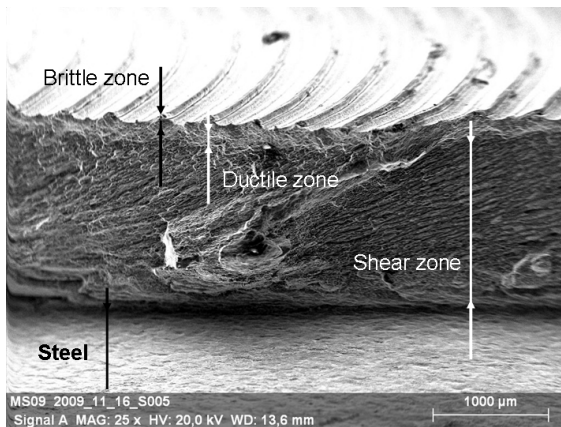

Figure 5.42: Fracture surface 2

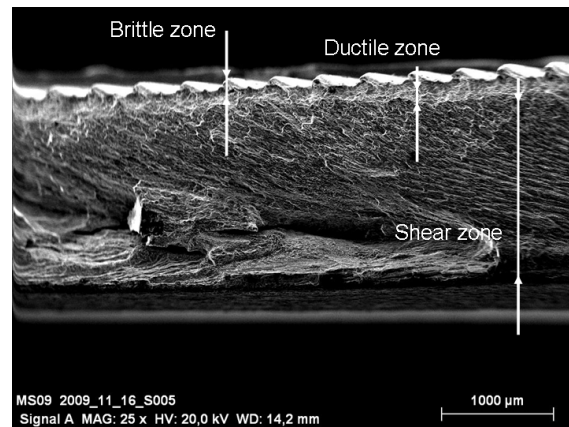Figure 5.43: Microstructure at position A in Figure **??**
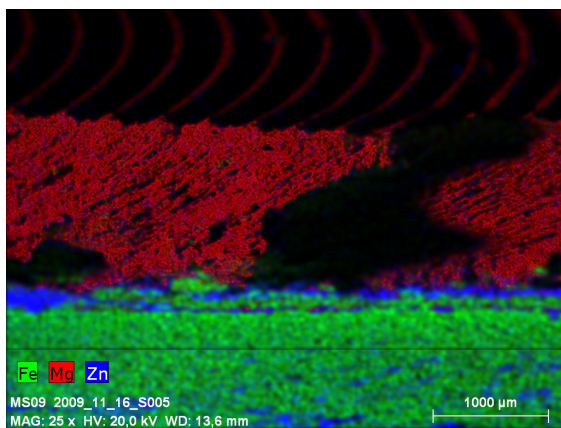

Figure 5.44: Microstructure at position B in Figure **??**

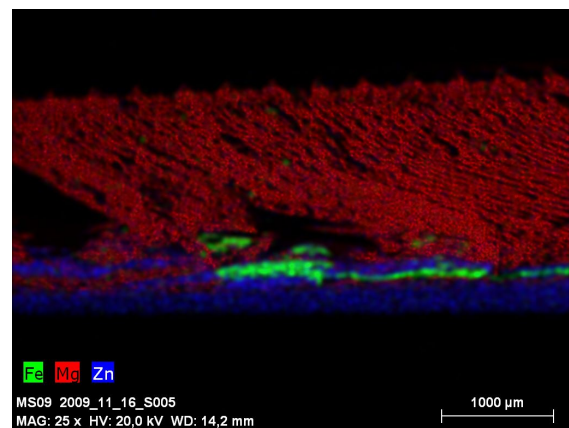Figure 5.45: Element analyses at position A in Figure **??**

Figure 5.46: Element analysis at position B in Figure **??**

5.4.2 Fracture at the Interface

The welding parameters for this sample were donated in table **??** which was the sample with the fracture at the interface.

The fracture path was through the interface and therefore one part was the steel sheet and the other the magnesium sheet. Figure **??** shows the tensile specimen after the tensile test. On the left-hand side is the steel sheet and on the right-hand side is the magnesium sheet.

On the steel sheet is a kind of notch through the specimen. This notch was produced by the pin of the friction stir welding tool. During the welding process, the pin was –0.2 mm in the steel sheet. The magnesium sheet shows the counterpart of the notch. In the notch on the steel sheet are some particles (detail D) and the zinc flows out of the interface.

Near the counterpart of the notch on the magnesium sheet some cracks were detected with the naked eye. The EDS - mapping (figure **??**) where green gives iron, red displays magnesium and the blue color stands for the zinc shows particles consisted of element zinc and magnesium on the steel sheet but the magnesium content is very low. At detail E on the magnesium sheet a zinc layer where iron particles were detected (see figure **??**). These particles could be from the sample preparation process.
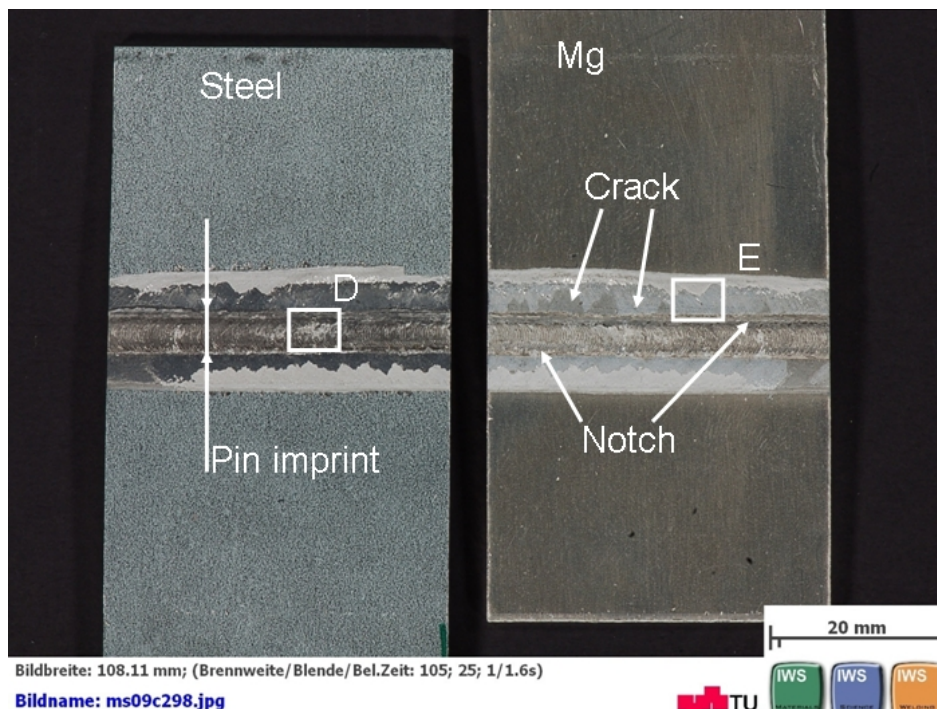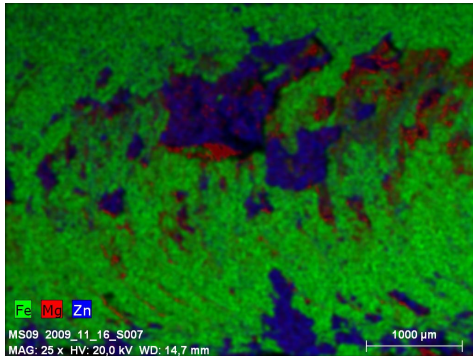

Figure 5.47: Fracture at the interface

Figure 5.48: Element analysis at position D in Figure **??**
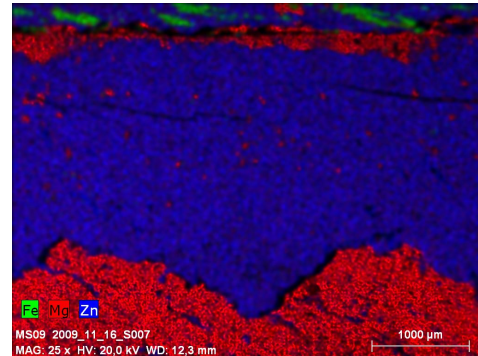

Figure 5.49: Element analysis at position E in Figure **??**

Conclusion and Discussion of the Investigation of the Fracture Surface

Fracture at the stir zone: Higher zinc content was detected near the clamp but not on the whole fracture surface. At this point of the investigation, no statement of the influence of the zinc layer on the fracture path or tensile strength is possible. Commin et al. [**?**] investigated the influence of friction stir welding process parameters on AZ31 magnesium alloy. They report about three different fracture zones. Below the shoulder they reported about a small brittle layer, than a larger ductile area and the biggest area was a shear area. Afrin et. al. [**?**] investigated the microstructure and tensile properties of friction stir welded AZ31B magnesium alloy. They reported that the butt welded samples fractured between the stir zone and TMAZ at the advancing side.

> *"These oxide particles present on the fracture surface could be the trapped oxide during friction stir welding and would be partially responsible for the reduction in the tensile strength and elongation of the joints" [**?**]*

Magnesium oxidizes very fast due to that it is easy to find oxide particles on the fracture surface.

Fracture at the interface: Most of the zinc coating is on the magnesium sheet which looks like the zinc layer could be the weakest part of the welding. This sample is difficult to compare with others ones because of the different welding parameters. The effective sheet thickness (thickness of the magnesium sheet minus plunge depth of the shoulder) was lower compared to the other samples but the difference in the measured tensile strength is very low.

5.5 Investigation of the Crack Path

The investigation of the fracture path is very important for the optimisation of the welding parameters. Changes in grain size, grain orientation voids or particles have a big influence on the fracture path and fracture strength.

The sample with the optimal welding parameters, with the low welding speed and fracture path at the interface were investigated (see table **??**). The samples were polished with the ion beam polishing machine and investigated with SEM, EDS and EBSD. It was impossible to polish the sample at the fracture path because of the scattering ion beam at the fracture surface.

The sample with the fracture path at the interface (see welding parameters at table **??**) was investigated during the investigation of the interface.

5.5.1 Optimal Welding Parameters

The welding parameters for this sample were donated in table **??** which was the sample with the optimal welding parameters.

The sample fractured in the magnesium sheet. Due to that one part consists of the magnesium and the other consists of steel and magnesium. Figure **??** show the cross fracture path of the steel magnesium sample where the steel is on the top and figure **??** the magnesium sample of the fracture.
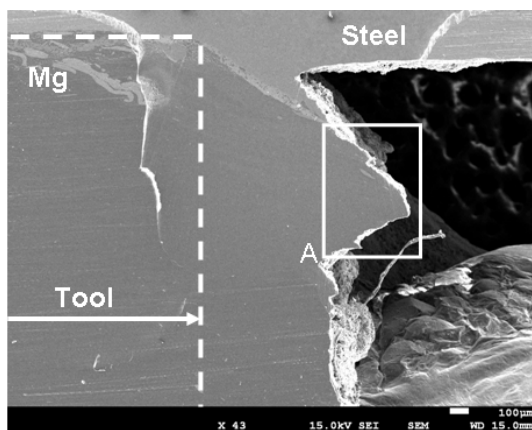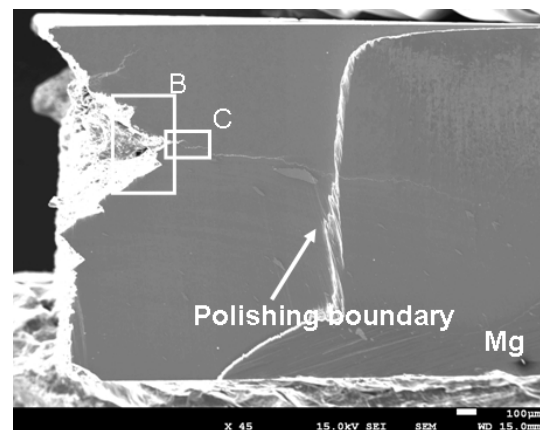

Figure 5.50: Fractured sample steel side

Figure 5.51: Fractured sample magnesium side

The crack path is at the top of the steel clamp. During the investigation of the cross section a magnesium - zinc layer was detected in the magnesium sheet. This layer was detected at the clamp as well but no higher zinc content was detected at the fracture path. The crack path is at the top of the

steel clamp. During the investigation of the cross section a layer consists of zinc and magnesium was detected in the magnesium sheet (see figure **??** and table **??**). This layer was detected at the clamp as well but no higher zinc content was detected at the fracture path. Figure **??** and **??** shows the pole figure of figure **??** and **??**. The orientation is about the same.

Figure **??** and **??** show the grain size and orientation of the grains which is on both sides of the fracture path about the same. On the top right of figure **??** the grains are bigger than on the other areas.
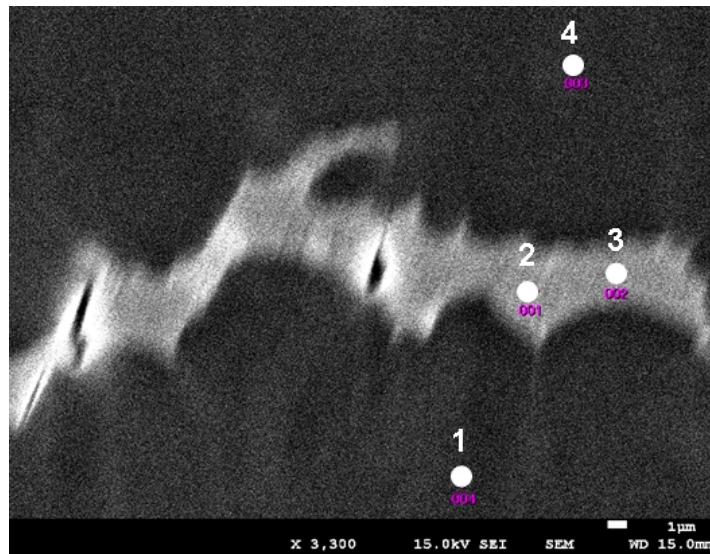

Figure 5.52: Detail C in figure **??**. The chemical composition at the EDS spots is given in table **??**

Table 5.4: EDS spots figure **??**

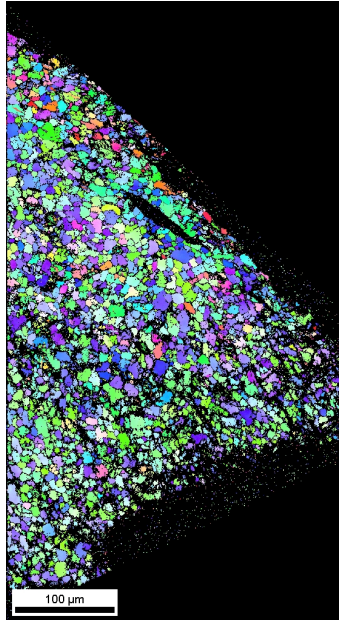| [wt.%]	Spot 1	Spot 2	Spot 3	Spot 4
Mg	46.45	47.74	96.79	95.43
Al	1.92	1.64	1.8	1.55
Fe	0.04	nd	0.11	0.15
Zn	51.53	50.37	1.3	2.72

Figure 5.53: Grain size and orientation steel side, detail A in figure **??**
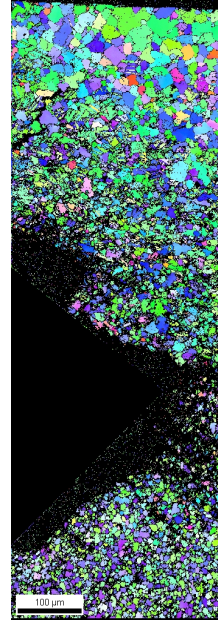

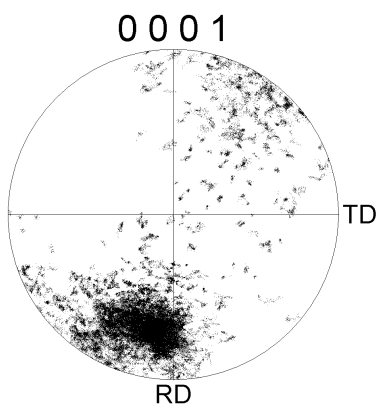Figure 5.54: Grain size and orientation magnesium side, detail B in figure **??**
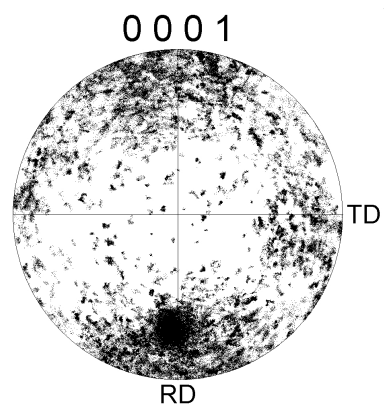

Figure 5.55: Pole figure of figure **??**

Figure 5.56: Pole figure of figure **??**

5.5.2 Low Welding Speed

The welding parameters for this sample were donated in table **??** which was the sample with the low weling speed parameters.

The crack starts at the clamp and grows through the magnesium sheet (see figure **??** and **??**). The grain size and grain orientation on the left and right-hand side of the fracture looks about the same (see figure **??**). No zinc layer could be detected and no higher zinc content could be identified at the fracture path. There are many iron particles around the fracture path but it looks like these particles have no influence on the fracture path.
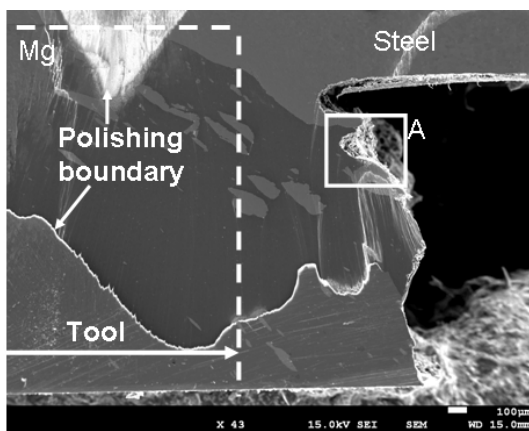

Figure 5.57: Fractured sample steel side
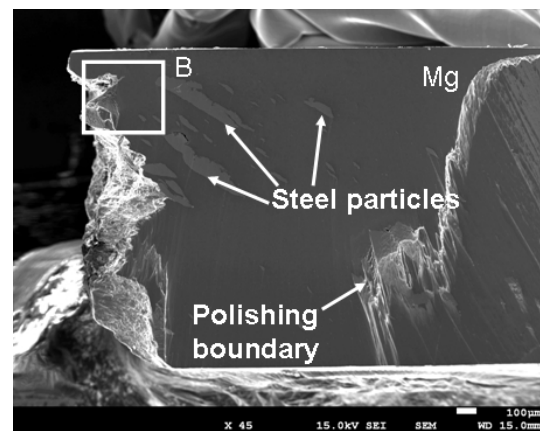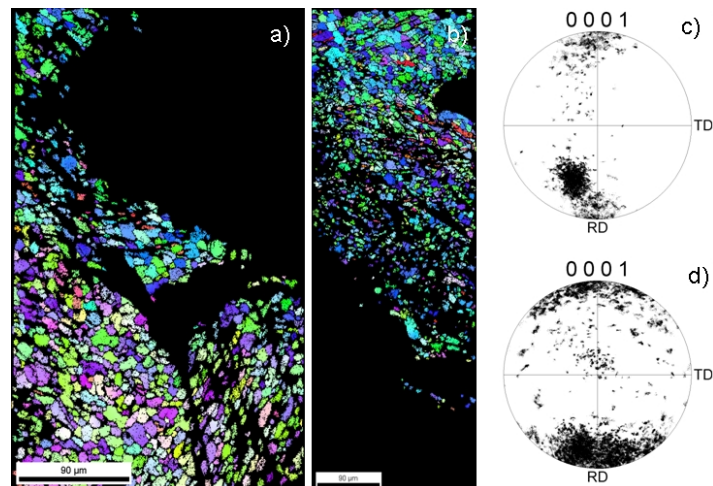
Figure 5.58: Fractured sample magnesium side

Figure 5.59: Grain structure and orientation, a) fracture steel side detail A in figure **??**, b) fracture magnesium side detail B in figure **??**, c) pole figure of a), d) pole figure of b)

5.5.3 Fracture at the Interface

The welding parameters for this sample were donated in table **??** which was the sample with the fracture at the interface speed parameters.

Figure **??** shows the magnesium sheet where the interface was on the bottom. The position of the clamp is easy to define and a layer near the clamp is a zinc - magnesium layer which gets thinner with the increasing distance to the centre of the stir zone. The stir zone is on the left-hand side. The crack starts at the top of the clamp and growth into the direction of the thickness of the material. Near the crack path some steel particles were detected. It looks like the steel particles have an influence on the crack path because there are small defects in the direction of steel particle. Figure **??** shows the grain orientation of detail A from figure **??** and the pole figure. The grain orientation is on both sides of the fracture path about the same and the pole figure shows a preferential orientation.
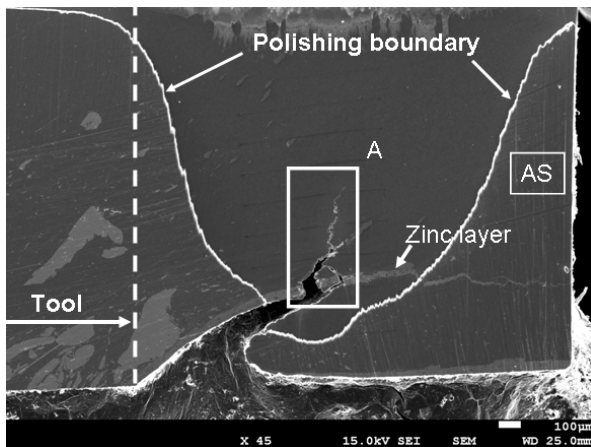
Figure 5.60: Fracture at the interface
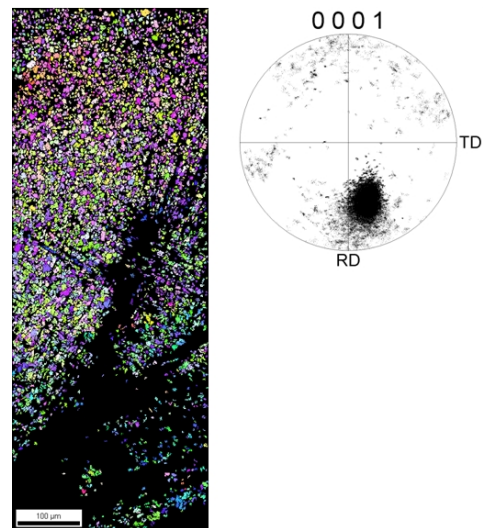
Figure 5.61: Grain size and orientation and the pole figure of detail A in figure **??**

Conclusion and Discussion of the Investigation of the Fracture Path

If the interface is strong, the crack starts at the top of the clamp and grow in thickness direction of the magnesium sheet. The top of the clamp is in the fracture path. Probably the clamp shape and length has a big influence on the tensile strength because of the stress concentration at the clamp top. For the investigated samples the load was on the advancing side. The clamp on the advancing side points

away from the stir zone and the clamp on the retreating side points into the stir zone.

The steel particles could have had an influence on the crack path due to voids around the steel particles but the influence of the zinc layer is not clear.

No change in the grain size around the fracture path or crack. It is very difficult to investigate a change of the grain orientation after a tensile test because the orientation changes during the tensile test and due to that it is necessary to investigate the grain orientation at a sample which was not influenced by the stress of the tensile test. To get more information why there is a difference in the measured strength of the grain orientation at the possible fracture path could answer this.

5.6 Investigation of the Clamp along the Joint Line

The investigation of the fracture path shows that the steel clamp has probably an influence on the fracture path and the strength of the joint. The steel clamp always was a part of the fracture path and the shape of the clamps was different. The clamp on the retreating side points into the stir zone and the clamp on the advancing side points out of the stir zone. Normally the clamp on the advancing side is smaller than the clamp on the retreating side.

To get more information about the shape of the clamp, the magnesium was removed. To remove the magnesium without destroying or change the shape of the clamp hydrochloric acid (HCl) was used. Because of the extremely generation of smoke and foam, the magnesium was only removed for a small sample. Figure **??** and figure **??** show the clamp from the top and from the front. This sample was welded with the following welding parameters:

- Welding speed: 150 mm/min

- Tool rotation: 1200 rpm

- Plunge depth: –0.15 mm

- Clamping distance: 40 mm

The welding direction was from the top down. The loaded advancing side is on the left side where the clamp is smaller. The clamp changes along the joint line.

Conclusion and Discussion of the Investigation of the Clamp

The clamp change it is shape along the joint line due to that it is very difficult to define the influence of the clamp on the fracture strength with only one sample. The change of the clamp was only
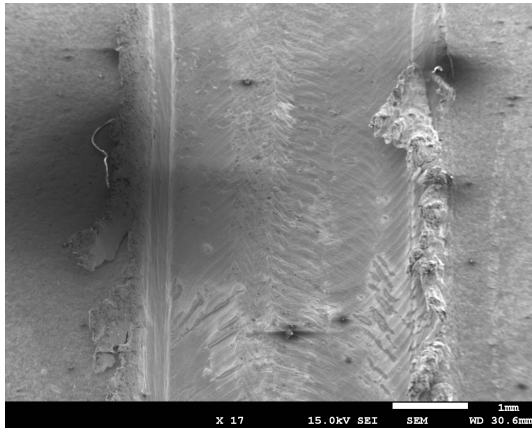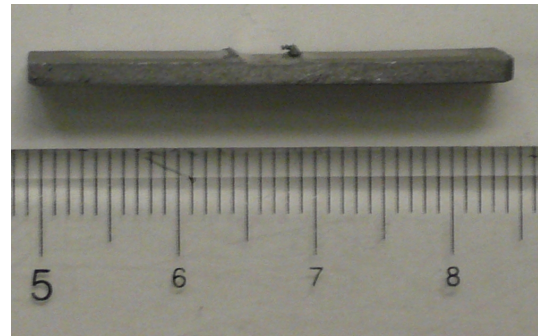
Figure 5.62: Top view of the clamps

Figure 5.63: Front view of the clamps

investigated for this small part but the change in shape of the clamp are detect for other welding parameters as well. During the parameter study the load on the retreating side and advancing side was compared (see chapter **??**).

The strength on the retreating side was 87MPa and on the advancing side the stress was 95MPa. Figure **??** and figure **??** shows a smaller clamp (lower notch effect) on the advancing side and probably this is the reason for the higher strength.

5.7 Investigation of the possible Fracture Path

This investigation is very important to get more information why the fracture path is at this position and why is a difference in the measured strength. The grain orientation, grain size and defects have a big influence on the strength. The different welding speeds could have had an influence on the grain orientation.

The possible fracture path was investigated for the sample with the optimal welding parameters which were the parameters with a low heat input per unit length, the sample with a high heat input and the sample which fractured at the interface. The difference to **??** "'Investigation of the Fracture Path"' is, that the tensile test had no influence on the grain orientiation.

5.7.1 Optimal Welding Parameters

The welding parameters for this sample were donated in table **??** which was the sample with the optimal welding parameters.

Figure **??** shows the clamp at the advancing side. The steel sheet is on the top and the stir zone on the left side. The joint interface is on the left hand side. The clamp points away from the stir zone and has a size of about 200 microns. The layer between the clamp and the magnesium is the zinc layer. On the right-hand side the steel and magnesium sheet were not joined but the zinc diffused in to the magnesium and the crack was between the zinc layer and the steel. Some steel particles are near the clamp.

Figure **??** shows the magnesium grains near the clamp and the pole figure of the area between the white lines. The grains top right are bigger than the other grains and the bigger part has a grain size of 7 microns. The pole figure for the area shows a preferential orientation of the grains.
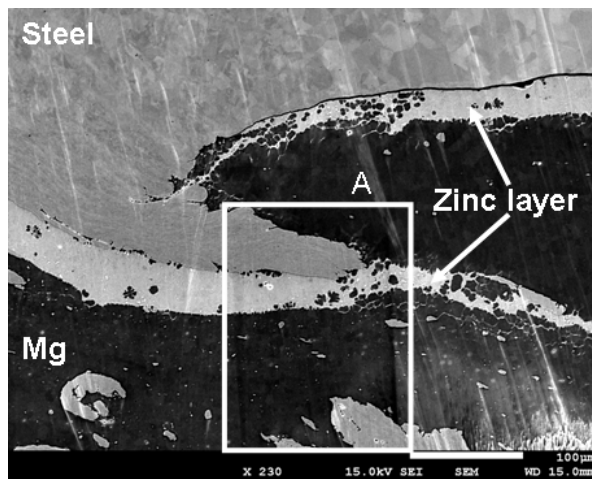

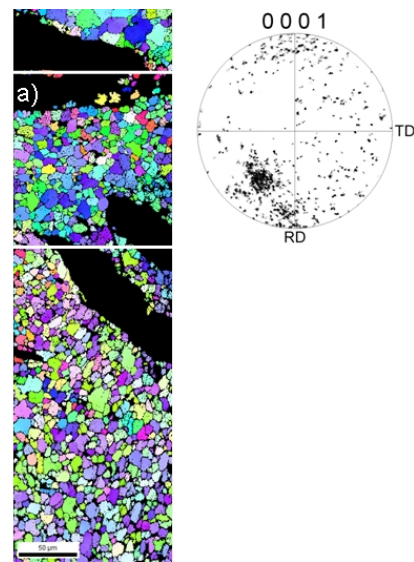Figure 5.64: Clamp at the advancing side

Figure 5.65: Grain orientation near the lamps and polefigure of detail A in figure **??**

5.7.2 Low Welding Speed

The welding parameters for this sample were donated in table **??** which was the sample with the low weling speed parameters.

Figure **??** a) shows the clamp on the advancing side. The steel sheet is on the top and the stir zone is on the left side. The clamp points away from the stir zone. There is no layer between the steel and the magnesium. Figure **??** b) shows the top of the clamp where a big pore is. The size of the pore is about 100 microns and the pore is not at the interface that means the pore is in the magnesium sheet. Figure **??** c) shows the grain structure near the clamp. The grains between the steel clamp and steel sheets are much bigger than the other grains because they are less deformed. Figure **??** d) shows the pole figure with a preferential orientation of the grains. The basal plan of the magnesium grain is more or less parallel to the interface.
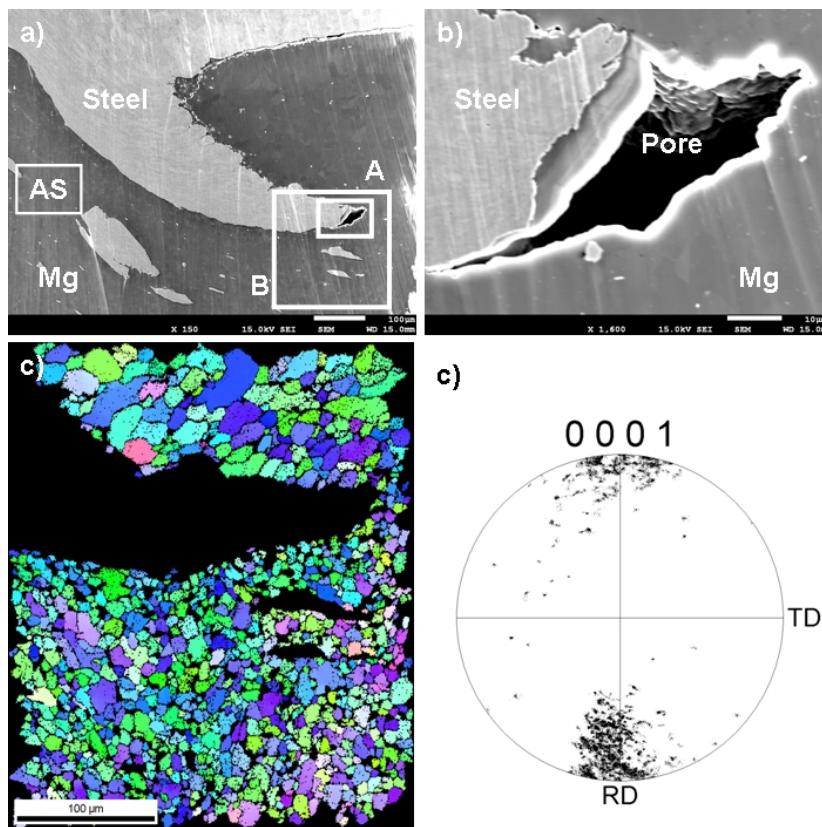

Figure 5.66: Clamp at the advancing side a)Overview, b) pore detail A in a), c) grain orientation detail B in a), d) polefigure

5.7.3 Fracture at the Interface

The welding parameters for this sample were donated in table **??** which was the sample with the fracture at the interface speed parameters.

Figure **??** shows the clamp on the advancing side. The steel is at the bottom and the stir zone is left-hand. The clamp points away from the stir zone. There are many defects at the interface which were one reason why the fracture path was at the interface. Figure **??** shows the magnesium grains, the colour code triangle and the pole figure. The grains are bigger between the steel clamp and the steel sheet and the basal plane of the magnesium is more or less parallel to the interface.
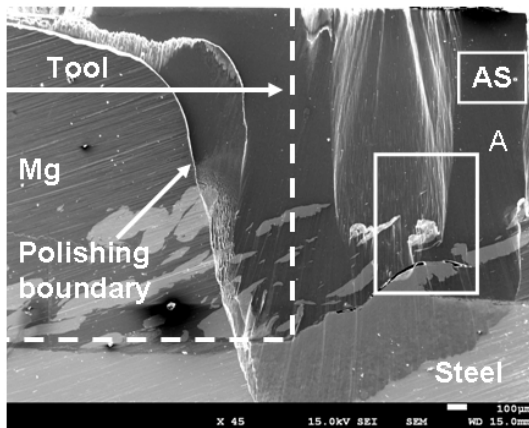

Figure 5.67: Clamp at the advancing side
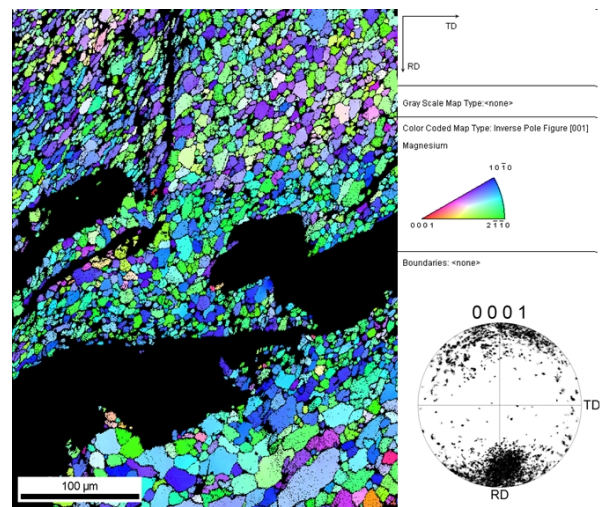
Figure 5.68: Grain size and orientation near the lamps, colour code triangle and pole-figure, detail A in figure **??**

5.7.4 Conclusion and Discussion

For the sample with the high welding speed no defect at the interface or at the possible fracture path were detect. Probably the zinc layer has a big influence or is on the fracture path.

The sample with the low welding speed has a big pore at the top of the clamp. This defect could be the reason why the measured strength is lower than for the sample with the high welding speed. The pole figures for these two samples look different. For the low welding speed (150 mm/min) the basal plane is more or less parallel to the interface but for the high welding speed (500mm/min) the grains tilt 30 degrees from the reference direction to the transversal direction and rotated on the transversal axis.

6 Additional Experiments and Investigations

Joining magnesium and steel is with many welding techniques impossible. It was possible to join magnesium and steel by friction stir welding but there are many open questions.

During the basic investigation zinc coated steel was used but the effect of the zinc is not clear. At the interface steel - magnesium a higher zinc content was detected. Is there a higher zinc content just because of the zinc coating or is higher zinc content at the interface necessary to join the samples? If the higher zinc content is necessary, would be the zinc form the magnesium alloy be enough or is an interlayer of zinc needed?

Zinc is a very important alloying element for magnesium alloys. Zinc improves the castability, improves the strength and acts as a grain refiner but increases the tendency for micro porosity and alloys with a zinc content higher than 3 wt.% has higher tendency to hot cracking [?].

6.1 FSW of Magnesium and uncoated Steel

The influence of the zinc coating on the interface strength is poorly investigated at the moment. Nakata et al. [?] investigated the effect of tool geometry on microstructure and mechanical properties of friction stir lap welded magnesium alloy and steel. They used a zinc coated steel and a brush finished steel for their investigation and reported that the fracture load was higher with a brush finished steel than with a zinc coated steel.

6.1.1 Experiment

To get more information about the zinc layer, some samples without zinc coating were welded by friction stir welding. The zinc coating was removed from the steel sheets to use the same base material. The welding parameters with the highest and lowest heat input per unit of length were used and the sample with a fracture path through the interface was investigated. The welding parameters were:

- Optimal welding parameters for zinc coated steel

- – Welding speed: 500 mm/min

- – Tool rotation: 1200 rpm

- – Plunge depth: –0.15 mm

- – Clamping distance 40 mm

- – Tensile strength: 120 MPa

- – Fracture in the stir zone

- • Low welding speed, high heat input

  - – Welding speed: 150 mm/min

  - – Tool rotation: 1200 rpm

  - – Plunge depth: –0.15 mm

  - – Clamping distance 40 mm

  - – Tensile strength: 96 MPa

  - – Fracture in the stir zone

- • Fracture at the Interface

  - – Welding speed: 300 mm/min

  - – Tool rotation: 900 rpm

  - – Plunge depth: –0.20 mm

  - – Clamping distance 40 mm

  - – Tensile strength: 107 MPa

  - – Fracture at the interface

6.1.2 Result

Three different samples were investigated by tensile test. The same tensile testing machine and sample preparation were used as for the samples with the zinc coated steel and the difference in strength was less than 2 MPa. The stress was calculated with the tickness of the base material. Table **??** shows the strength of the samples for the three different parameter conditions. All samples fractured at the stir zone which means that the interface is stronger than the measured value. The sample with the welding speed of 500 mm/min reached the highest strength.

Table 6.1: Fracture strength for the samples without and with zinc coating

	Optimal parameters	Low welding speed	900rpm
Strength without zinc coating	98MPa	78MPa	92MPa
Strength with zinc coating	120MPa	96MPa	107MPa

6.1.3 Metallography of the Interface

The samples were ion beam polished and investigated with EDS and EBSD.

Optimal Welding parameters

Figure **??** shows an EDS map of the interface. The steel sheet is at the top and the advancing side on the right hand side. The steel particles in the magnesium moved to the advancing side. No zinc could be detected at the interface.
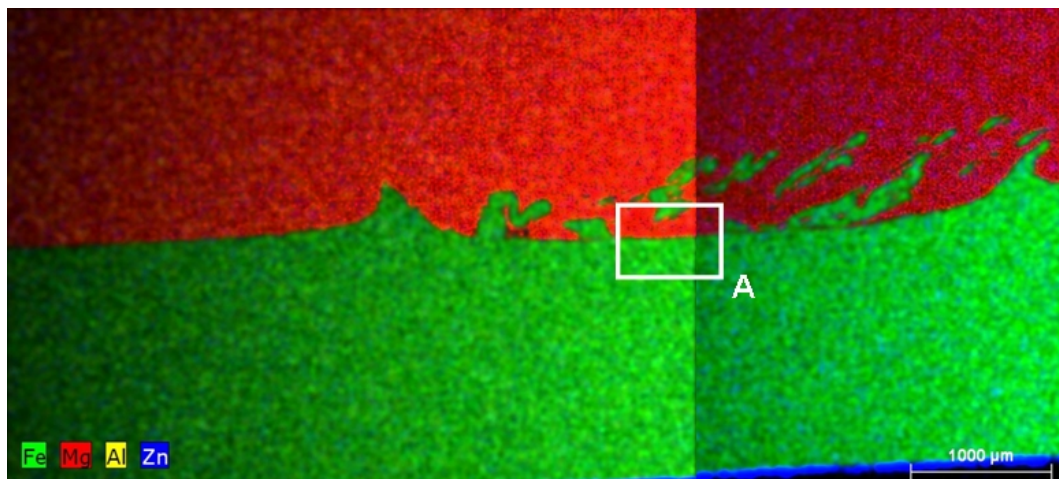

Figure 6.1: EDS map of the cross section

Figure **??**, detail A in figure **??** shows the interface in the stir zone. The top sheet is the steel sheet and the bottom sheet is the magnesium sheet. The advancing side is on the right-hand side. Some particles were in the stir zone and voids with a size less than 3 microns were detected. The voids are in the stir zone and not at the interface.

Figure **??** shows the EDS line scans over the interface. The steel sheet is at the top and the magnesium sheet is at the bottom. Diagram **??** and **??** show no higher content of aluminium or zinc at the interface. Line scan 2, figure **??** shows an area with a higher steel content in the magnesium sheet. The reason for the higher content are the steel particles in the magnesium sheet.
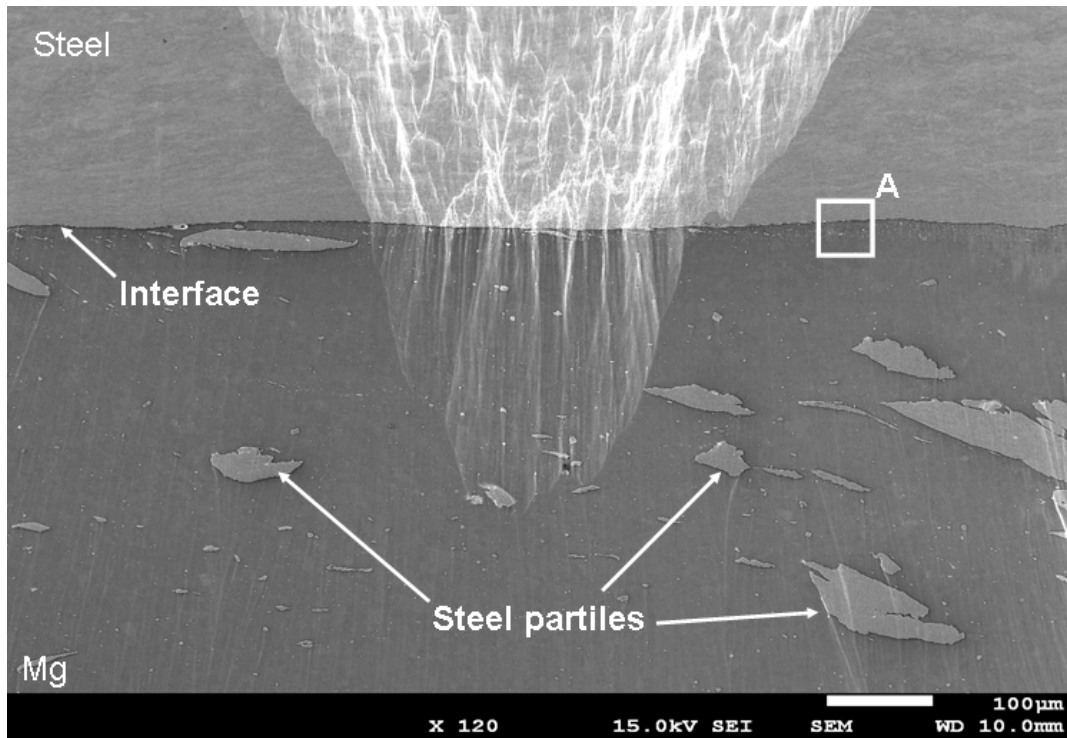
Figure 6.2: Interface for the welding speed 500 mm/min, detail A in figure **??**
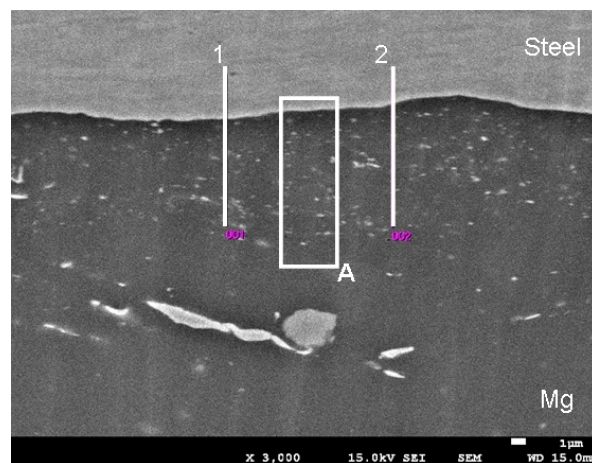
Figure 6.3: Cross section with EDS lines, welding speed 500 mm/min
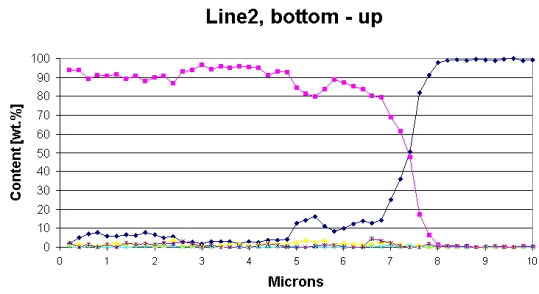
Figure 6.4: EDS line 1 from figure **??**
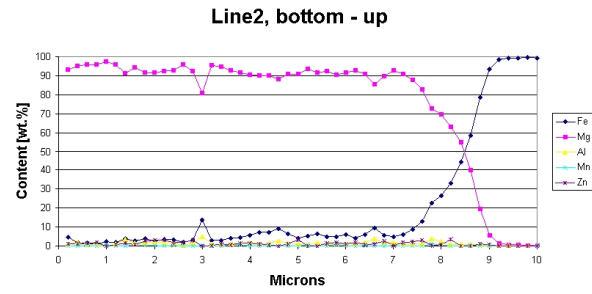
Figure 6.5: EDS line 2 from figure **??**

Figure **??** shows the grain orientation and pole figure of the magnesium sheet. The steel sheet is on top. At the interface is a layer with a thickness of about 20 microns with a grain size of about 1 micron. With a distance of 20 microns from the interface the grain size is about 15 microns. The pole figure shows a preferential orientation.

Figure 6.6: Grain structure and pole figure of detail A in figure **??**

Low Welding Speed and 900rpm

Only the sample with the highest welding speed was discussed. The figures for the samples with the lower welding speed (EDS cross section **??**, Interface **??**, EDS lines **??** and figure **??**, grain orientation **??**) and the sample which was welded with the 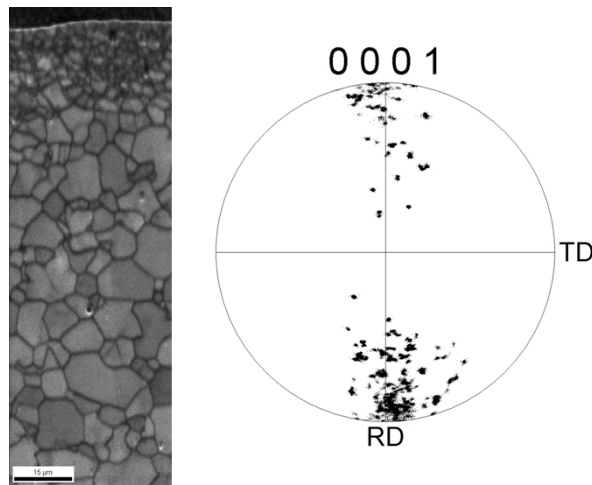tool rotation of 900 rpm (Interface **??**, EDS line scan **??**, grain orientation **??**) are in the appendix. Steel particles are in the stir zone. No zinc or aluminium could be detected at the interface. The grain size at the interface is not significant smaller than in the stir zone. All samples have voids with a size up to 30 microns.

6.1.4 Discussion

It is possible to join magnesium and steel without a interlayer of zinc. Some defects are in the stir zone but not at the interface. The reason for these defects could be the material flow in the stir zone. The sample with welding speed 500 mm/min was the best sample. The grain size at the interface is smaller than in the stir zone. All investigated areas had a preferential orientation of the grains in reference direction.

6.2 Diffusion Welding

The grains in the FSW stir zone were very small but the reason for the small grains is not clear. Due to the measurement of the temperature and the measurement of forge force from the FSW process all parameters for diffusion welding could be estimated.

For the diffusion welding process the Thermecmaster-Z (Fuji. Electric Ind. Co., Ltd.) was used which is a dilatometer that allows making simulations of thermo-mechanical treatments on small cylinder samples.

The cylindrical samples had a diameter of 8 mm and were cut out of the magnesium and steel sheets which were used for investigation by FSW. The magnesium was AZ31B-O and the steel was zinc coated. After the cutting process the thickness of the zinc coating was checked and it was about 15 microns which is the same as for the investigation. The FSW process is a welding process without inert gas. The welding took place at atmosphere pressure.

6.2.1 Experiment

Figure **??** and figure **??** in the appendix shows the FSW thermocycle from the measuring point at the interface. The measured peak temperature was 320 °C because of the distance of the thermocouple to the interface the lowest temperature was assumed to be 350 °C for the diffusion welding.

For the diffusion welding a pressure is required. The forge force for the welding speed 500 mm/min was about 7 kN and for the welding speed of 150 mm/min the forge force was 5 kN. These forces are not the peak forces at the beginning of the process but rather the forces during the middle and end of the joint seam. At the beginning the tool plunges into the magnesium and steel and because of that the forge force is very high. The used pressure for the diffusion welding was 100 MPa and 150 MPa. This pressure was set before heating up the samples. If a pressure of 100 MPa or higher act on samples which have a temperature of 350 °C, the samples would get destroyed. Due to the higher temperature the material gets softer and high pressure will deform the sample extremely.

Table **??** shows the thermocycles for the diffusion welding. Experiment 1 represents the welding speed of 500 mm/min, Experiment 2 stands for the welding speed of 150 mm/min and Experiment 3 was a modified experiment with a thermocycle for a welding speed of 150 mm/min but a higher pressure.

Table 6.2: Thermocycles for the diffusion welding

Experiment	1	2	3
Pressure	100MPa	100 MPa	150MPa
Peak tempterature	350 °C	450 °C	450 °C
Heating	50 °C per sec.	50 °C per sec.	50 °C per sec.
Holding time	0	0	0
Cooling to 200 °C	4 sec.	7 sec.	7 sec.
Cooling to 100 °C	7 sec.	18 sec.	18 sec.

6.2.2 Results

Sample 1 The peak temperature for sample 1 was 350 °C and the pressure 100 MPa. It was impossible to join this sample, the zinc did not melt and the sample was not investigated further.

Sample 2 The peak temperature of the thermocycle were increased. During the joining process the zinc layer melted and because of the pressure the zinc flowed out of the joining interface. This sample split during the preparation for the ion beam polishing process and due to that the sample was not investigated more.

Sample 3 The peak temperature was 450 °C and the pressure 150 MPa before heating up. During the joining process a big part of the zinc flows out of the interface. The interface is very weak due to the voids. Figure **??** shows a detail of the interface where the steel sheet is on top. Many voids are along the joint. The EDS line 1 scan over the interface shows an aluminium peak at the interface (see figure **??** and **??**). The layer at the interface has a lamellar micro structure. The grain size is of the magnesium grains is about 50 microns. (see figure **??**)

6.2.3 Conclusion and Discussion

It was impossible to join the sample with a peak temperature of 350 °C. After increasing the temperature to 450°C the zinc melts and it was possible to join it but the interface was very weak. The sample which was joined with a pressure of 100MPa fractured during the sawing. The third sample was possible to prepare for the investigation of the interface but the interface had many voids and looks very weak. 450 °C are definitely less than the melting temperature of the magnesium alloy which is about 650 °C. At the interface there is a layer with a lamellar micro structure which is eutectic. This layer is a product of the diffusion from the zinc into the magnesium which decreases the melting point and
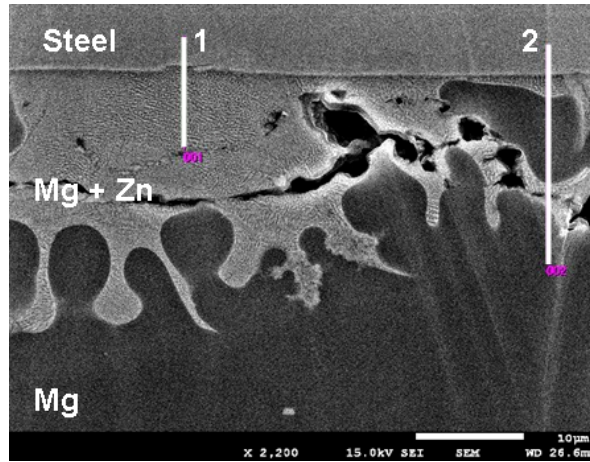
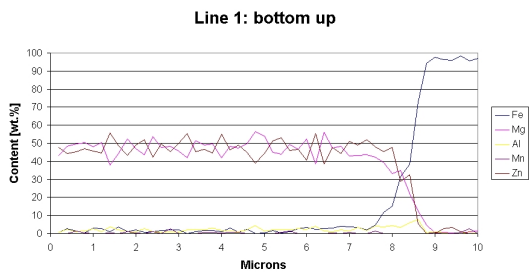Figure 6.7: Interface of the diffusion welded sample 3
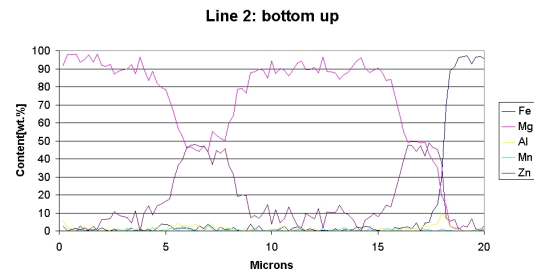

Figure 6.8: EDS line 1 from figure ??
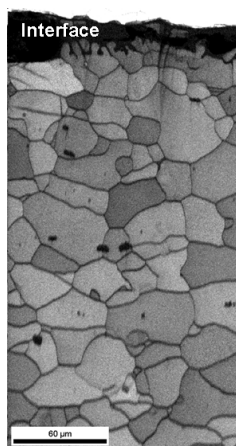

Figure 6.9: EDS line 2 from figure ??

Figure 6.10: EBSD of diffusion welded magnesium sheet shows the grains with a size of about 50 microns

make it is possible to melt.

Figure **??** shows the measured thermocycle and the force acting on sample 3. At the beginning, the force was set to 8.25kN to get a pressure of 150 MPa at the interface. It is impossible to have a pressure of 150MPa during the welding process because the samples would flow away. At the beginning the pressure increases with increased temperature but after reaching about 200 °C the pressure decreases very fast. This means that at peak temperature the pressure is much lower than 150MPa. The pressure is about 20MPa at peak temperature.
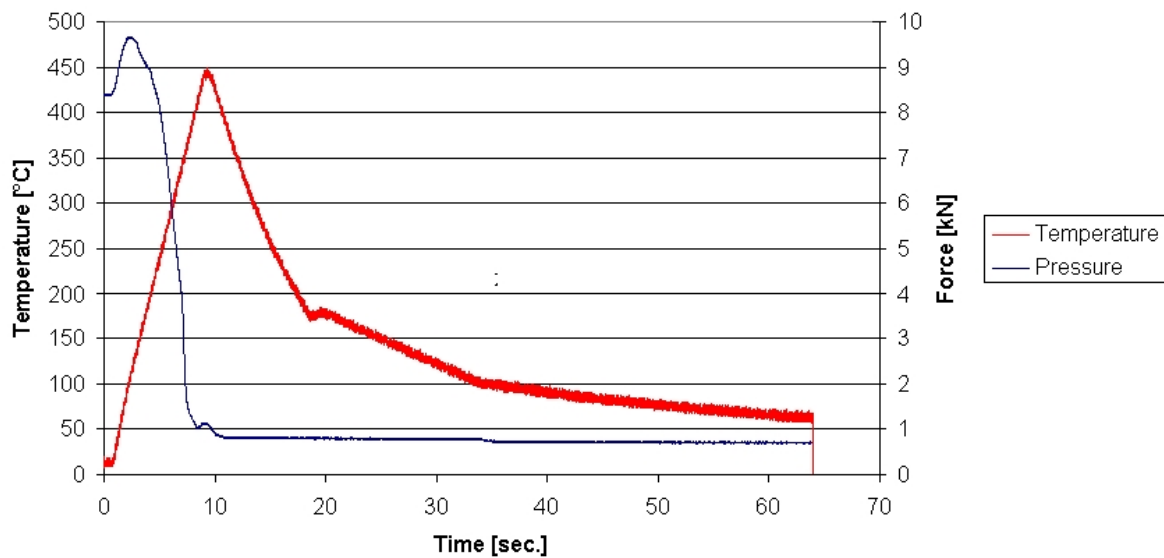
Figure 6.11: Diffusion welding: pressure and temperature over the time.

There are many differences between FSW and diffusion welding. The heating up rate is much higher by FSW and the pressure at high temperature at the interface is probably higher by FSW as well. A higher pressure at high temperature at the interface is probably only possible because of the material flow in the stir zone. The line scan shows a higher content of aluminium but for the FSW sample it was a higher zinc content. The grain size is much bigger at the diffusion welded sample; this means that the influence of the zinc on the grain size could only be very low.

7 Conclusion and Discussion

In this thesis, zinc coated steel and a magnesium alloy were joined by FSW and investigated. To study the influence of zinc some samples were joined without zinc coating and in order to get more information about the stirring process of FSW some experiments with diffusion welding were done.

7.1 Friction Stir Welding and Parameters Study

The friction stir welding process has different welding parameters which have different influence on the quality of the joint. The parameter study started with parameters from the literature and during the investigation only one parameterat a time was changed.

It was not the goal of this thesis to find the best welding parameters for this material combination, but rather to join two totally different materials and investigate the interface to describe mechanisms.

During the parameter study different parameter combinations were tested with a shear tensile test. The most of the combinations were tested only once. The key parameters (1200 rpm, 150 mm/min or 500 mm/min, –0.15mm) were tested up to 5 times but the differences in the strength were less than 5%.

For overlap welding the bending moment has a big influence on the strength due to the fact that the measured strength is always a combination of different stresses. To compare the different samples the strength was calculated with the cross section of the base material. The cross section of the base material was reduced by the plunge depth of the shoulder and the clamp. If the strength would be calculated with the real thickness the values would be up to 15% higher.

The optimal parameter combination found after the parameter study were:

- Tool rotation: 1200 rpm

- Welding speed: 500 mm/min

- Plunge depth: –0.15 mm

- Distance of clamping: 40 mm

The friction stir welding process is well known as a solid state joining process which is easily repeatable. Friction stir welding is a computer controlled joining process but that means not that the parameters on the screen are the real parameters. During the investigation with welding speeds higher than 500 mm/min the welding process got unstable which means that the plunge depth was not constant along the joint line.

7.2 Interface

The investigation of the interface after mechanical polishing or etching was not possible due to the oxide layer at the interface was too big or the surface was too rough and /or the confidential index of EBSD was too low. To investigate the interface cross section the samples were polished with ion beam polishing and afterward SEM, EDS and EDSB were used.

The grain size in the base material was about 25 microns and the grains have a preferential orientation in rolling direction. During the FSW process with the zinc coated steel the grains refined to a size of 7 microns. It is very difficult to polish at the same place of each sample at the interface and because of that it is not possible to compare the grain orientation.

In all investigated samples steel particles and aluminum particles were detected. The size of the steel particles and the number of particles increases with increasing welding speed and increasing plunge depth.A lower welding speed means a higher heat input which makes the material softer and due to this the particles are smaller. With increasing tool rotation the particles are getting smaller.

For a higher welding speed (500 mm/min) which means lower heat input per unit length, the zinc diffused into the magnesium sheets and reduced the melting temperature of the of the magnesium - zinc alloy, due to that the magnesium zinc layer melted during the joining process. This layer had a lamellar micro structure.

Firouzdour et al. [**?**] investigated Al - to - Mg friction stir welding, effect of positions of Al and Mg

with respect to the welding tool. They reported that aluminum diffused into Mg which reduced the melting temperature and due to that a melted area was at the interface. This is the same effect as in this investigation but with different elements.

At some areas magnesium at the interface and in other areas the magnesium - zinc layer was at the interface. The magnesium at the interface and the magnesium particles in the layer were segregations from the melted magnesium - zinc alloy. The process temperature was higher than the about 330°C which is the eutectic temperature of magnesium zinc. The measured temperature was about 320°C but this was about 4 mm away from the interface and on the retreating side.

During the investigation of the interface, the stir zone was assayed and a line with many cracks parallel to the interface was detected. An EBSD map over this crack shows different orientation of the grains which could be an indication that this sample was stirred too less, that means the parameter for the welding speed, tool rotation or the shape of the tool was wrong. The cracks influence on measured strength is very low because the weakest point was not in the stir zone and the crack was parallel to the stress direction.

For a low welding speed (150 mm/min) which means a high heat input per unit length the eutectic magnesium - zinc alloy flow out of the joining area and no eutectic zinc layer was at the interface only a higher amount of zinc could be detected at the interface. No defects were detected at the interface or in the stir zone.

A sample was investigated which fractured at the interface because the fracture strength of 103 MPa was very high. The steel particles in this sample were much larger than in the other investigated samples. The reason for this is the deeper plunge depth of 0.2 mm into the steel. The other samples had a plunge depth of 0.15 mm. At the interface there were many defects due to that the fracture path was at the interface.

7.3 Fracture Investigation

The fracture surface, the fracture path and the possible fracture path were investigated during this study.

Fracture surface: The fracture at the interface showed that magnesium - zinc alloy was flowing out of the joining area. Some big magnesium - zinc particles were at the joining area. The Fracture surface at the stir zone showed that the big part fractured due to shear but small areas were ductile or brittle.

Fracture Path The fracture path of only one sample with a fracture path through the interface was investigated because this sample had compared to the other samples relatively high fracture strength. Near the clamp there were cracks which mean that this sample would fracture at the clamp if the interface would be stronger.

The samples with the high (150mm/min) and low heat (500mm/min) input fractured at the stir zone and the fracture starts always from the clamp. During the tensile test, the bending moment is higher at the clamp than on the top of the magnesium sheet. No differences in grain size and grain orientatoin could be detected. The clamps on the advancing side pointed away from the stir zone and the clamps on the retreating side pointed toward the stir zone.

Along a joint line the shape of the clamps changes and this is could be one reason why the measured strength varied. For the low welding speed a pore at the top of the clamp was detected which could be the reason for the difference in the fracture strength. For the higher welding speed no defects at the possible fracture path were detected but the zinc layer was at the clamp and the effect of the zinc layer is not clear.

7.4 Additional Experiments

FSW of magnesium and uncoated steel
Only the three different welding parameters (500 mm/min, 150 mm/min and tool rotation 900rpm) which were investigated in detail were welded. All samples fractured in the stir zone which means that the interface is stronger than the stir zone.

For The samples with the steel sheet without zinc coating, the fracture strength was about 15 percent lower than than with zinc coating (see table **??**). The grain size in the sample with the zinc coated steel was 7 microns but during the investigation without zinc coating the grain size was 15 microns. At the interface no interlayer was detected.

Diffusion Welding

With the Thermecmaster-Z it was tried to join the magnesium and steel sample with diffusion welding. For this investigation small cylinders with a diameter of 8 mm were cut out of the same sheets which were used for FSW. Due to that the zinc layer and the chemical composition was the same. For the joining process the thermo cycles from the FSW was used.

It was impossible to join the samples with the thermo cycles from the high welding speed (500mm/min). After increasing the pressure and temperature it was possible to join the samples but many defects were at the interface. The grain size was much bigger than in the base material. The grain size in the base material was about 20 microns and in the diffusion welded sample the size was 50 microns.

The grain size from the FSW joined sample where zinc coated steel was used had a grain size of about 7 microns. The EDS lines over the interface showed an aluminium peak at the interface. All EDS lines over the FSW interfaces showed a zinc peak or non interlayer

7.5 Influence of Zinc

Zinc is the reason for melting during the FSW process. Zinc diffused into the magnesium and due to that the melting temperature decreased and the magnesium - zinc alloy melted. Without zinc no melting during the friction stir welding was detected. The eutectic melted zinc layer at the interface filled up pores and other defects and this could be the reason why the fracture strength with a zinc layer in the stir zone is higher. If the heat input and/or the stirring was too extensive, the magnesium zinc alloy flows out of the joining interface and the pores were at the advancing side. No signs that the zinc layer was weaker than the magnesium sheet could be detected.

The grain size was for the samples with zinc layer about 7 microns and for the samples without zinc layer about 15 microns. The difference between these samples was only the zinc layer, this means that the zinc layer had an influence on the grain size.

Zinc as alloying element in magnesium alloys refines the grains but there is an eutectic magnesium zinc layer at the interface or the eutectic alloy flows out of the joining area. Zinc particles could act as nuclides but the influence from the zinc on the grain size is not clear. The investigation of the grain size was just a two dimensional investigation which means that the shape in the third direction is not clear.

7.6 Influence of the Welding Speed

Most of the investigation was done with a tool rotation of 1200 rpm and the welding speed was varied. With an increased welding speed the heat input and stirring per unit length decreased. If the heat input and the stirring per unit length is high, the eutectic magnesium - zinc alloy flows out of the joining interface. The deformation of magnesium is only possible by shear in the basal plane due to that the liquid layer should remain in the joining area to reduce the deformation of magnesium and fill up the pores at the interface.

The grain orientation at the advancing clamp was investigated for the possible fracture path and the orientation was different for a different welding speed which means that the welding speed has an influence on the grain orientation. The influence from the welding speed on the orientation is not clear.

7.7 Outlook

At the moment, many different universities and companies are researching at joining magnesium and steel with different techniques. Some techniques were under shilding gas or vacuum and very time consuming. Friction stir welding is one of the fastest joining techniques but the results are not good investigated to other techniques at the moment. One result of this investigation is that the weakest point was not at the interface. To reduce the defects the welding parameters or tool shape could be changed to get a better material flow. A FEM-simulation of the tensile test and material flow would be interesting for tool development in future.

During this investigation the clamp had a big influence on the fracture path and probably on the fracture strength as well. Figure **??** shows an idea how to reduce the influence of the clamp. It is a kind of multi - pass welding by friction stir welding. The first pass is like the passes done during this investigation. This means the tool plunges into the steel and joins steel and magnesium together. During this process a clamp was produced but this clamp has a negative influence on the strength. Due to that the second pass reduced or destroy this clamp. The second pass is displaced to the first path and the tool plunges only into the magnesium and mills the clamp away. A positive secondary action is that the joining area between steel and magnesium gets larger. This would be only necessary on the loaded side.

Reynold et al. [**?**] investigated the multi-pass friction stir welding in alloy 7050-T7451: Effects on weld response variables and on weld properties. They reported that the tensile strength and hardness
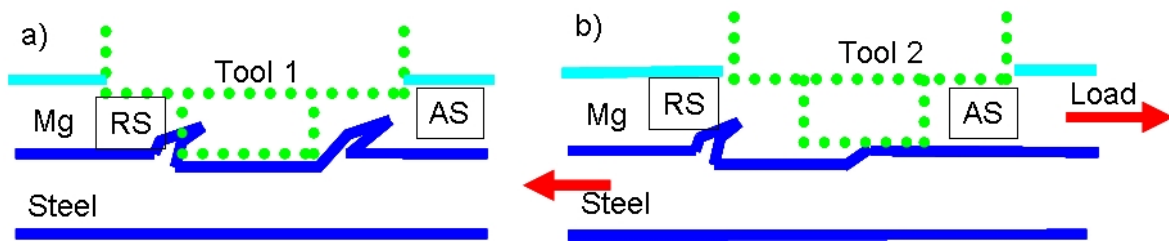
Figure 7.1: Multi pass FSW, a) first pass, b) second pass

were reduced with increasing welding pass number. The tensile strength decreases from the first to the second pass less then 5 %. This investigation was for aluminum and the effect of multi pass friction stir welding on magnesium is not investigated today.

The eutectic magnesium - zinc layer, the grain orientation in the stir zone, the influence of zinc on the grain size is not fully understood today and should be investigated in more detail in further works.

List of Figures

List of Tables

Bibliography

[1] N. Afrin, D.L. Chen, X. Cao, and M. Jahazi. Microstructure and tensile properties of friction stir welded AZ31B magnesium alloy. *Materials Science and Engineering: A*, 472(1-2):179 – 186, 2008.

[2] M. Aonuma and K. Nakata. Effect of alloying elements on interface microstructure of Mg-Al-Zn magnesium alloys and Titanium joint by friction stir welding. *Materials Science and Engineering: B*, 161(1-3):46 – 49, 2009.

[3] Rohr L. Befford O. Magnesium - Verbundwerkstoff neue Leichtbaukonzepte für das angehende Jahrhundert. *Nachhaltige Material- und Systemtechnik*, pages 21–28, 2001.

[4] Boron and Ultra high Strength Steel. Boron and Ultra-high Strength Steel. Website, March 2010. `http://www.boronextrication.com/search/label/Magnesium`.

[5] R Brown, W. Tang, and A.P. Reynolds. Multi-pass friction stir welding in alloy 7050-T7451: Effects on weld response variables and on weld properties. *Materials Science and Engineering A*, 513-514:115 – 121, 2009.

[6] Kammer C. *Magnesium Taschenbuch*. Aluminium Verlag Marketing & Kommunikation GmbH, 1 edition, 2000.

[7] X. Cao and M. Jahazi. Effect of welding speed on the quality of friction stir welded butt joints of a magnesium alloy. *Materials & Design*, 30(6):2033 – 2042, 2009.

[8] S. Carabajar, J. Merlin, V. Massardier, and S. Chabanet. Precipitation evolution during the annealing of an interstitial-free steel. *Materials Science and Engineering A*, 281(1-2):132 – 142, 2000.

[9] Center for Research in Computational Thermochemistry. Phase diagram. Website, Mai 2010. `http://www.crct.polymtl.ca/fact/documentation/SGTE/SGTE_Figs.htm`.

[10] Y.C. Chen and K. Nakata. Friction stir lap joining aluminum and magnesium alloys. *Scripta Materialia*, 58(6):433 – 436, 2008.

[11] Y.C. Chen and K. Nakata. Effect of tool geometry on microstructure and mechanical properties of friction stir lap welded magnesium alloy and steel. *Materials & Design*, 30(9):3913 – 3919, 2009.

[12] L. Commin, M. Dumont, J.-E. Masse, and L. Barrallier. Friction stir welding of AZ31 magnesium alloy rolled sheets: Influence of processing parameters. *Acta Materialia*, 57(2):326 – 334, 2009.

[13] F. Czerwinski. *Magnesium Injection Molding*. Springer, 12 edition, 2000.

[14] DIN. DIN 1729 1, Magnesiumlegierungen Knetlegierungen. *DIN Standart*, 1982.

[15] DIN. DIN EN 10327,Continuously hot-dip coated strip and sheet of low carbon steels for cold forming. *DIN Standart*, 2004.

[16] M. Ericsson, Lai-Zhe Jin, and R. Sandström. Fatigue properties of friction stir overlap welds. *International Journal of Fatigue*, 29(1):57 – 68, 2007.

[17] W.M. Thomas et al. Friction welding. United States Patent Number: 5,460,317, Ocotber 1995. US005460317A.

[18] V. Firouzdor and S. Kou. Al-to-Mg Friction Stir Welding: Effect of Positions of Al and Mg with Respect to the Welding Tool. *Supplement to the Welding Journal*, 88:213–224, 2009.

[19] MgF Magnesium Flachprodukte GmbH. Anwendungen. Website, Ocotber 2009. `http://thyssenkrupp-mgf.com/de/anwendungen/index.jsp`.

[20] Cantin G.M.D, David S.A., Thomas W.M., Lara-Curzio E., and Babu S.S. Friction Skew-stir welding of lap joints in 5083 0 aluminium. *Science and Technology of Welding & Joining*, 10(3):268 – 280, 2005.

[21] OMEGA Engineering INC. Thermocouples an introduction. Website, January 2010. `http://www.omega.com/thermocouples.html`.

[22] S. F. James. *Introduction to materials science for engineers*. Macmillan Publishing Company, 3 edition, 1992.

[23] Callister William D. Jr. *Material Science and Engineering, An Introduction.* Wiley-VCH, 7 edition, 2007.

[24] A. Kostka, R.S. Coelho, J. dos Santos, and A.R. Pyzalla. Microstructure of friction stir welding of aluminium alloy to magnesium alloy. *Scripta Materialia*, 60(11):953 – 956, 2009.

[25] K. N. Krishnan. On the formation of onion rings in friction stir welds. *Materials Science and Engineering A*, 327(2):246 – 251, 2002.

[26] I. Kusnir. Magnesium metal, its perspectives. *Acta Montanistica Slovaca*, 7:119–121, 2002.

[27] Y.J. Kwon, I. Shigematsu, and N. Saito. Dissimilar friction stir welding between magnesium and aluminum alloys. *Materials Letters*, 62(23):3827 – 3829, 2008.

[28] Cederqvist L. and Reynolds A. P. Factors affecting the properties of friction stir welded aluminum lap joints. *Welding Journal*, 80(12):281 – 287, 2001.

[29] T. Laser, M.R. Nürnberg, A. Janz, Ch. Hartig, D. Letzig, R. Schmid-Fetzer, and R. Bormann. The influence of manganese on the microstructure and mechanical properties of AZ31 gravity die cast alloys. *Acta Materialia*, 54(11):3033 – 3041, 2006.

[30] C. Liu, D.L. Chen, S. Bhole, X. Cao, and M. Jahazi. Polishing-assisted galvanic corrosion in the dissimilar friction stir welded joint of AZ31 magnesium alloy to 2024 aluminum alloy. *Materials Characterization*, 60(5):370 – 376, 2009.

[31] O. T. Midling and G. Rorvik. Effect of tool shoulder material on the heat input during friction stir welding. *1st International Symposium on Friction Stir Welding*, 1(1), 1999.

[32] R.S. Mishra and Z.Y. Ma. Friction stir welding and processing. *Materials Science and Engineering: R: Reports*, 50(1-2):1 – 78, 2005.

[33] Mahoney M. W. Mishra R.S. *Friction Stir Welding and Processing.* ASM International, 1 edition, 2007.

[34] R. Nandan, T. DebRoy, and H.K.D.H. Bhadeshia. Recent advances in friction-stir welding - Process, weldment structure and properties. *Progress in Materials Science*, 53(6):980 – 1023, 2008.

[35] Y. S. Sato, S. H. C. Park, M. Michiuchi, and H. Kokawa. Constitutional liquation during dissimilar friction stir welding of Al and Mg alloys. *Scripta Materialia*, 50(9):1233 – 1236, 2004.

[36] A. C. Somasekharan and L. E. Murr. Microstructures in friction-stir welded dissimilar magnesium alloys and magnesium alloys to 6061-T6 aluminum alloy. *Materials Characterization*, 52(1):49 – 64, 2004.

[37] P. Bala Srinivasan, R. Zettler, C. Blawert, and W. Dietzel. A study on the effect of plasma electrolytic oxidation on the stress corrosion cracking behaviour of a wrought AZ61 magnesium alloy and its friction stir weldment. *Materials Characterization*, 60(5):389 – 396, 2009.

[38] ASTM Standart. AASTM A275 / A275M - 08 Standard Practice for Magnetic Particle Examination of Steel Forgings. *ASTM Standart*, 2008.

[39] ASTM Standart. ASTM B296, Standard Practice for Temper Designations of Magnesium Alloys, Cast and Wrough. *ASTM Standart*, 2008.

[40] U.F.H.R. Suhuddin, S. Mironov, Y.S. Sato, H. Kokawa, and C.-W. Lee. Grain structure evolution during friction-stir welding of AZ31 magnesium alloy. *Acta Materialia*, 57(18):5406 – 5418, 2009.

[41] K. Wierzbzanoski, A. Baczmanski, P. Lipinski, and A. Lodini. Elasto-plastic models of polycrystalline material deformation and their applications. *Archives of Metallurgy and Materials*, 52(1):77 – 85, 2007.

[42] W. Woo, H. Choo, M.B. Prime, Z. Feng, and B. Clausen. Microstructure, texture and residual stress in a friction-stir-processed az31b magnesium alloy. *Acta Materialia*, 56(8):1701 – 1711, 2008.

[43] J. Yang, B.L. Xiao, D. Wang, and Z.Y. Ma. Effects of heat input on tensile properties and fracture behavior of friction stir welded mg-3al-1zn alloy. *Materials Science and Engineering: A*, 527(3):708 – 714, 2010.

[44] H. Zhang, S.B. Lin, L. Wu, J.C. Feng, and Sh.L. Ma. Defects formation procedure and mathematic model for defect free friction stir welding of magnesium alloy. *Materials & Design*, 27(9):805 – 809, 2006.

List of Symbols

AS	Advancing side
$ASTM$	American Society for Testing Materials
$at.\%$	Atomic Percent
BCC	Body Center Cubic
DIN	German Institute for Standardization (Deutsches Institut für Normung)
$EBSD$	Electron Back Scatter Diffraction
EDS	Energy Dispersive X-ray Spectroscopy
IPF	Inverse Pole Figure
FSW	Fricton Stir Welding
HAZ	Heat affected zone
HV	Vickers hardness
IF	Interstitial Free
IWS	Institute of Material Science and Welding at Graz University of Technology
RD	Reference Direction
rpm	Rotation per Minute
RS	Retreating side
SEM	Scanning Electron Microscopy
TD	Transverse Direction
$TMAZ$	Thermomechanically affected zone

TWI The Welding Institute

$wt.\%$ Weight Percentt

A Appendix

A.1 Used Equipments

Tensile Test Machine

The tensile testing machine at IWS was a produced by Zwick Roell type RMC 100. The tensile specimens were 40mm wide. The sampling was 35 to 75mm from the beginning of the weld joint. The tensile tests were made on the base of ISO 6892-1:2009 (Metallic materials - Tensile testing - Part 1: Method of testing at room temperature) and ISO 14273:2000 (Specimen dimensions and procedure for shear testing resistance spot, seam and embossed projection welds). The testing speed was 0.1 mm/min. The force and the path of the traverse were measured.

Hardness Testing Machine

For the characterization of the joint, a hardness measurement was necessary. The hardness testing machine at IWS was an EMCOTEST hardness testing machine type M1C 010. The hardness testing machine was calibrated for Vickers hardness HV1. For measuring the hardness at University of Tokyo the testing machine was a Shimadzu HMV-2 which was calibrated for HV 0.1. Both measurements took place at room temperature and were according to ISO 6507 -1:2005(Metallic materials - Vickers hardness test). The load duration was 10 seconds.

Ion Beam Polishing

For investigations with SEM the samples were ion beam polished with the JOEL SM-09010 cross section polisher.

SEM

For the investigation of the fracture surface and cross section a SEM type LEO 1450VP with EDS detector at Graz, University of Technology was used. At the University of Tokyo a SEM type JEOL JSM 7001FA with EDS detector and EBSD system was used.

A.2 Additional Figures

A.2.1 FSW of Magnesium and uncoated Steel: Low welding speed
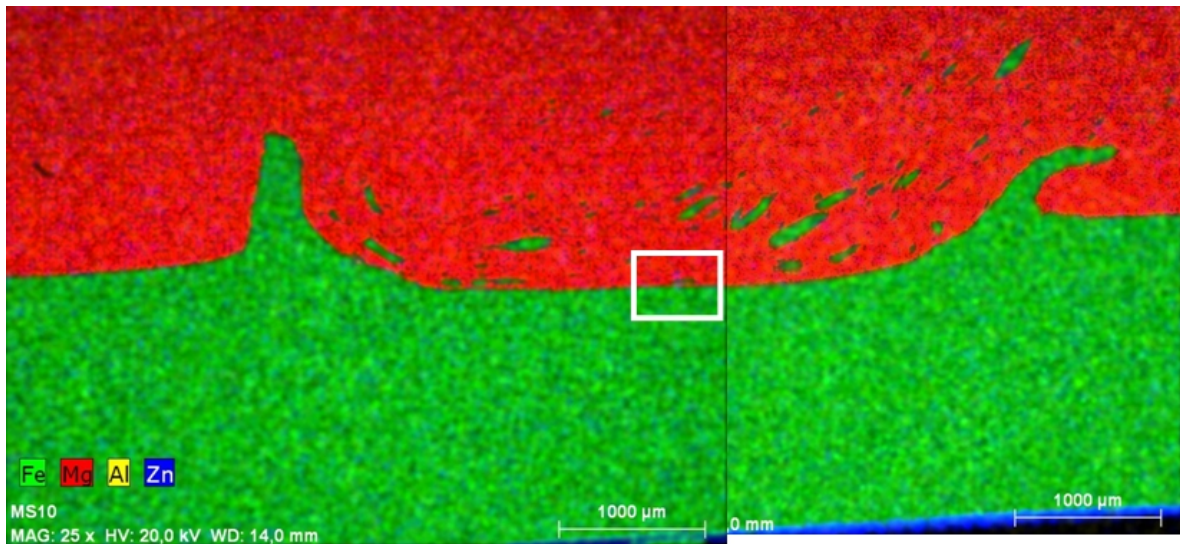
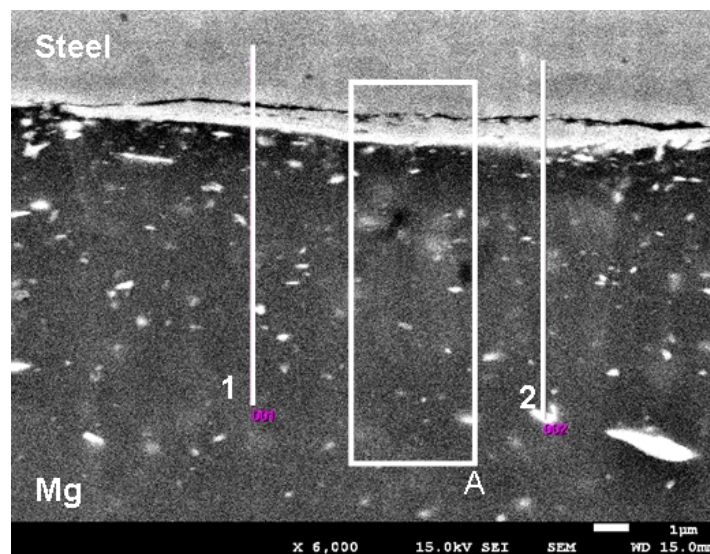Figure A.1: EDS map of the cross section, low welding speed

Figure A.2: Interface with EDS lines, low welding speed, detail A in figure **??**
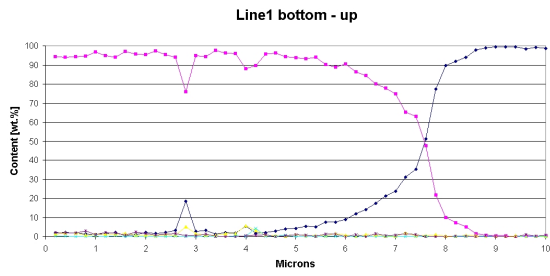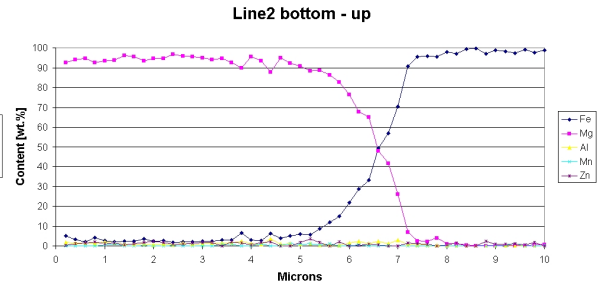
Figure A.3: EDS line 1 of figure **??**
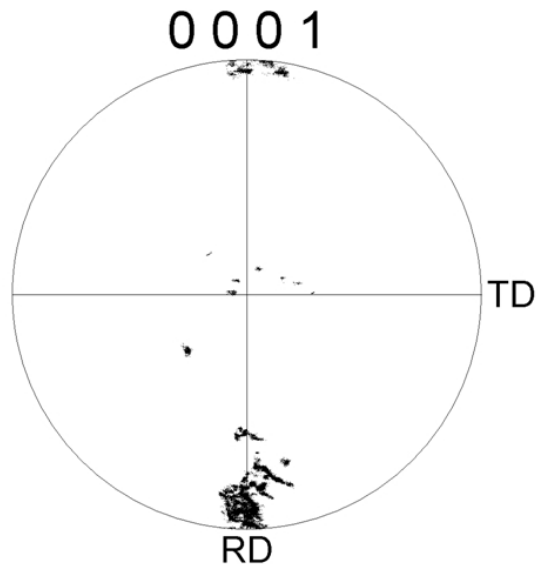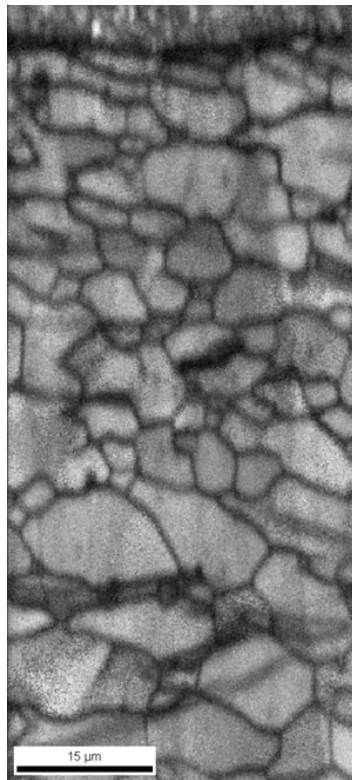

Figure A.4: EDS line 2 of figure **??**

Figure A.5: Grain structure and pole figure, low welding speed, detail A in figure **??**
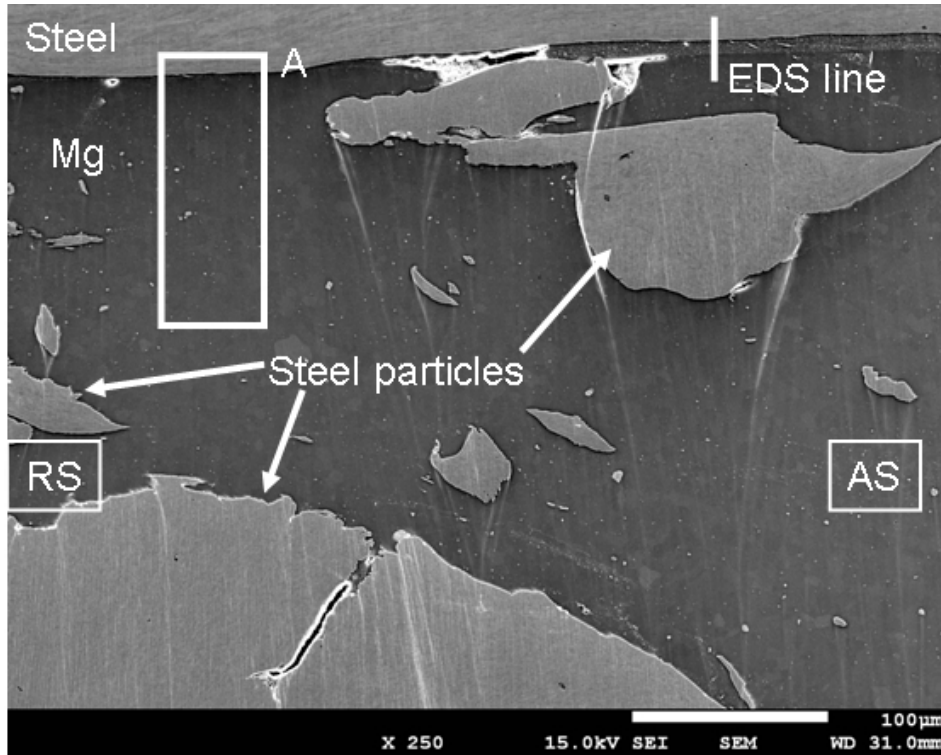
A.2.2 FSW of Magnesium and uncoated Steel: 900rpm

Figure A.6: Interface with EDS lines, tool rotation 900rpm
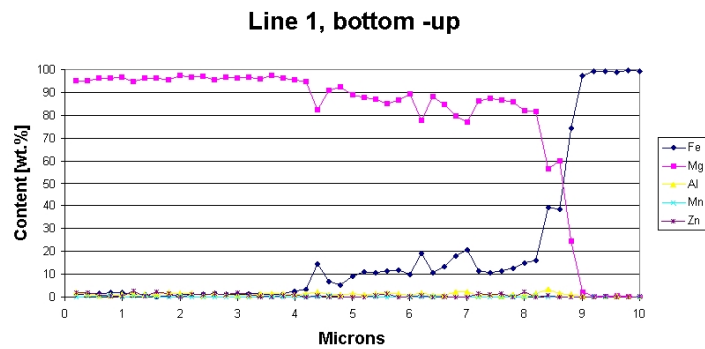
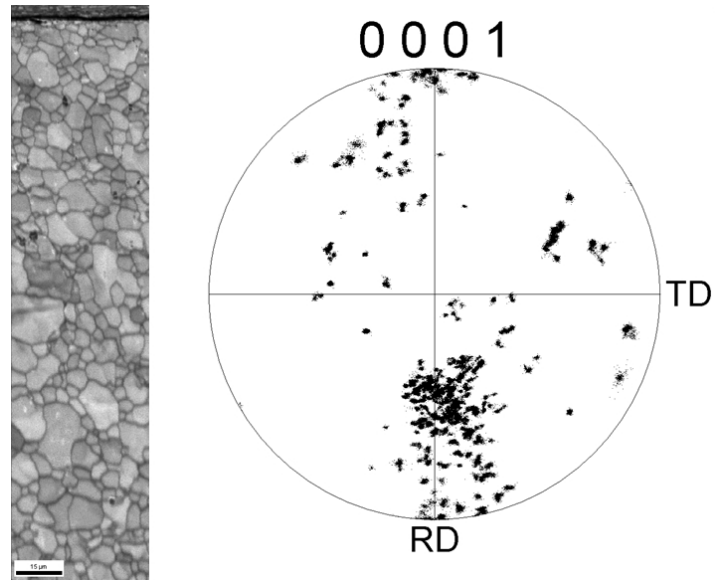Figure A.7: EDS line scan, tool rotation 900 rpm, without zinc coating

Figure A.8: Grain structure and pole figure, tool rotation 900 rpm, detail A in figure **??**

A.2.3 FSW Thermocycles at the Interface
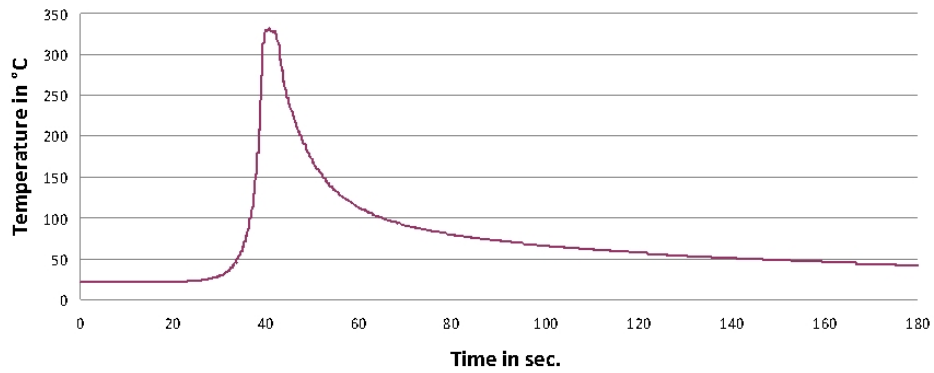
Figure A.9: Measured thermocylce at the interface Mg - steel for a welding speed of 150 mm/min
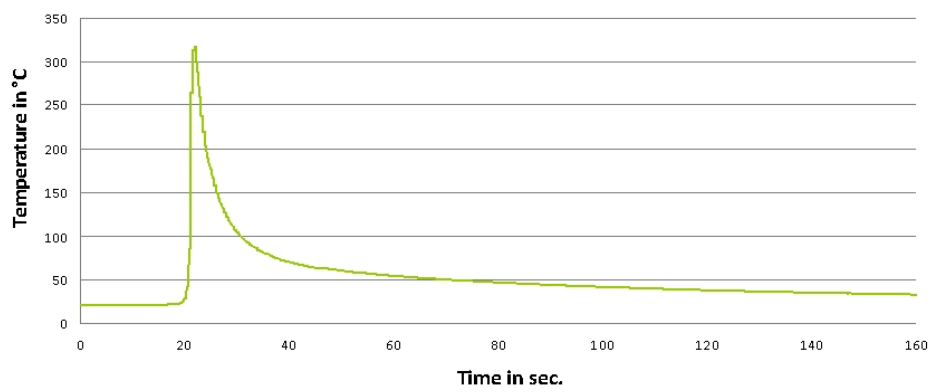
Figure A.10: Measured thermocylce at the interface Mg - steel for a welding speed of 500 mm/min